UNIVERSITÄT ZU LÜBECK

From the Institute of Experimental Endocrinology
of the University of Lübeck

Director: Prof. Dr. Jens Mittag

"BAT, can you feel the stream of dopamine?
—
Peripheral administration of dopamine or specific dopamine receptor agonists does not spark BAT thermogenesis in mice"

Dissertation for Fulfillment of Requirements
for the Doctoral Degree of the University of Lübeck
from the Department of Natural Sciences

Submitted by

Francesca-Maria Raffaelli

from
Kühlungsborn

Lübeck 2024

First Referee: Prof. Dr. Jens Mittag
Name

Second Referee: Prof. Dr. Henrik Oster
Name

Oral Examination: Lübeck, 24.02.2025
Date

Approved for Printing: Lübeck, 25.02.2025
Date

DECLARATION OF ORIGINALITY

I, Francesca-Maria Raffaelli, confirm that the submitted thesis is original work and was written by myself without further assistance. All direct or indirect sources used are acknowledged as references. Further, appropriate credit has been given to individuals who contributed to experiments or analyses.

This thesis has not been previously presented to an examination board, nor has it been published before.

The submitted electronic version of this thesis matches the printed version.

Lübeck, 16.10.2024 _____

Date Signature

PUBLICATIONS

Parts of the work compiled in this thesis have previously been published in a journal due to priority reasons:

Raffaelli, F.-M., Resch, J., Oelkrug, R., Iwen, K. A., & Mittag, J. (2020). Dopamine receptor D1- and D2-agonists do not spark brown adipose tissue thermogenesis in mice. *Scientific Reports*, *10*(1), 20203.

List of publications that are not related to this thesis:

Au, C. C., Docanto, M. M., Zahid, H., **Raffaelli**, F.-M., Ferrero, R. L., Furness, J. B., & Brown, K. A. (2017). Des-acyl ghrelin inhibits the capacity of macrophages to stimulate the expression of aromatase in breast adipose stromal cells. *Journal of Steroid Biochemistry and Molecular Biology*, *170*.

Djiogue, S., Halabalaki, M., Njamen, D., Kretzschmar, G., Lambrinidis, G., Hoepping, J., **Raffaelli**, F. M., Mikros, E., Skaltsounis, A. L., & Vollmer, G. (2014). Erythroidine alkaloids: A novel class of phytoestrogens. *Planta Medica*, *80*(11), 861–869.

Taudien, S., Szafranski, K., Felder, M., Groth, M., Huse, K., **Raffaelli**, F., Petzold, A., Zhang, X., Rosenstiel, P., Hampe, J., Schreiber, S., & Platzer, M. (2011). Comprehensive assessment of sequence variation within the copy number variable defensin cluster on 8p23 by target enriched in-depth 454 sequencing. *BMC Genomics*, *12*(1), 243.

ACKNOWLEDGMENTS

I would like to express my heartfelt appreciation for those who have paved and lined the path of this journey.

First and foremost, I would like to thank Prof. Dr. Jens Mittag for being an outstanding PhD supervisor. Thank you for the exceptionally good balance of trust, encouragement and brilliant input Jens. You are truly one of a kind and I am proud to call you my "Doktorvater".

I also thank my "Bonus-Doktorvater" PD Dr. Alexander Iwen for his highly valued contributions and advice from a clinician's point of view. I am forever grateful for your support Alex.

My work was funded by the German Research Foundation, my training further supported by the European Society of Endocrinology and the Bioscientifica Trust, and my experiments aided by the CBBM Core Facility and the Animal Facility of the University of Lübeck – all of whom I greatly appreciate.

To the MolEndo team – those who were there to greet me in the beginning, those who were there through thick and thin, and those who are there now to say farewell – you are a fantastic bunch of people, and I am going to miss every single one of you. Good group energy is the backbone of our work and not to be taken for granted. Thank you all for an amazing team spirit.

Especially, I would like to thank Dr. Rebecca Ölkrug, for happily sharing her knowledge and experience and backing me up whenever needed; and for her excellent feedback in every single presentation she ever attended. You are an ace Rebecca.

I would like to thank my office mates Julia, Rose, Lisa, Nocki, and Mehdi for a splendid time. We have shared joy and frustration up close and had good laughs almost every day, which is priceless to me. I am so glad I had you. Next door, but just as close, I would like to thank Lisbeth, Sogol, Beate and Conni for being great sports. You have all made my arrival in the group so easy and fun and supported me whenever needed.

I would also like to thank the neighboring groups of Prof. Dr. Oster, Dr. Kirchner, Dr. Schulz and Dr. Fliedner, for contributing to a very pleasant and cooperative work environment.

I further thank my fellow GRK 1957 students and all PIs for contributing to the unique experience this graduate college was. Our collaborations, events and everyday support of each other have brought us closer across our diverse fields of research and I am thankful

for the network these bonds have supplied us with. Many thanks in this regard also to Chaoqun, who has organized our meetings, schedules, curriculums, and events and was always there to support me and hold the back-office fort.

I would like to explicitly thank Martina and Conni, my colleagues who soon became very close friends. I am so thankful our paths crossed during this exciting time in life, and I hope they will stay closely intertwined in the future.

Further, my collaborators in Vienna deserve a big thank you. Prof. Dr. Gert Lubec, who invited me to his laboratory and made the collaboration possible; Fernando who is an outright genius, patient tutor, and very good friend; Roman, Martina, Edit, Ana, and Pedrag, who all made me feel very welcome and shared their experience and knowledge with me; Nassim, who joined the group and instantly became a dear friend; and Georg, my host, without whom my stay in Vienna would not have been the same.

My Lübeck family – Diane, Jens, Sieglinde, Uwe, Flame und Fire. You all are dear to me and made me feel like a family member from day one. Living with you has given me the perfect base and strength to perform well at work and I cannot imagine what this time would have been like without you all in my life. You were there through all highs and lows and even through the lowest low of my life. I owe a lot to you!

Finally, I thank my parents for supporting and loving me unconditionally no matter the distance, and my partner, best friend, and soon to-be-husband Christian for being my rock, my cheerleader, and my lifeline. Thank you for doing life with me, including this rollercoaster passage of it.

"The pain of parting is nothing to the joy of meeting again."

– Charles Dickens

ABSTRACT

Combatting overweight and obesity is one of the major concerns in healthcare in the world at the moment. Over two thirds of the world's population present with an above average BMI, which is the root cause for metabolic diseases, sky rocketing costs in healthcare, and eventually premature death.

Recent advances in the field include injections of antidiabetics that promote weightloss, but are essentially black boxes regarding long term side effects, sustainability, and overall consumer safety. An even deeper understanding of adipose tissue biology and its effects on whole body metabolism must be achieved to uncover safe ways for individuals to manage their body weight and therefore lead a healthier life – however long it may be.

One mechanism that has been investigated as a potential route to aid weight loss is brown adipose tissue (BAT) thermogenesis activation. Brown adipocytes differ from white adipocytes in cell size, fat vacuole distribution, mitochondrial density and a protein unique to their cell type, called uncoupling protein 1 (UCP1). This protein enables brown adipocytes to combust excess energy into heat, instead of intracellular storage, as is the case in white adipocytes.

The current state of the knowledge is, that BAT thermogenesis is activated through cold exposure and food intake which lead to hypothalamic signalling via the sympathetic nervous system and increase the release of norepinephrine in BAT, which consequently initiates G protein-coupled receptor-dependent molecular pathways leading to increased UCP1 expression.

Interestingly, observations in the 1980s have described dopamine to have similar effects on BAT temperature increases in rodents, as norepinephrine does. A more recent study by Kohlie *et al.* followed this lead and investigated this observation on a molecular level in rodent cells *in vitro*; concluding dopamine and dopamine receptor D1-agonists did increase thermogenesis in brown adipocytes.

This study therefore aims to further investigate the role of dopamine and dopamine receptors in BAT thermogenesis *ex vivo* and *in vivo* in mice using direct tissue treatment, single injection short term approaches, as well as repeated injection and constant release methods over the course of one week in wild type C57BL/6NCrl mice, respectively. Furthermore, the presence of dopamine receptors in BAT of mice was investigated meticoulously in a proteomics approach. Neither BAT thermogenesis activation, nor dopamine receptor presence were detected in these experiments, leading to the conclusion, that dopamine or dopamine receptors D1 and D2 do not directly contribute

to BAT thermogenesis. However, an indirect role of dopamine, as the direct metabolic precursor of norepinephrine in the catecholamine synthesis pathway, via the central axis, can not be excluded and should be investigated further.

ZUSAMMENFASSUNG

Die Bekämpfung von Übergewicht und Fettleibigkeit ist derzeit weltweit eines der größten Anliegen im Gesundheitswesen. Über zwei Drittel der Weltbevölkerung haben einen überdurchschnittlichen BMI, der die Hauptursache für Stoffwechselerkrankungen, explodierende Kosten im Gesundheitswesen und schließlich vorzeitigen Tod ist.
Zu den jüngsten Fortschritten auf diesem Gebiet gehören Injektionen von Antidiabetika, die die Gewichtsabnahme fördern. Mit Hinblick auf langfristige Nebenwirkungen, Nachhaltigkeit und allgemeine Verbrauchersicherheit, stellen diese Medikamente jedoch bislang *Black Boxes* dar. Daher muss ein noch tieferes Verständnis der Fettgewebsbiologie und derren Auswirkung auf den Gesamtstoffwechsel erreicht werden, um sichere Wege zur Körpergewichtskontrolle für Individuen zu ergründen, und der Bevölkerung, ungeachtet der Lebensdauer, ein gesünderes Leben zu ermöglichen.
Ein Mechanismus, der als möglicher Weg zur Unterstützung der Gewichtsabnahme untersucht wurde, ist die Aktivierung der Thermogenese des braunen Fettgewebes (BAT). Braune Adipozyten unterscheiden sich von weißen Adipozyten in der Zellgröße, der Fettvakuolenverteilung, der Mitochondriendichte und einem für ihren Zelltyp einzigartigen Protein – dem sogenannten *Uncoupling Protein 1* (UCP1). Dieses Protein ermöglicht es braunen Adipozyten überschüssige Energie in Form von Wärme freizusetzen, statt sie intrazellulär zu speichern, wie es bei weißen Adipozyten der Fall ist. Nach aktuellem Wissensstand wird die BAT-Thermogenese durch Kälteeinwirkung und Nahrungsaufnahme aktiviert, was hypothalamische Signale über das sympathische Nervensystem sendet und die Freisetzung von Noradrenalin in BAT erhöht, was wiederum molekulare Signalwege initiiert, die durch G-Protein-gekoppelte Rezeptoren gesteuert werden und letztlich die UCP1-Expression erhöhen.
Interessanterweise zeigten Beobachtungen der 1980er Jahre, dass Dopamin ähnliche Auswirkungen auf den BAT-Temperaturanstieg in Nagern hat wie Noradrenalin. Eine neuere Studie von Kohlie *et al.* folgte diesem Hinweis und untersuchte diese Beobachtung auf molekularer Ebene in Nagetierzellen *in vitro*, mit der Schlussfolgerung, dass Dopamin und Dopaminrezeptor-D1-Agonisten die Thermogenese in braunen Adipozyten steigern.
Die vorliegende Studie untersucht daher die Rolle von Dopamin und Dopaminrezeptoren in der BAT-Thermogenese *ex vivo* und *in vivo* in Mäusen. Zum Einsatz kamen hierbei direkte Gewebebehandlung, kurzfristige Einzelinjektionsansätze sowie wiederholte Injektions- und konstante Freisetzungsmethoden im Laufe einer Woche in Wildtyp-C57BL/6NCrl-Mäusen. Darüber hinaus wurde das Vorhandensein von Dopamin-

rezeptoren in BAT von Mäusen im Rahmen einer Proteomics-Studie akribisch untersucht. In diesen Experimenten wurde weder die Aktivierung von BAT-Thermogenese noch das Vorhandensein von Dopaminrezeptoren festgestellt, was zu der Schlussfolgerung führt, dass Dopamin bzw. Dopaminrezeptoren D1 und D2 nicht direkt im Gewebe zu BAT-Thermogenese beitragen. Allerdings kann eine indirekte Rolle von Dopamin, welches die metabolische Vorstufe von Noradrenalin im Katecholaminsyntheseweg darstellt, über die zentrale Achse nicht ausgeschlossen werden und sollte weiter untersucht werden.

LIST OF ABBREVIATIONS

1° antibody	Primary antibody
2° antibody	Secondary antibody
ACN	Acetonitrile
Adrb3	Adrenoceptor β3
APS	Ammonium persulfate
BAT	Brown adipose tissue
BCA	Bicinchononic acid
BSA	Bovine serum albumin
cAMP	Cyclic adenosine monophosphate
CHAPS	Cholamidopropyl-dimethylammonio-propanesulfonate
CNS	Central nervous system
DA	Dopamine
DAT	Dopamine transporter
DBP	Diastolic blood pressure
DEPC	Diethyl pyrocarbonate
DIO2	Deiodinase 2
DMSO	Dimethyl sulfoxide
DRD1	Dopamine receptor D1
DRD2	Dopamine receptor D2
DTT	Dithiothreitol
EDTA	Ethylenediaminetetraacetic acid
ELISA	Enzyme-linked immunosorbend assay
FFA	Free fatt acids
$G_{\alpha i}$, $G_{\alpha q}$	Inhibitory G protein
$G_{\alpha s}$	Stimulatory G protein
GPCR	G protein-coupled receptor
gWAT	Gonadal white adipose tissue
H&E	Hematoxylin and eosin
i.c.v.	Intracerebroventricular
i.p.	Intraperitoneal
IAA	Indoacetamide
iBAT	Interscapular brown adipose tissue
IHC	Immunohistochemistry
IRT	Infrared thermography
iWAT	Inguinal white adipose tissue
LC-MS/MS	Liquid chromatography with tandem mass spectrometry
MAP	Mean arterial pressure

NE	Norepinephrine
O.C.T.	Optimal cutting temperature
OD	Optical density
OXPHOS	Oxidative phosphorylation
P1	Pellet 1
P2	Pellet 2
PAGE	Polyacrylamide gel electrophoresis
PCA	Perchloric acid
PMSF	Phenlymethylsulfonyl fluoride
PVDF	Polyvinylidene difluoride
SN	Supernatant
SBP	Systolic blood pressure
SDS	Sodium dodecyl-sulfate
SPE	Solid phase extraction
T3	Triiodothyronine
TBE	Tris-borate-EDTA
TCA	Trichloracetic acid
TEAB	Triethylammonium bicarbonate buffer
TEMED	Tetramethylethylendiamin
TFA	Trifluoroacetic acid
TRP	Transient receptor potential ion channel
UCP1	Uncoupling protein 1
Wt	Wild type

LIST OF FIGURES

LIST OF TABLES

TABLE OF CONTENTS

1 INTRODUCTION

With more than half the world's population being overweight or obese (body mass index BMI ≥ 25 and BMI ≥ 30, respectively) (Hepatology, 2021; Roth et al., 2004), humanity is facing a persistent and rampant global epidemic of not only obesity, but also all its comorbities. Apart from being a key diagnostic criterion for metabolic syndrome, obesity is also a key driver in the development of all other metabolic syndrome diagnostic criteria, and their associated health conditions – amongst which are some of the leading causes of death, such as cardiovascular disease (World Health Organization, 2018) (Figure 1-1).
Obesity typically is a consequence of chronic dysbalance between energy intake and energy expenditure. Energy expenditure is commonly surpassed by energy intake due to dietary choices and a lack of physical activity. Despite increasing awareness of factors contributing to overweight and obesity, this burden to health continues to affect more people every year, with prevalences having tripled since the 1970s (Fryar, 2018). Besides the potentially detrimental personal effects, this phenomenon is also of great socio-economic relevance, since healthcare costs associated with excessive body weight are tremendous (BMI ≥ 30 +65% costs; BMI ≥ 35 +157% costs) (Simon et al., 2011).
Accordingly, it is of great interest to identify novel approaches to balance energy metabolism despite modern lifestyle challenges, to positively regulate body weight.

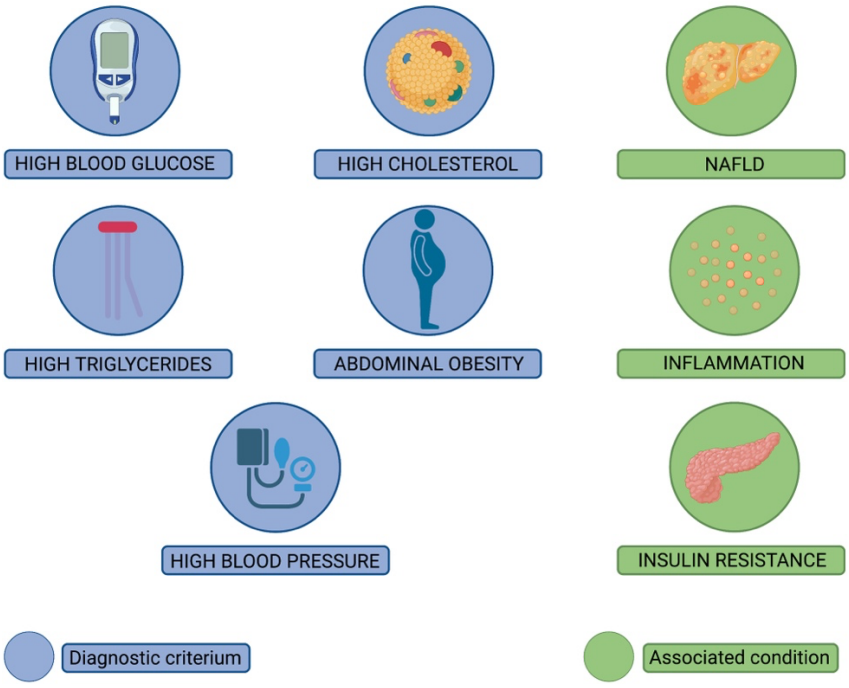

Figure 1-1: Diagnostic criteria of metabolic syndrome and associated conditions. (Geerling et al., 2022)

1.1 Brown adipose tissue (BAT)

One approach to positively influence energy balance is to increase energy expenditure by triggering combustion of excess energy into heat through the process of non-shivering thermogenesis, which takes place in a specialized adipose tissue.

There are two fundamentally different types of adipose tissue present in mammals: white adipose tissue (WAT) and brown adipose tissue (BAT); both of which are present in different depots throughout the body (Figure 1-2 B, C). Essentially, they serve opposite purposes. WAT is first and foremost responsible for energy storage, in form of lipids stowed in a unilocular fat vacuole (Petito et al., 2023). BAT, on the other hand, is responsible for energy combustion and heat generation (referred to as BAT thermogenesis), and characterized by smaller, multilocular lipid droplets and a large number of mitochondria per cell, the latter of which contribute to its brown appearance (Figure 1-2 A) (Cedikova et al., 2016).

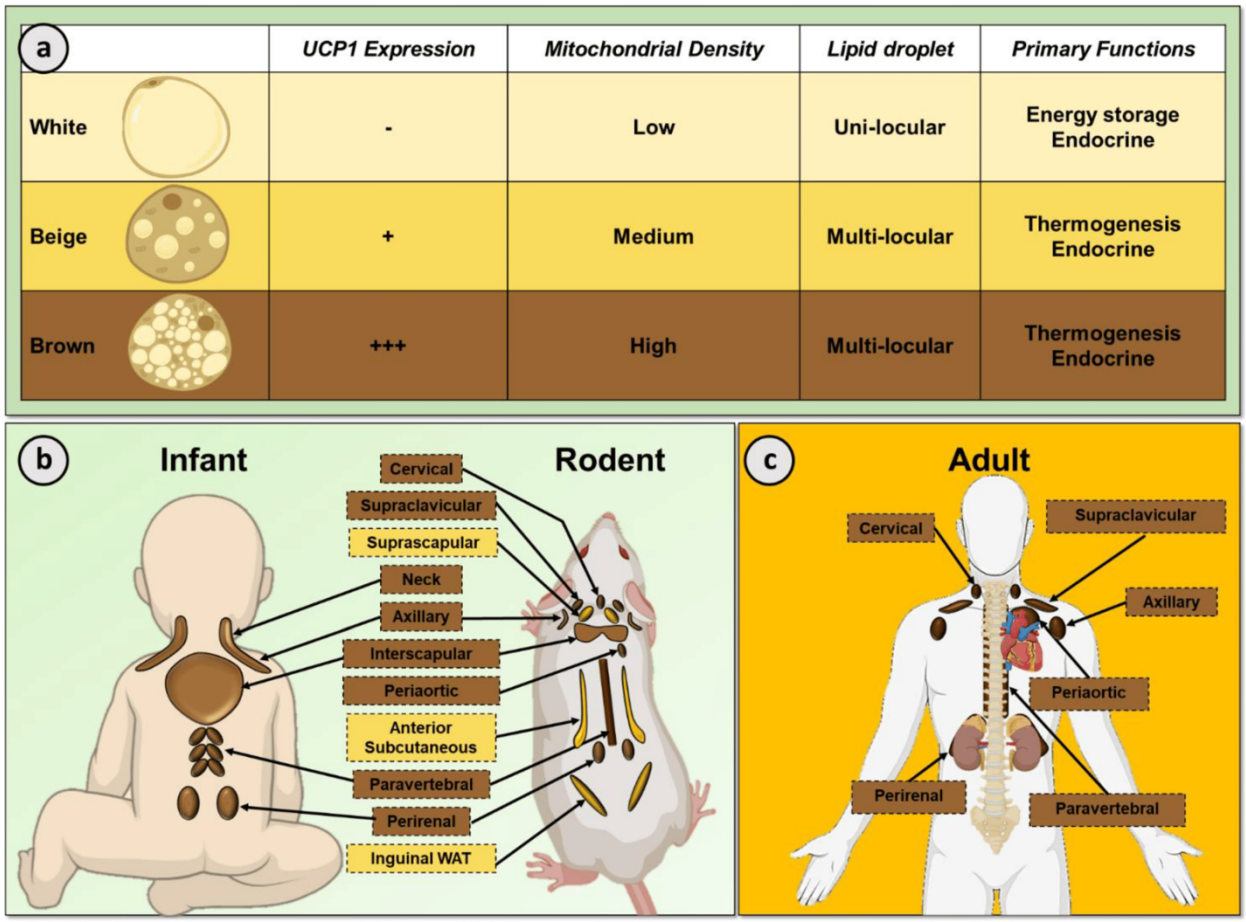

Figure 1-2: Overview of adipocyte subtypes (A) and localization of various adipose depots in mice and humans (B, C). (Suchacki & Stimson, 2021)

Of course, both types of adipose tissue are subject to remodeling and shifts in fat metabolism in the overall concertation of whole body energy homeostasis – with key modulators being feeding and fasting cycles, as well as environmental temperature changes. For example, white adipocytes can expand and contract their lipid depot, depending on whether energy needs to be stored or released. But also, they can be thermogenically activated (recruited) by, e.g., cold exposure, thus turning into an intermiediate cell type, called beige adipocytes (Wu et al., 2012). Likewise, the level of thermogenic activity of brown adipocytes depends on environmental stimuli, such as feeding state (Rothwell & Stock, 1983) and cold exposure (Virtanen et al., 2009). Despite this mechanism existing in both tissue types, the overall capacity for thermogenesis is significantly larger in BAT compared to beige adipose tissue or WAT (Nedergaard & Cannon, 2013).

1.1.1 Physiological Relevance of BAT Thermogenesis

Debates around these adipose tissue phenotypes and their contribution to balancing energy metabolism have increased since the discovery of active BAT in adult humans. Brown adipose tissue has been known to be present and active in adult, hibernating animals, i.e., tenreks; but also in rodents like mice and rats, as well as in newborn humans, where BAT serves the vital purpose of body temperature maintenance through non-shivering thermogenesis as a response to the sudden cold exposure post-natally (Aherne & Hull, 1966; Cannon & Nedergaard, 2004; Lidell, 2019). Newborns lack the ability to shiver sufficiently as a consequence of insufficiently developed muscle mass . Therefore, they rely on non-shivering thermogenesis as a source of heat production, which is why BAT thermogenesis is an essential mechanism of body temperature homeostasis after birth (Lidell, 2019).

Up until 2007 the consensus prevailed that BAT activity decreased with age and was no longer detectable in adult individuals. However, with the observation of active BAT in some adult humans by (Nedergaard et al., 2007; Virtanen et al., 2009) this view was challenged and ultimately had to be refuted. Since then, BAT thermogenesis has become a hot topic with the aim to unravel its molecular pathways and regulation, in order to use its energy expending properties to potentially counteract overweight and obesity.

1.1.2 Medical Intervention Potential of BAT Thermogenesis

Opinions differ about whether activation of BAT and recruitment of WAT are sufficient to have a beneficial effect on energy balance, to a degree where significant weight loss and therefore combatting of comorbidities of overweight and obesity can be achieved. In humans, an increase in metabolic rate between 1% and 20% has been attributed to activated BAT (Marlatt & Ravussin, 2017). More studies using standardized cold exposure protocols and cohorts of test subjects are needed to narrow down these varying results to come to realistic conclusions. Regardless of the net sum of additional energy excess generated by activated BAT, the effect of BAT activiation and browning of WAT on overall remodeling of adipose tissue depots and associated shifts in endocrine signalling also need to be taken into account (Petito et al., 2023; Suchacki & Stimson, 2021; Warner & Mittag, 2016). While an extra 100 kcal of energy expenditure may not lead to significant weightloss in a short amount of time, it can potentially help with weight loss maintenance, glucose tolerance, fat to body mass ratio and certainly be an additional measure in weight loss protocols, which currently focus on dietary changes and physical activity (Cho et al., 2023). Therefore, the molecular function of BAT thermogenesis needs to be further investigated for an improved understanding of its complex role in whole-body metabolism and how it can be safely activated. Only then, its properties can be securely exploited for interventions serving metabolic profile improvements, without, e.g., the danger of hyperthermia – as was the case with chemical uncouplers such as 2,4-dinitrophenol (DNP). The weight-loss effects of DNP were observed in munition factory workers during World War I, which is why the compound became widely used for obesity treatment in the 1930s, despite its deadly side effects (Goldgof et al., 2014; Grundlingh et al., 2011).

1.1.3 Molecular Mechanisms of BAT Thermogenesis Activation

BAT thermogenesis is the result of “unchained” energy metabolism. Brown adipocytes contain uncoupling protein 1 (UCP1), a protein that is unique to this cell type (Ricquier, 2000). Expression of UCP1 can be increased upon external stimulation, e.g. through cold exposure or food intake. As a result, the efficiency of mitochondrial oxidative phosphorylation decreases, and energy expenditure through lipid and glucose oxidation increases, which leads to significantly increased heat dissipation (De Meis et al., 2010).

The molecular mechanisms of cold-induced BAT thermogenesis are described in detail below.

1.1.3.1 Environmental Signal Reception, Integration, and Response

Thermosensation in mammals takes place through thermoceptors, which ultimately transmit an electric signal via afferent neurons to the central nervous system (CNS) and the hypothalamus in particular (Ezquerra-Romano & Ezquerra, 2017; Lv & Liu, 2007; Mackenzie et al., 1975) Once a cold stimulus is sensed and signalled to the hypothalamus via the according receptor and neuron types, it is processed by the preoptic area (POA) in the hypothalamus (Boulant, 2000; Contreras et al., 2017). The POA then projects to the dorsomedial and ventral nucleus of the hypothalamus (DMH and VMH). These nuclei and others (e.g., the arcuate nucleus) are also involved in sensing nutritional signals and mediating food-induced thermogenesis. In these regions, the received signals from cold and feeding status are being integrated and from here, excitatory projections are being sent to areas of the brainstem, like the rostral raphe pallidus (rRPA) (Contreras et al., 2017; Labbé et al., 2015), which in turn mediates sympathoexcitatory responses in peripheral organs (Cao & Morrison, 2006; Houtz et al., 2021). Both WAT and BAT are highly innervated by the sympathetic nervous system (SNS). Upon activation of the aforementioned neurotransmission cascade, neurotransmitter release from nerve terminals in WAT and BAT increases, leading to BAT thermogenesis activation.
Notably, BAT thermogenesis activation is also referred to as non-shivering thermogenesis. As the term suggests, it is different from shivering thermogenesis, which defends body temperature against a cold environment by generating heat through frequent contraction of muscles – an immediate response. Non-shivering thermosgenesis, on the other hand, requires recruitment and/or activation of BAT (W. Zhang & Bi, 2015). However, once recruited, activation can be immediate, while the magnitude of heat production depends on the amount of recruited BAT (Cannon & Nedergaard, 2004).

1.1.3.2 Catecholamine Signalling in BAT thermogenesis

In mice, non-shivering BAT thermogenesis is first and foremost activated through release of catecholamine neurotransmitter norepinephrine (NE) from nerve terminals spanning adipose tissue (Bartness et al., 2010a).

The synthesis pathway of catecholamine neurotransmitters, such as dopamine (DA), NE, and epinephrine (E) starts with the uptake of the amino acid L-tyrosine into the cytoplasm of the respective neurons (Vincent, 2004). In the cytoplasm, tyrosine hydroxylase (TyrH) catalyzes the conversion of tyrosine into L-dihydrophenylalanin (L-DOPA), which, in turn, is enzymatically converted into DA by DOPA-decarboxylase (DDC). DA itself is a neurotransmitter and synthesized mainly by various cell types in the brain, postganglionic fibres, and especially chromaffin cells in the adrenal medulla (Seeman, 2010). While some of the synthesized DA is being released into systemic circulation, some is being further converted into NE by dopamine-β-hydroxylase (DβH) inside chromaffin granule or synaptic amine storage vesicles of chromaffin cells or NE neurons, respectively. Finally, NE can be converted into E by phenylethanolamine-N-methyltransferase (PNMT) in adrenergic neurons or chromaffin cells (Grandbois et al., 2016).

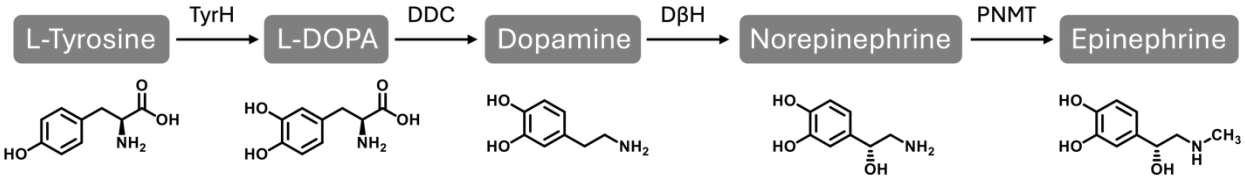

Figure 1-3: Catecholamine synthesis pathway.

TyrH – tyrosine hydroxylase, L-DOPA – L-dihydrophenylalanin, DDC – DOPA-decarboxylase, DβH – dopamine-β-hydroxylase, PNMT – phenylethanolamine-N-methyltransferase

Catecholamine neurotransmitters exclusively bind to and activate G-protein coupled receptors (GPCR) (Purves et al., 2001). GPCR are transmembrane receptors that transduce extracellular signals into intracellular second messenger signalling (Walsh et al., 2008). They can be classified into three categories depending on their α subunit: $G_{\alpha s}$, $G_{\alpha q}$, and $G_{\alpha i}$. $G_{\alpha s}$ and $G_{\alpha q}$ are stimulatory subunits, which activate cyclic adenosine monophosphate (cAMP) and phospholipase C, respectively; while $G_{\alpha i}$ is an inhibitory subunit, which inhibits multiple intracellular signalling pathways (Wettschureck & Offermanns, 2005).
BAT thermogenesis is most potently activated by catecholamine NE (Morrison et al., 2012). In mice, NE binds to the vastly abundant GPCR subtype adrenoceptor β3 (ADRB3) ($G_{\alpha s}$-coupled) on the adipocyte membrane (Bartness et al., 2010b, 2014), initiating a cAMP-mediated signal transduction cascade inside the cell, ultimately leading to thermogenesis activation, as described in detail in 1.1.3.3 and Figure 1-4. Notably, in humans this process is mediated mainly via adrenoceptor β2 instead of β3 (Blondin et al., 2020).

1.1.3.3 *Intracellular Mechanisms in Brown Adipocytes Leading to BAT-Thermogenesis Activation*

The NE-mediated intracellular increase in cAMP in brown adipocytes leads to increased protein kinase A (PKA), which in turn activates the lipase-mediated breakdown of triglycerides into free fatty acids (FFA), which ultimately fuel thermogenesis (Park et al., 2019). Additionally, increased cAMP and PKA activate transcription factors and co-factors, e.g., thyroid hormone receptor (TR), peroxisome proliferator-activated receptor (PPAR), retinoid X receptor (RXR), PPARγ coactivator 1α (PGC1α), CCAAT/enhancer

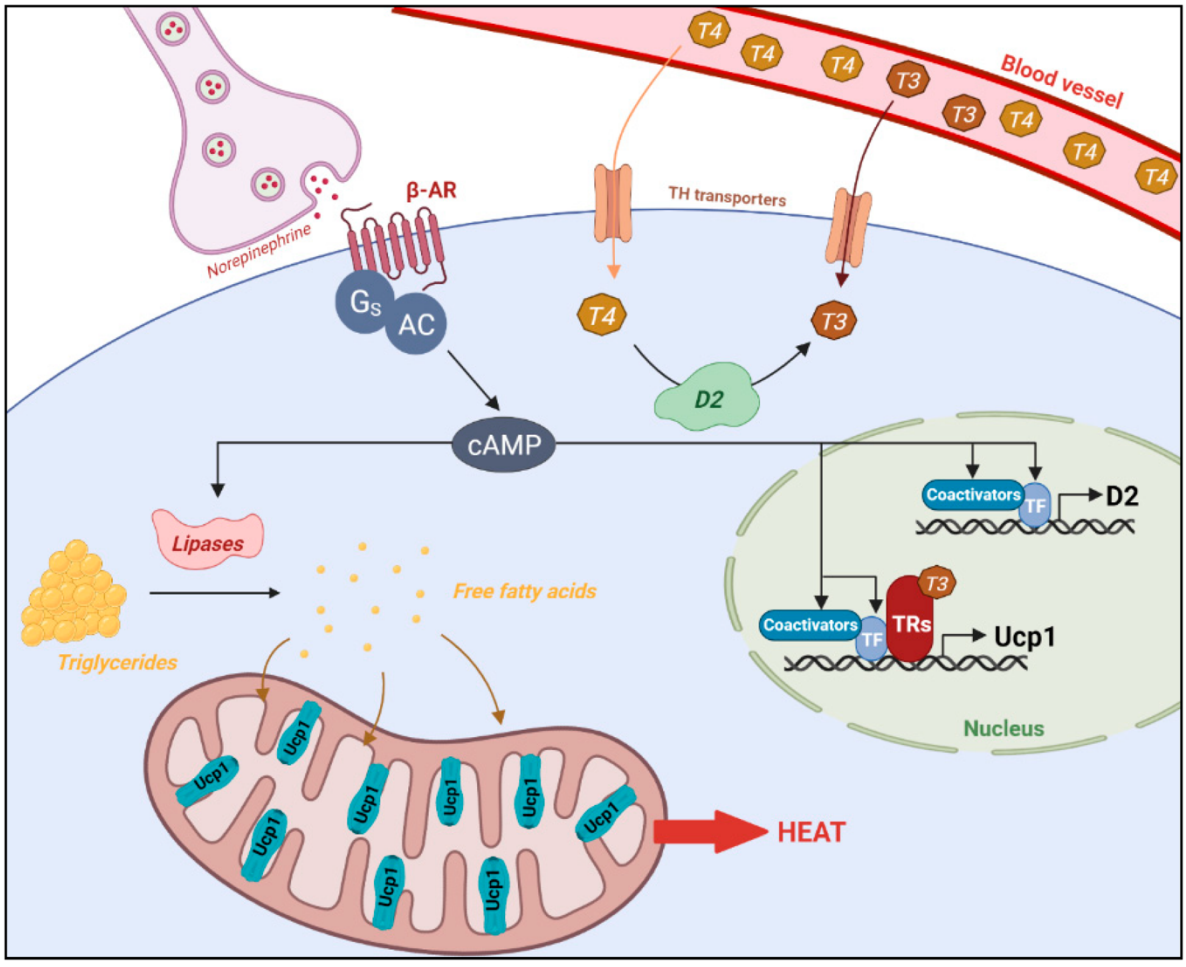

Figure 1-4: Molecular mechanisms of BAT thermogenesis activation. (Zekri et al., 2021)

β-AR - β-adrenergic receptor, AC – adenylate cyclase, cAMP – cyclic adenosine monophosphate, TF – transcription factor, TRs – thyroid hormone receptor, TH – thyroid hormone, T3 - triiodothyronine, T4 - thyroxine, D2 (Dio2) – deiodinase 2, Ucp1 – uncoupling protein 1.

binding proteins (C/EBPs), cyclic AMP response element binding protein (CREB), and PR domain containing 16 (PRDM16) (Seale, 2015; Tapia et al., 2018). Binding of transcription factors and co-activators to their according response elements in promotor or enhancer

regions leads to increased expression of key thermogenesis activating genes, including *Ucp1*.

Another key thermogenesis activating gene is deiodinase 2 (*Dio2*), which increases intracellular levels of the active thyroid hormone 3,3',5-triiodo-L-thyronine (T3) in brown adipocytes by deiodination of thyroxine (T4) (Bianco & Silva, 1987; de Jesus et al., 2001). T3, in turn, acts as a transcription co-factor in *Ucp1* gene expression (Bianco & McAninch, 2013). UCP1 protein then localizes to the inner mitochondrial membrane, where it acts as a FFA-activated H^+-carrier, thereby uncoupling the proton flux from oxidative phosphorylation, and generating heat, instead of ATP (Fedorenko et al., 2012).

1.1.4 Dopamine in BAT Thermogenesis

Interestingly, DA, as the direct precursor of NE in catecholamine synthesis, has been observed to have similar effects on BAT thermogenesis activation as NE in rats in the 1980s (Maxwell et al., 1985; Rothwell et al., 1982).

Interestingly, besides sharing a biosynthesis pathway, DA and NE are also overlapping in their receptor binding specificity. On the one hand, there are five types of DA-receptors, which are classified into two groups: dopamine receptor D1 (DRD1)-like and DRD2-like receptors. DRD1-like receptors are of the stimulating $G_{\alpha s}$ type, namely DRD1 and DRD5; while DRD2-like receptors are of the inhibiting $G_{\alpha i}$ type, namely DRD2, DRD3, and DRD4 (Bhatia et al., 2024). On the other hand, there are nine types of adrenoceptors, which are classified into three groups: α1-, α2-, and β-adrenoceptors (Hein & Kobilka, 1995; Qu et al., 2019). Namely, adrenoceptors α1A, α1B, α1D, adrenoceptors α2A, α2B, α2C, and adrenoceptors β1, β2, β3. Both DA and NE have been reported to act via non-canonical pathways by binding to subtypes of each other's receptor subtypes (Cornil & Ball, 2008; Sánchez-Soto et al., 2016).

Almost 40 years after the first implications for a possible role of DA in BAT thermogenesis activation were discovered by observations, this possible function of DA and its molecular mechanisms were followed by *in vitro* analyses. Specifically, the direct effects of DA and DRD-receptor agonists on immortalized murine white and brown adipocytes were studied by Kohlie et al., 2017. The study showed that DA, as well as a specific DRD1-agonist increased oxygen consumption rate, mitochondrial membrane potential, mitochondrial mass, and UCP1 in these brown adipocytes, which all hint at activation of thermogenesis in these cells.

However, whether this effect also occurs *in vivo* and which DRs might be involved in a complex physiological model, remains enigmatic.

1.2 Aim

While BAT thermogenesis activation through NE is well described, the question whether other catecholamines, such as DA, also play a role in this process has yet to be analyzed in detail.

While there are mainly two ways in which DA could impact BAT thermogenesis activation – via indirect, central signalling or via direct, peripheral receptor interaction on brown adipocytes – the latter of these is being analyzed in this study. While observations in rodents back in the 1980s, as well as more recent molecular analyses by Kohlie et al., 2017 in murine immortalized brown adipocytes suggest a direct role for DA in BAT thermogenesis activation *in vitro*, *in vivo* studies are yet to confirm these findings.

Thus, this study aims to a) analyze whether DA or DRDs directly trigger thermogenesis in BAT of mice *ex vivo* and *in vivo*, b) investigate whether DA receptors are truly present in brown adipocytes, allowing the tissue to respond directly to DA via canonical pathways, and c) employ the generated proteomic data set to identify novel markers that facilitate assessing the degree of BAT thermogenesis activity.

These efforts will progress the knowledge of molecular mechanisms in BAT thermogenesis and therefore advance aspirations to safely exploit this physiological energy wasting mechanism for metabolically beneficial therapies to counteract overweight and obesity.

2 MATERIAL AND METHODS

2.1 Material

The following lists provide information on substances (Table 2-1), reagent kits (Table 2-2), buffer and medium recipes (Table 2-3), primers (Table 2-4), antibodies (Table 2-5), consumables (Table 2-6), devices (Table 2-7), and software (Table 2-8) used in experiments that were performed for this thesis.

Table 2-1: List of substances

Substance	Catalog #	Supplier
2-Mercaptoethanol	M3148	Sigma-Aldrich
3,3',5-Triiodo-L-thyronine Sodium Salt (T3)	T6397	Sigma-Aldrich
Acetic Acid 100 %	3738.4	Roth
Acetone ≥ 99,9 %, HPLC	270725	Sigma-Aldrich
Acetonitrile (ACN) ≥ 99,9 %, HPLC Plus	34998	Sigma-Aldrich
Acrylamide ≥ 99,5 %	01696	Sigma-Aldrich
Agarose Neeo, Ultra-Quality	2267.4	Roth
Ammonium Persulfate (APS) ≥ 98 %	9592.1	Roth
Bepanthen Eye Ointment	01578675	Bayer
Bicinchononic Acid (BCA)	B9643	Supelco
Bovine Serum Albumin (BSA) 98 %	A7906	Sigma-Aldrich
Bromophenol Blue	111746	Millipore
Calcium Chloride Dihydrate ≥ 99 %	HN04.2	Roth
Carprofen, Rimadyl	462986	Pfizer
Cell Culture DMEM Medium, High Glucose, L-Glut	21063-029	Gibco
Cell Culture Medium 199	31150022	Gibco
CHAPS hydrate ≥ 98 %	C3023	Sigma-Aldrich
Chloroform ≥ 99,5 %	C2432	Sigma-Aldrich
CL316,243 Hydrate	C5976	Sigma-Aldrich
D-Glucose ≥ 99,5 %	G7021	Sigma-Aldrich
Dexamethasone ≥ 97 %	D4902	Sigma-Aldrich
Diethyl Ether ≥ 99,5 %	3942.1	Roth
Dimethyl Sulfoxide (DMSO) ≥ 99,8 %	4720.4	Roth
Dimethylformamide ≥ 99 %	D4551	Sigma-Aldrich
Dipotassium Hydrogen Phosphate ≥ 98 %	6875.2	Roth
Disodium Hydrogen Phosphate ≥ 99 %	P030.1	Roth
Disodium Tetraborate ≥ 99 %	4403.1	Roth
Dithiothreitol (DTT) ≥ 99 %	D0632	Sigma-Aldrich

DNA Marker 100bp, FastGene	MWD100	Nippon
DNase, RNase-free	79254	Qiagen
DNase, Turbo, 2U/µl	AM2238	Invitrogen
dNTP Mix 10 mM	R0191	Thermo Scientific
Dopamine Hydrochloride	AB120565	Abcam
DPBS 10x	14190144	Gibco
Eosin Y Solution 0,5 %	X883.2	Roth
Ethanol ≥ 99,5 % purest	5054.4	Roth
Ethanol ≥ 99,8 % denatured	K928.4	Roth
Ethylene Glycol ≥ 99,5 %	6881.1	Roth
Ethylenediaminetetraacetic Acid (EDTA) ≥ 99 %	8043.1	Roth
Ethylenediaminetetraacetic Acid (EDTA) 0,5 M, pH 8	31.450.500	AppliChem
Gentamicin Sulfate 50 mg/ml	17-518Z	Lonza
Glycerol ≥ 99,5 %	2006	Gerbu
Glycine ≥ 99 %, Blotting Grade	0079.3	Roth
Hemalum Solution Acid	T865.3	Roth
HEPES, Ultra-Pure	05288	Biomol
Hydrochloric Acid	K025.1	Roth
Hydrochloric Acid 37 %	9277.1	Roth
Indoacetamide (IAA) ≥ 99 %	I1149	Sigma-Aldrich
Insulin	I6634	Sigma-Aldrich
Isoflurane 100 %, IsoFlo	TU061220	Zoetis
Isopropyl Alcohol 99 %	17024	Fischar
L-Ascorbic Acid ≥ 99 %	L5960	Sigma-Aldrich
LC-MS Acetonitrile with 0,1 % Formic Acid, Chromasolv	34668	VWR
LC-MS Rinsing Solution I, 50 % 2-Propanol, Chromasolv	34689	VWR
LC-MS Trifluoroacetic Acid (TFA), Chromasolv	302031	VWR
LC-MS Water HiPerSolv, Chromanorm	23595.328	VWR
LC-MS Water with 0,1 % Formic Acid, Chromasolv	34673	VWR
Lugol Solution	L6146	Sigma-Aldrich
Magnesium Chloride Hexahydrate ≥ 99 %	HN03.2	Roth
Magnesium Sulfate Heptahydrate ≥ 99 %	T888.1	Roth
Methanol ≥ 99,9 %	0082.2	Roth
Milk Powder	T145.3	Roth
Mounting Medium ProLong Antifade, DAPI	P36971	Invitrogen
Mounting Medium Pertex	LEIC811	VWR
Mounting Medium, Vectashield, DAPI	VEC-H-1500	Biozol
Nonidet P-40	n/a	Fluka
Norepinephrine (+)-Bitartrate Salt Monohydrate (*ex vivo*)	A9512	Sigma-Aldrich
Norepinephrine (NE), Arterenol (*in vivo*)	03870227	Sanofi

Paraffin Wax, Shandon Histoplast	6774060	Thermo Scientific
Paraformaldehyde Solution 4 % in PBS	19943	Affymetrix
Perchloric Acid (PCA) 48-50 %	44464	Alfa Aesar
Phenlymethylsulfonyl Fluoride 0,1 M (PMSF)	93482	Sigma-Aldrich
Phenol	0038.1	Roth
Phenylephrine Hydrochloride	P6126	Sigma-Aldrich
Potassium Acetate	T874.2	Roth
Potassium Chloride ≥ 99 %	P017.1	Roth
Potassium Dihydrogen Phosphate ≥ 98 %	P018.2	Roth
ProSieve EX PAGEr Protein Gel 12 Well, 4-12 %	BMA59722	Lonza
ProSieve EX Running Buffer 10x	00200307	Lonza
ProSieve EX Transfer Buffer 10x	00200309	Lonza
Protease Inhibitor Cocktail, cOmplete Ultra Mini	5892791001	Roche
Protein Ladder PageRuler Plus, Prestained	26619	Thermo Scientific
Proteinase K Solution 20 mg/ml	25530049	Invitrogen
RNase ZAP Spray	R2020	Sigma-Aldrich
(±)-SKF-38393 Hydrochloride	D047	Sigma-Aldrich
Saline Solution, Isotonic 0,9 %	02337169	Berlin Chemie
Sample Buffer 4x Laemmli	1610747	Bio-Rad
Sodium Acetate	106268	Supelco
Sodium Chloride ≥ 99,8 %	9265.2	Roth
Sodium Deoxycholate ≥ 98 %	30970	Sigma-Aldrich
Sodium Dihydrogen Phosphate Monohydrate ≥ 98 %	K300.1	Roth
Sodium Dodecyl Sulfate (SDS)	817034	SAFC
Sodium Fluoride Solution 0,5 M	67414	Sigma-Aldrich
Sodium Hydrogen Carbonate ≥ 99,5 %	6885.2	Roth
Sodium Hydroxide ≥ 98 %	6771.3	Roth
Sodium Hypochlorite Solution 5-10 %	6846.1	Roth
Sodium Orthovanadate 99 %	0735.2	Roth
Standard Diet Mice, Breeding Diet	1314	Altromin
Standard Diet Mice, Maintenance Diet	1324	Altromin
Sucrose ≥ 99,5 % (GC)	S9378	Sigma Aldrich
Sumanirole Maleate	2773/50	Tocris
SYBR Green Master, FastStart Universal (ROX)	4913914001	Roche
SYBR Safe DNA Gel Stain	S33102	Invitrogen
Tetramethylethylendiamine (TEMED) ≥ 99 %	2367.1	Roth
Thiourea ≥ 99 %	T7875	Sigma-Aldrich
Tissue-Tek O.C.T. Compound	4583	Sakura
Tri-Sodium Citrate Dihydrate ≥ 99 %	4088.3	Roth
Trichloracetic Acid (TCA) ≥ 99 %	T9159	Sigma-Aldrich

Triethylammonium Bicarbonate Buffer (TEAB) 1M	T7408	Sigma-Aldrich
Trifluoroacetic Acid (TFA) ≥ 99 %	302031	Sigma-Aldrich
Tris 1 M, pH 8,0, RNase-Free	AM9855G	Invitrogen
Tris Base, Trizma, BioUltra ≥ 99,8 %	93362	Sigma-Aldrich
Tris Pufferan, Buffer Grade	AE15.2	Roth
Tris-Borate-EDTA (TBE) Buffer 10x, pH 8,3	106177	Millipore
Tris-EDTA 100x Buffer Solution	T9285	Sigma-Aldrich
Triton X-100	8059	Th. Geyer
Trizol Reagent	15596026	Invitrogen
Trypsin, Proteomics Grade	T6567	Sigma-Aldrich
Tween 20	P1379	Sigma-Aldrich
Urea ≥ 98 %	U5378	Sigma-Aldrich
Vaseline, White	n/a	Pharmacy
Water, Molecular Biology, AccuGene	51200	Lonza
Water, Nuclease-Free, DEPC-treated	AM9906	Invitrogen
Water, Nuclease-Free, Non-DEPC-Treated	AM9938	Invitrogen
Western Blot Stripping Buffer Restore Plus	46430	Thermo Scientific
Western ECL Substrate Clarity	1705060	Bio-Rad
Western ECL Substrate Clarity Max	1705062	Bio-Rad
Xylene (Isomers) ≥ 97 %	9713.3	Roth

Table 2-2: List of reagent kits

Kit	**Catalog #**	**Supplier**
Avidin / Biotin Blocking Kit	SP2001	Vector
cAMP Direct Biotrak EIA	RPN225	GE Healthcare
Chemiluminescence Substrate Quantum Kit	K-12042-C20	Advansta
Free Glycerol Reagent Kit	F6428	Sigma-Aldrich
Glycerol Standard Solution	G7793	Sigma-Aldrich
Leptin ELISA Kit 96 Well, Mouse	EZML-82K	Sigma-Aldrich
Lipase Activity Assay Kit, Colorimetric	AB102524	Abcam
LTQ Velos ESI Positive Ion Calibration Solution, Pierce	88323	Thermo Scientific
MemCode Reversible Protein Stain Kit	1485.1	Thermo Scientific
Peptide Assay Kit, Pierce Fluorometric	23290	Thermo Scientific
Peptide Fractionation, Pierce High pH Reversed-Phase	84868	Thermo Scientific
Protein Assay Kit II DC	5000112	Bio-Rad
Protein Assay Kit, Pierce BCA	23227	Thermo Scientific
Protein Assay Standard BSA, Pierce, Pre-Diluted	23208	Thermo Scientific
QIAzol Lysis Reagent	79306	Qiagen
Revert Aid First Strand cDNA Synthesis Kit	K1622	Thermo Scientific
RNeasy Fibrous Tissue Mini Kit	74704	Qiagen

RNeasy Lipid Tissue Mini Kit	74804	Qiagen
RNeasy Micro Kit	74004	Qiagen
RNeasy Mini Kit	74106	Qiagen
TGX Stain Free Fast Cast Acrylamide Kit 10 %	1610183	Bio-Rad
TGX Stain Free Fast Cast Acrylamide Kit 12 %	1610185	Bio-Rad

Table 2-3: List of buffer and medium recipes

Buffer	Conc.	Ingredient	Input	Total
Blocking Solution 5 %	~5 % (w/v)	Milk Powder	2,5 g	50 ml
	1x	TBS-T 1x	to 50 ml	
Explant Medium	100 %	Medium 199	250 ml	0,25 l
	25 mM	HEPES	1,49 g	
	2 % (w/v)	BSA	5 g	
Basic	0,25 mg/ml	Gentamicin Sulfate	1,25 ml	
Explant Medium	100 %	Explant Medium Basic	52 ml	52 ml
	0,7 nM	Insulin 7 µM	5,2 µl	
	2 nM	T3 10 µM	10,4 µl	
	2,5 nM	Dexamethasone 2,5 µM	52 µl	
Complete	150 µM	L-Ascorbic Acid 150 mM	52 µl	
Lugol Reaction Mix	30 parts	KCl 25 % (w/v)	30 ml	30 ml
	0,5 parts	Lugol Solution	500 µl	
	0,2 parts	HCl 5 M	200 µl	
Lysis Buffer	90 %	RIPA Buffer	9 ml	10 ml
	1 mM	Na_3VO_4 200 mM	50 µl	
	10 mM	NaF 500 mM	200 µl	
	1x	Protease Inhib. Cockt.	1 tbl	
			aliquot -20°C	
	1 mM	PMSF 100 mM	add fresh	
PBS 10x	1,37 M	NaCl	80 g	1 l
	26,8 mM	KCl	2 g	
	14,7 mM	KH_2PO_4	2 g	
	104,4 mM	$N_2HPO_4*H_2O$	14,4 g	
pH 7,4	32 %	NaOH	titrate	
RIPA Buffer	0,05 M	Tris-HCl 1,5 M pH 7,4	3,33 ml	0,1 l
	150 mM	NaCl 5M	3 ml	
	1 % (v/v)	Nonidet P40	1 ml	
	1 ml	EDTA Solution 0,5 M	200 µl	
	0,5 % (v/v)	Sodium Deoxychol. 10 % (w/v)	5 ml	
Running Buffer 10x	0,25 M	Tris Base	30,3 g	1 l

		1,92 M	Glycine	144,13 g	
		1 % (w/v)	SDS	10 g	
Sample Buffer 4x		50 % (v/v)	Glycerol	10 ml	20 ml
		10 %	SDS	2 g	
		312,5 mM	Tris-HCl 1,0 M pH 6,8	6,25 ml	
		n/a	Bromophenol Blue	Sp. Tip	
TBS 10x		0,1 M	Tris Base	12,1 g	1 l
		1,5 M	NaCl	87,7 g	
	pH 7,4	1,0 M	HCl	titrate	
TBS-T 1x		10 x	TBS	200 ml	2 l
		0,1 % (w/v)	Tween 20 10 % (w/v)	2 ml	
Transfer Buffer 10x		0,25 M	Tris	30,3 g	1 l
	Basic	1,92 M	Glycine	144,13 g	
Transfer Buffer 1x		10 x	Blotting Buffer Prep	100 ml	1 l
	Final	20 % (v/v)	Methanol	200 ml	
Tris-HCl 0,5 M		0,5 M	Tris Base	30,3 g	0,5 l
	pH 6,8	1,0 M	HCl	titrate	
Tris-HCl 1,0 M		1,0 M	Tris Base	12,1 g	0,1 l
	pH 6,8	1,0 M	HCl	titrate	
Tris-HCl 1,0 M		1,0 M	Tris Base	30,3 g	0,25
	pH 7,5	1,0 M	HCl	titrate	
Tris-HCl 1,5 M		1,5 M	Tris Base	45,4 g	0,25 l
	pH 7,4	1,0 M	HCl	titrate	
Tris-HCl 1,5 M		1,5 M	Tris Base	90,9 g	0,5 l
	pH 8,8	1,0 M	HCl	titrate	
Vienna Proteomics		7 M	Urea	4,2 g	10 ml
Protein Solubilization Buffer		2 M	Thiourea	1,5 g	
		4 % (v/v)	CHAPS	0,4 g	
		100 mM	DTT	154 mg	
		50 mM	TEAB 1 M	0,5 ml	
		1x	Protease Inhib. Cockt.	1 tbl.	
Vienna Proteomics		8 M	Urea	9,6 g	10 ml
Sample Cleaning Buffer		0,1 M	TEAB 1M	1,0 ml	
Vienna Western		1,5 % (w/v)	SDS 10 %	3 ml	20 ml
SDS Buffer for Subfractions		100 mM	NaCl 4 M	0,5 ml	
		20 mM	Tris 1 M pH 7,5	0,4 ml	
		1x	Protease Inhib. Cockt.	2 tbl	
Vienna Western		0,32 M	Sucrose 2 M	1,6 ml	10 ml
Lysis Buffer for Subfractions		10 mM	HEPES 1M	100 µl	
		0,1 mM	$CaCl_2$ 0,1 M	10 µl	

	1x	Protease Inhib. Cockt.	1 tbl	
Vienna Western	0,2 M	Glycine	15 g	
Mild Stripping Buffer	0,1 % (w/v)	SDS	1 g	1 l
	1 % (v/v)	Tween 20	10 ml	

Table 2-4: List of primers (supplier: Integrated DNA Technologies)

Target	Gene Name		Sequence 5' → 3'	bp	Tm [°C]
Abcd2	ATP-binding Cassette D	fw	CATGGCGCGGATGTTTTACC	115	60,25
		rev	AATCCCAGCCCCAATAGCAG		59,81
Acc1	Acetyl-CoA Carboxylase	fw	GTCCCCAGGGATGAACCAATA	132	59,15
		rev	GCCATGCTCAACCAAAGTAGC		60,14
Adig	Adipogenin	fw	TTTCCTGGTGAGGAGGACGG	121	61,19
		rev	TGACAACGGGAGATCCCAGG		61,26
Adipoq	Adiponectin	fw	TGTTCCTCTTAATCCTGCCCA	104	58,73
		rev	CCAACCTGCACAAGTTCCCTT		61,03
Adrb3	Adrenoceptor β3	fw	AGAAACGGCTCTCTGGCTTTG	190	60,88
		rev	TGGTTATGGTCTGTAGTCTCGG		58,98
Akr1b7	Aldo-Keto Reductase 1 b 7	fw	GCCATTCTCAGCCTCAACAG	105	58,91
		rev	TCAAGCGAACCAACATCAGT		57,75
Aldh2	Aldehyde Dehydrogenase 2	fw	GCAGGCCTACACGGAAGTG	129	60,74
		rev	TGCTTGGTGGTGGCTTTTCTC		61,36
C12orf73	Chromosome 12 Orf 73	fw	CCAGGTGGTGCATTGGTACT	107	59,96
		rev	CGTGGCGTCTCTCTTTCAGT		60,04
Cd209d	CD209d Antigen	fw	AATGAAGCCACATGGCACTGG	104	61,50
		rev	GCACAATCTTCATCACCGACATT		59,87
Cdnf	Cerebral Dopamine	fw	TTGCGCCGGGTTTTGTATCT	120	60,61
	Neurotrophic Factor	rev	AGCAGGGAGTTGTAGAATCGG		59,52
Cidea	Cell Death-Inducing DNA	fw	TGACATTCATGGGATTGCAGA	171	57,63
	Fragmentation Factor, Alpha	rev	GGCCAGTTGTGATGACTAAGA		57,67
Cpt1c	Carnitine Palmitoyltransferase	fw	GGCTTCTGGAACCTCATGG	104	57,82
	1c	rev	GCGTTGGAAGCTGAAGAGC		59,50
Dio2	Deiodinase,	fw	ATGGGACTCCTCAGCGTAGAC	151	61,02
	Iodothyronine, Type II	rev	ACTCTCCGCGAGTGGACTT		60,60
Drd1	Dopamine Receptor D1	fw	GACATACGCCATTTCATCCTCC	108	59,19
		rev	ATGCGCCGGATTTGCTTCT		60,75
Drd2	Dopamine Receptor D2	fw	ACCTGTCCTGGTACGATGATG	105	59,24
		rev	GCATGGCATAGTAGTTGTAGTGG		59,19
Drd3	Dopamine Receptor D3	fw	TGGGGCAGAAAACTCCACTG	106	60,18
		rev	TACCAGACCGTTGCCAAAGAT		59,65
Drd4	Dopamine Receptor D4	fw	GCCTGGAGAACCGAGACTATG	142	59,93

		rev	CGGCTGTGAAGTTTGGTGTG		59,97
Drd5	Dopamine Receptor D5	fw	CTCGGCAACGTCCTAGTGTG	92	60,73
		rev	GAGACGGCCAGAGATACGATG		60,07
Epx	Eosinophil Peroxidase	fw	CCCCTGGAAAGAGGCGTAAT	85	59,45
		rev	AGTTTCTTGCTGGGGAAGCG		60,89
Fasn	Fatty Acid Synthase	fw	GGAGGTGGTGATAGCCGGTAT	140	61,10
		rev	TGGGTAATCCATAGAGCCCAG		58,66
Gamt	Guanidinoacetat-N-	fw	CACGCACCTGCAAATCCTG	119	59,79
	Methyltransferase	rev	TACCGAAGCCCACTTCCAAGA		61,11
Gatm	Glycine Amidinotransferase	fw	GCTTCCTCCCGAAATTCCTGT	100	60,34
		rev	CCTCTAAAGGGTCCCATTCGT		59,16
Gstm6	Glutathione	fw	GCCTTCCCAAACCTGAAGGA	95	59,89
	S-Transferase, Mu 6	rev	ACAGGACTTGGAAGGAAGCG		59,96
Hprt	Hypoxanthine Guanine	fw	GCAGTACAGCCCCAAAATGG	85	59,47
	Phosphoribosyl Transferase	rev	AACAAAGTCTGGCCTGTATCCAA		60,18
Lep	Leptin	fw	GAGACCCCTGTGTCGGTTC	139	59,71
		rev	CTGCGTGTGTGAAATGTCATTG		59,02
Letmd1	LETM1 Domain Containing 1	fw	GTGTCTCTTCGTTGGCCTCA	110	59,97
		rev	TGGGGGTCCAGAAATGCTTG		60,25
Mlycd	Malonyl-CoA Decarboxylase	fw	CTGTCGCCTATCCCTGGATTC	122	60,00
		rev	CCGGTAACCGCTGAGATTTCT		60,13
Mpz	Myelin Protein Zero	fw	AGTTTCATGTTGGTAGCAGTGG	87	58,85
		rev	ATAGCTGGGGTAGGGCAAAGG		61,61
Mtfp1	Mitochondrial Fission Process 1	fw	TGGCCATCCCCGTCATAATC	85	59,60
		rev	ACTGACGGGTACAGCTTGC		60,00
Mtg1	Mitochondrial Ribosome-	fw	ACATGGCCAAGGGACTAAAGA	109	59,01
	Associated GTPase	rev	TGGAACAGAGGGTTTCGACC		59,60
Npr3	Natriuretic Peptide Receptor 3	fw	TTGGGGCCCTTTGAAACTGA	99	59,74
		rev	ACTGCAGATTCTTCTAGGCCAC		60,09
Pepck	Phosphoenolpyruvate	fw	ATCTTTGGTGGCCGTAGACCT	199	61,18
	Carboxykinase 1	rev	GCCAGTGGGCCAGGTATTT		60,00
Pgc1a	PPARG Coactivator 1 Alpha	fw	TTGTCAGGCTGGAGTGTACC	99	59,31
		rev	CACCATGGTCGTATCAGAGG		57,48
Phospho	Phosphoethanolamine/Phosph	fw	ATGAGCGGGTGTTTTCCAG	102	58,05
1	ocholine Phosphatase 1	rev	ATCGAAGTCGAAGGTGAGGAG		59,25
Pnkd	Paroxysmal Non-Kinesiogenic	fw	AAGAACCCCATGAAAGCCGT	113	59,89
	Dyskinesia	rev	TTGGGATAGCGATTCCGAGC		59,97
Prdm16	PR Domain Containing 16	fw	CCCCACATTCCGCTGTGAT	184	60,08
		rev	CTCGCAATCCTTGCACTCA		58,15
Prg2	Proteoglycan 2	fw	CTTGACAAGACCCAGGAGGG	200	59,67

		rev	TAGCTCTTCCCCTGGAGGAC		60,03
Prx	Periaxin	fw	GAATCTTTGTCCGCGAGCTG	86	59,63
		rev	ACGGGCGCTCAGAAGTTG		60,36
Pyrk	Pyruvate Kinase Liver	fw	TCAAGGCAGGGATGAACATTG	131	58,55
		rev	CACGGGTCTGTAGCTGAGTG		60,11
Serca2	Sarcoplasmic/Endoplasmic	fw	TCCGCTACCTCATCTCATCC	161	58,38
	Reticulum Calcium ATPase 2	rev	CAGGTCTGGAGGATTGAACC		57,59
Slc25a42	Solute Carrier 25 a 42	fw	GGGTGTCATTCCCTATGCGG	107	60,54
	(CoA and PAP Transporter)	rev	CCATGCGCTCAAAGGGGTA		60,08
Slc27a2	Solute Carrier 27 a 2	fw	TGAATGTGTATGGCGTGCCT	121	60,04
	(Fatty Acid Transporter FATP2)	rev	AGGTACTCCGCGATGTGTTG		60,11
Slc6a2	Solute Carrier 6 a 2	fw	CTGGCTCTGGGGCAATACAA	108	60,03
	(Noradrenalin Transporter NAT)	rev	GCCGACATAGAGGGCAATGA		59,89
Slc6a3	Solute Carrier 6 a 3	fw	GGAGGTTTCCCTACCTGTGC	102	60,04
	(Dopamine Transporter DAT)	rev	GCTCCATGTAGAAGAGGGGC		59,89
Slc6a8	Sodium- & Chloride-Dependent	fw	GTCTGGTGACGAGAAGAAGGG	161	60,07
	Creatine Transporter 1	rev	CCACGCACGACATGATGAAGT		61,27
Ucp1	Uncoupling Protein 1	fw	ACTCAGGATTGGCCTCTACG	110	58,88
		rev	CCACACCTCCAGTCATTAAGC		58,64
Ugt1a6	UDP Glucuronosyltransferase 1	fw	TCACGTGCGCAGGTCTCTA	106	60,97
	Polypeptide A6A	rev	AACTGAGCCCCAGAGCACTA		60,55
Vnn1	Vanin 1	fw	CACAGTGAGGCTCTGGCATT	130	60,32
		rev	TGGTGAAACGCACACCGTAT		60,25

Table 2-5: List of antibodies

Class	Target	Type	Host	Catalog #	Supplier
1°	Anti-DAT	Monoclonal Antibody	Rat	MAB369	Sigma-Aldrich
1°	Anti-DAT	Monoclonal Antibody	Rabbit	AB184451	Abcam
1°	Anti-DRD1	Monoclonal Antibody	Rat	D2944	Sigma-Aldrich
1°	Anti-DRD1	Monoclonal Antibody	Rat	MAB5290	Sigma-Aldrich
1°	Anti-DRD2	Monoclonal Antibody	Mouse	SC-5303	Santa Cruz
1°	Anti-DRD2	Polyclonal Antibody	Rabbit	TA328799	OriGene
1°	Anti-DRD2 L/S	Polyclonal Antibody	Rabbit	AB5084P	Sigma-Aldrich
1°	Anti-MAO-A	Monoclonal Antibody	Rabbit	AB126751	Abcam
1°	Anti-OxPhos	Rodent Clone Cocktail	Mouse	45-8099	Thermo Scientific
2°	Anti-Mouse	HRP-linked Polyclonal Antibody	Goat	P0447	Dako
2°	Anti-Rabbit	HRP-linked Polyclonal Antibody	Goat	P0448	Dako
2°	Anti-Rat	HRP-linked Polyclonal Antibody	Goat	7077	Cell Signaling
2°	Anti-Rat	HRP-linked Polyclonal Antibody	Goat	AB97057	Abcam

Table 2-6: List of consumables

Items	Catalog #	Supplier
Alcohol Pads	9160612	B. Braun
Aluminum Foil Labsolute, 15 µm	9106106	Korff
Alzet Micro-Osmotic Pump Model 1002	0004317	Charles River
Cell Culture Plates 6 Well	83.3920	Sarstedt
Cell Culture Plates 12 Well	83.3921	Sarstedt
Cell Culture Plates 24 Well	83.3922	Sarstedt
Cell Strainer 100 µm Pore Size, Yellow	83.3945.100	Sarstedt
Ceramic Beads Precellys 1,4 mm	432-0356	Bertin
Dounce Tissue Grinder Set Kimble 2 ml	D8938	Sigma-Aldrich
Dounce Tissue Grinder Set Kimble 7 ml	D9063	Sigma-Aldrich
Filter Column 3K Pierce Protein Concentrator	88512	Thermo Scientific
Filter Column 10K Vivacon 500 Protein Concentrator	518-0001	VWR
Filter Paper Western Blotting 0,83 mm	88600	Thermo Scientific
Filter Tips 0,5-20 µl	70.1114.210	Sarstedt
Filter Tips 2-100 µl	70.760.212	Sarstedt
Filter Tips 50-1000 µl	70.762.211	Sarstedt
Gloves Nitrile Micro-Touch Accelerator-Free, M	700103	Ansell
Gloves Nitrile Micro-Touch Nitra-Tex, M	700113	Ansell
Microplate ELISA 96 Well, Skirted, Flat Base	82.1581.200	Sarstedt
Microplate PCR 96 Well, Semi-Skirted, Flat Base	72.1979.102	Sarstedt
Microplate PCR Seal Sheets, Adhesive, Clear	600208	Biozym
Microscope Slides SuperFrost Plus	J18AMNZ	Thermo Fisher
MicroSpin Columns 5-60 µg, 200 µl, Solid Phase Extraction	SEM SS18V	Nest Group
Microtome Blades, Epredia MB35	3050835	Thermo Scientific
Parafilm M, PM992	P7542	Sigma-Aldrich
Pasteur Pipettes 2 ml, Disposable, 150 mm	612-1701	VWR
Petri Dishes 60x15 mm	82.1194.500	Sarstedt
Petri Dishes 92x16 mm	82.1472.001	Sarstedt
pH-Indicator Strips MColorpHast, pH 0-6,0	1.09531	Supelco
Protein Transfer Power Blotter Pierce	15319134	Thermo Scientific
PVDF Transfer Membrane Immobilon-P 0,45 µm	IPVH00010	Millipore
Scalpel Figure 10, Disposable	0200130010	Feather
Scalpel Figure 11, Disposable	020013011	Feather
Serological Pipettes 2 ml, Wadded, Sterile	86.1252.025	Sarstedt
Serological Pipettes 5 ml, Wadded, Sterile	86.1253.025	Sarstedt
Serological Pipettes 10 ml, Wadded, Sterile	86.1254.025	Sarstedt
Serological Pipettes 25 ml, Wadded, Sterile	86.1685.020	Sarstedt
Silk Suture, Absorbable, Perma-Hand, Purple	V396H	Ethicon

Silk Suture, Non-Absorbable, Perma-Hand, Black	681H	Ethicon
Slide Boxes “SliBo”, 100 Spaces, Kork, White	733010	Biozym
Sterican Disposable Cannulae, 23G, 0,50x25mm	4657667	B. Braun
Sterican Disposable Cannulae, 26G, 0,45x12mm	4665457	B. Braun
Syringe Filter 0,2 µm, Filtropur S, PES Membrane	83.1826.001	Sarstedt
Syringes 1 ml, Injekt-F Solo, Fine Dosage	9166017V	B. Braun
Syringes 10 ml 3-part Luer-Lock, Plastipak	BD305959	BD
Syringes 20 ml 3-part Luer-Lock, Plastipak	BD300629	BD
Syringes 0,5 ml, Micro-Fine + U100 Needle Insulin	BD324825	BD
Tissue Embedding Base Mold, 15x15, Parafree	39LC7052	Leica
Tissue Processing/Embedding Casettes, Histosette	720-0932	VWR
Tube Boxes 4x4, Cardboard	95.64.916	Sarstedt
Tube Boxes 9x9, Cardboard	95.64.981	Sarstedt
Tube Boxes 10x10, Cardboard	95.64.997	Sarstedt
Tubes 0,2 ml Strips of 8, Domed Caps	AB0451	Thermo Scientific
Tubes 0,2 ml, Sapphire PCR, Flat Lid	683271	Greiner
Tubes 1,5 ml, Safe Seal	72.706	Sarstedt
Tubes 2 ml, Safe Seal	72.695.500	Sarstedt
Tubes 2 ml, Screw Cap	72.694.406	Sarstedt
Tubes 5 ml, Eppendorf Quality, Snap-Cap	0030119.401	Eppendorf
Tubes 15 ml, Screw Cap	62.554.512	Sarstedt
Tubes 50 ml, Screw Cap	62.559.001	Sarstedt
Vacuum Filtration Filter & Bottle 250 ml, 0,2 µm Pore Size	83.3940.001	Sarstedt

Table 2-7: List of devices

Device	**Catalog #**	**Supplier**
Absorption Microplate Reader SPECTROstar Nano	n/a	BMG Labtech
Anesthesia Unit Univentor 410	U-410	Agnthos
Animal Cage Changing Station CS5 EVO GP	9CS5ETS0	Tecniplast
Animal Cages GM500 Mouse IVC Green Line	DGM70CPSU	Tecniplast
Animal Cages Rack System Mouse AERO 7x10	AERO70	Tecniplast
Autoclave Vertical Floor-Standing V-Series	Systec-V	Systec
BAT-12 Microprobe Thermometer	BAT-12	Physitemp
Blood Pressure Analysis System for Mice	SC-1000	Hatteras
Cell Culture CO2 Incubators CB 170	9640-0010	Binder
Centrifuge MC6 Mini Benchtop	90.186.102	Sarstedt
Centrifuge Non-Refrigerated	5430	Eppendorf
Centrifuge Refrigerated	5430R	Eppendorf
Centrifuge Rotor A-2-MTP (2 Microplates)	5427700005	Eppendorf
Centrifuge Rotor FA-45-48-11 (48 Tubes 1,5-2 ml)	5427754008	Eppendorf

Centrifuge Vacuum Concentrator Plus	5305000509	Eppendorf
Gel Imaging System ChemiDoc Touch	1708370	Bio-Rad
Heating Mat Thermolux	S89947	Voelkner
Infrared Photo Camera FLIR T335	T335	Flir
Infrared Video Camera VarioCam hr Head 600	n/a	Infratec
Isofluran Evaporator Delta Veterinarian	0206041-1	Löwenstein
LCMS PepMap C18 HPLC Trap Column 2 µm, 75 µm	164942	Thermo Scientific
LCMS PepMap C18 HPLC Trap Column 3 µm, 75 µm	164946	Thermo Scientific
LCMS Q Exactive Plus Hybrid Quadrupol-Orbitrap	IQLAAEGAAPFALGMBDK	Thermo Scientific
LCMS UltiMate 3000 RLSCnano HPLC System	5200.0355	Thermo Scientific
Magnetic Stirrer with Heater	VMS-C4	VWR
Microplate Washer Wellwash Versa 2x8	5165010	Thermo Scientific
Microscope ECLIPSE Ci-E	MBA93000	Nikon
Microtome Rotary Electronic Microm HM340E	56550	Thermo Scientific
Pipette Eppendorf Research Plus 0,5-10 µl	3123000020	Eppendorf
Pipette Eppendorf Research Plus 10-100 µl	3123000047	Eppendorf
Pipette Eppendorf Research Plus 10-100 µl, 8 Ch.	3125000036	Eppendorf
Pipette Eppendorf Research Plus 100-1000 µl	3123000063	Eppendorf
Pipette Multipette E3	4987000371	Eppendorf
Pipetting Aid Easypet	4420815005	Eppendorf
Precision Scale Atilon Analytical Balance	ATL-124-I	Acculab
Precision Scale PCB 1000-1	PCB1000-1	Kern
Precision Scale SE 203 LR Draft-Shielded	611-2600	VWR
Real-Time PCR System QuantStudio 5	A28569	Applied Biosystems
RET-3 Rectal Probe for Mice	RET-3	Physitemp
Roller Tilt Mixer RS-TR 05	XK30.1	Phönix
Scale Pro Pocket (Animal Facility)	TOP500	Smart Weigh
Shaker Duomax 1030	543-32205-00	Heidolph
Shaker Orbital Titramax 100	544-11200-00	Heidolph
Staining Jar Macro	073.05.001	Isolab
Staining Jar Rack	073.06.001	Isolab
Stereo Microscope 0,7x-4,5x SZB250	630-1577	VWR
Stereo Microscope Micrometric Eyepiece	630-1774	VWR
Take3 Micro-Volume Plate	10626785	BioTek
Take3 Microplate Spectrophotometer Epoch	17287989	BioTek
Temperature Control Unit HB 101/2	n/a	Agnthos
Temperature Logger EasyLog	EL-USB-1-LCD	Lascar Electronics
Thermal Cycler PTC-200 Dual	MJ-200D	MJ Research
Thermal Incubator Shaker 71 l INCU-Line ILS6	444-0733	VWR
Thermal Shaker Thermomixer Comfort 1,5 ml	5355000011	Eppendorf

Tissue Homogenizer Fisherbrand Bead Mill 24	15-340-163	Thermo Scientific
Tissue Homogenizer Hybaid RiboLyser	THO150	Hybaid
Ultra-Freezer -80°C	n/a	Thermo Fisher
Vortex Mixer Grant Instruments PV1	11466367	Thermo Scientific
Western Mini Trans-Blot Module Set	1703935	Bio-Rad
Western Mini-PROTEAN Tetra Cell Set	1658001	Bio-Rad
Western Power Supply PowerPac HC	1645052	Bio-Rad
Western Semi-Dry Transfer Cell Trans-Blot SD	1703940	Bio-Rad

Table 2-8: List of software and databases

Software	**Supplier**
Allen Mouse Brain Atlas, Brain Explorer 2	Allen Institute
BioTek Gen5 Microplate Reader and Imager	Agilent
FLIR Tools	FLIR
Image Lab Version 6.1	Bio-Rad
IRBIS 3 Plus	Infratec
LabChart 8.1	AD Instruments
Microsoft Excel, Word, and PowerPoint	Microsoft
Primer Bank	Harvard Medical School
Primer-BLAST	NCBI
Prism 6	GraphPad
Proteome Discoverer 2.3 – 3.0	Thermo Scientific
PubMed	NCBI
Q Exactive Plus	Thermo Scientific
QuantStudio Design and Analysis	Applied Biosystems
Sci-Hub Library	Sci-Hub Project
Tick@Lab Animal Research Facility	A-Tune Software AG
Tune 2.8.1.2806	Thermo Scientific
Xcalibur 4	Thermo Scientific
Zotero	Corporation for Digital Scholarship

2.2 Methods

In the following descriptions of applied methods, relevant material, in addition to foreign terms, has been highlighted in cursive style, indicating information on its catalog number and supplier or recipe can be found under 2.1 Material.

2.2.1 Animal Husbandry

All studies – *ex vivo* and *in vivo* – were conducted with 10 - 12 weeks old male wild type C57BL/6NCrl mice, purchased directly from Charles River, Germany. The mice were 9 - 10 weeks old upon arrival and were ensured to have at least one week to acclimate to the *Animal Cage System* and facility with an ambient temperature of 23 ± 1 °C, a constant 12 h light-dark cycle, and *ad libitum* access to the *Standard Diet Mice* and water. The animals were housed in groups of up to five for the "*Ex Vivo* Study" (2.2.3.1), in groups of three for the "Repeated Injection *In Vivo* Study" (2.2.4.2), and individually housed for the "Single Injection *In Vivo* Study" (2.2.4.1) and "Constant Release *In Vivo* Study" (2.2.4.3). Preceding dissection, the animals were anesthetized with CO_2 until vital signs had completely ceased. Immediately subsequent blood collection ensured death. All animal procedures were approved by the *Ministerium für Energiewende, Landwirtschaft, Umwelt, Natur und Digitalisierung (MELUND)* in Schleswig-Holstein, Germany. All methods were performed in accordance with relevant guidelines and regulations.

2.2.2 Active Compounds

Active compounds used for *ex vivo* or *in vivo* treatments of iBAT tissue or animals, respectively, and their molecular function are listed below (Table 2-9). Purchasing information is disclosed in the List of Substances (Table 2-1).

Table 2-9: List of active compounds and their molecular function

Active Compound	**Molecular Function**
Dopamine Hydrochloride	General Catecholamine Neurotransmitter
Norepinephrine	General Catecholamine Neurotransmitter
CL316,243	Specific Adrenoceptor β3 (ADRB3)-Agonist
(±)-SKF-38393 Hydrochloride	Specific Dopamine-Receptor D1 (DRD1)-Agonist
Sumanirole Maleate	Specific Dopamine-Receptor D2 (DRD2)-Agonist

The individual compounds were solubilized in water or *Saline Solution, Isotonic 0,9 %* for *ex vivo* or *in vivo* application, respectively, yielding stock solutions of identical concentration. From these stock solutions, final dilutions were freshly prepared in *Complete Explant Medium* or *Saline Solution, Isotonic 0,9 %* for *ex vivo* or *in vivo* treatment, respectively.

2.2.3 Ex Vivo Studies

2.2.3.1 Dose-Response Studies in iBAT Explant Tissue Culture

Tissue culture of iBAT explants was performed similarly as described in previous studies (Cannon & Nedergaard, 2001; Chen *et al*., 2013; Lee *et al*., 2016; Pulinilkunnil *et al*., 2011). In brief, iBAT was dissected from eight mice (12 weeks of age) per experiment and each cut into four pieces. All 32 iBAT pieces for one experiment were pooled in a covered petri dish filled with *Basic Explant Medium*. The process was completed within 40 minutes at most.

All further steps were carried out in a laminar flow work bench. First, the tissue was minced into pieces of 1 - 2 mm in diameter, transferred to a 100 µm cell strainer placed on top of a 50 ml tube, rinsed thoroughly with 100 ml 1x DPBS, and distributed evenly into 12-well culture plates (~ 10 mg tissue/well), each well of which was pre-filled with 1 ml *Complete Explant Medium*. Explants were synchronized in 37 °C and 5 % CO_2 for 24 h. Subsequently, each well was rinsed with 1x DPBS. Finally, 1 ml of *Complete Explant Medium* with added treatment substances was added per well. Treatment of iBAT explants consisted of DRD1-agonist SKF-38393, DRD2-agonist Sumanirole, and DA (each at 10 nM, 50 nM, 100 nM, and 500 nM) as well as ADRB3-agonist CL316,243 (1 µM) as a positive control.

For each treatment condition, three technical replicates were performed (n = 3). The experiment was carried out twice, yielding a total of n = 6 technical replicates. After incubation at 37 °C and 5 % CO_2 for 24 h, iBAT explants were rinsed with 1x DPBS, collected, snap frozen, and stored at -80 °C until further processing.

2.2.4 In Vivo Studies

2.2.4.1 Single Injection In Vivo Study (1 h)

To study the immediate effects of peripheral application of the DRD1-agonist, DRD2-agonist, and DA on iBAT thermogenesis, mice (n = 6) were injected intraperitoneally (i.p.)

with *Saline Solution, Isotonic 0,9 %*, DRD1-agonist SKF-38393 (10 mg/kg), DRD2-agonist Sumanirole (3,2 mg/kg), or DA (100 µg/kg). Each animal received all four conditions in random order with a recovery time of three days between treatments. As a positive control reference, one additional animal was injected with NE (1 mg/kg) (credit to Dr. Rebecca Ölkrug).

Animals, in their accustomed cages with open lids, were placed underneath the fixed *Infrared Video Camera VarioCam hr head 600* and infrared thermography (IRT) videos were recorded for a total duration of 70 min at a rate of 1 frame/s. Ambient temperature was kept at 23 ± 1 °C and draft was prevented. First, 10 min were recorded for baseline establishment. Then, animals were briefly restrained for i.p. injection, released back into the cage, and filmed for another 60 min.

iBAT temperature was scored in one representative IRT image per minute using the *IRBIS3 Plus* software. Changes in iBAT temperature were calculated by subtracting the 10 min-baseline average from each 5 min-treatment interval average.

2.2.4.2 Repeated Injection In Vivo Study (1 week)

To study the effects of repeated peripheral DRD1- and DRD2-agonist injections on iBAT thermogenesis, mice were monitored for two weeks. Measurements of the first week were collected for baseline establishment, while measurements of the second week were collected to account for treatment effects. Treatment during the second week consisted of daily i.p. injections with either DRD1-agonist SKF-38393 (10 mg/kg, $t_{1/2}$ > 4 h) (Jackson et al., 1988; McCall et al., 2005a) or DRD2-agonist Sumanirole (3,2 mg/kg, $t_{1/2}$ > 4 h) (Baker *et al*., 2008).

The two different treatment groups were studied successively. Therefore, each treatment group (n = 6) had its own independent saline control group (n = 6) that was monitored and analyzed simultaneously with the treatment group.

During both weeks, the documented physiological data comprised body weight, food intake, water intake, core body temperature, iBAT temperature, tail root temperature, heart rate, and blood pressure.

Body weight, food and water intake were determined daily by weighing the animal, food, and water, respectively.

Core body temperature was measured rectally, using the *RET-3 Rectal Probe for Mice* connected to the *BAT-12 Microprobe Thermometer*.

iBAT and tail root temperature were determined by IRT photos, taken with the *Infrared Photo Camera FLIR T335*. IRT photos were taken on day six and seven of both the first (baseline) and second (treatment) week. From these IRT photos, iBAT and tail root temperature were scored using the *FLIR Tools* software. For statistical analysis, the scored temperatures were averaged within each group of animals over two consecutive days, and normalized to the rectally measured T_b, which was averaged in the same way.
Heart rate and blood pressure were determined using the non-invasive *Blood Pressure Analysis System for Mice*. In detail, mice were restrained on the heated plate (37 °C), while their tail was threaded through the balloon-lined tail cuff. The tail root was positioned in the tail cuff, the tail middle in the v-notch over the pulse detector, and the tail tip was gently fixated with tape. The tail was accurately aligned, so the ventral artery would face straight down towards the pulse detector. After a two-minute acclimation phase, an automated sequence of 15 measurements of heart rate, systolic blood pressure (SBP), diastolic blood pressure (DBP), and mean arterial pressure (MAP) (all four readouts were generated simultaneously during each measurement) was recorded. A minimum of 12 valid values for each parameter (SBP, DBP, and MAP) per session were set as mandatory to calculate the mean for statistical analysis. Two sessions were conducted as training. Two further sessions within two consecutive days during the second (treatment) week were used for statistical analysis to compare the groups.
At the end of day seven of the treatment week, the animals were sacrificed for blood sampling and organ collection.

2.2.4.3 Constant Release In Vivo Study (1 week)

Following up on the "Repeated Injection *In Vivo* Study" 2.2.4.2, the effect of constant peripheral release of the DRD1-agonist on iBAT thermogenesis was investigated. This was achieved by implanting the *Alzet Micro-Osmotic Pump Model 1002*. The approach further allowed to study the effect of DA itself, given its extremely short half-life ($t_{1/2} < 2$ min) (Bachmann *et al*., 2007; Sturgill *et al*., 2011). Hence, the osmotic pumps were loaded to release DRD1-agonist SKF-38393 or DA at a rate of 10 µg/kg/min and 7 µg/kg/min, respectively, for the duration of one week, following the manufacturer's instructions.
The *Alzet Micro-Osmotic Pump Model 1002*, by default, provides a constant flowrate of 0,25 µl/h, is 1,5 cm long and 0,6 cm in diameter; and was implanted into the peritoneal cavity in a minimally invasive surgery procedure.

Briefly, animals were anesthetized with 4 % isoflurane at a flowrate of 400 ml/min, followed by 2 % isoflurane at 200 ml/min to maintain anesthesia. Reflexes were tested regularly to ensure sufficient narcosis. Mice were placed on a heating mat, eyes protected with Bepanthen eye ointment, fur shaved along the *linea alba*, and an initial dose of i.p. analgesic Carprofen (5 mg/kg) applied. Through a small (0,5 – 1 cm) incision along the *linea alba*, the loaded osmotic pump was inserted, the peritoneum closed with absorbable suture material and the abdominal wall closed with non-absorbable suture material. Bepanthen was dabbed on the suture to aid the healing process. The animals recovered for two full days post operation before any measurements other than body weight were taken. A second dose of Carprofen (5 mg/kg) was administered i.p. one day post operation.
Starting on the third day post operation, physiological measurements were collected as described in 2.2.4.2.

2.2.5 Molecular Analyses

2.2.5.1 mRNA Expression Analysis

To analyze mRNA expression in adipose tissue, brain, liver, abdominal aorta and ventral tail artery, total RNA was isolated according to the manufacturer's instructions supplied with the *RNeasy Lipid Tissue Mini Kit*, *RNeasy Mini Kit*, *RNeasy Fibrous Tissue Mini Kit*, and *RNeasy Micro Kit*, respectively. RNA concentration was determined using the *Take3 Microplate Spectrophotometer Epoch* with the *Take3 Micro-Volume Plate* and *BioTek Gen5 Microplate Reader and Imager* software. Then, quantitative real-time reverse transcription PCR (qRT PCR) was performed in two steps. First, to obtain cDNA, reverse transcription PCR (RT PCR) was performed according to the manufacturer's instructions for the *Revert Aid First Strand cDNA Synthesis Kit*. The cDNA was diluted 1:50 (samples) or 1:25 (standards) for every 1000 ng total RNA input. Subsequently, qPCR was performed using the *Real-Time PCR System QuantStudio 5*. Primers for qPCR were generated aiming to have melting temperatures (T_m) of about 60 °C and a length of approximately 120 base pairs (bp). Primer sequences, regardless of their source (e.g., primer bank, publications, or new design) were verified using the *Primer-BLAST* tool to ensure correct sequences, orientation, and properties. Lyophilized primers were reconstituted to form 50 µM stock solutions. Primer mixes for each target were prepared by diluting forward (fw) and reverse (rev) primers 1:100 in 1 ml *Water, Nuclease-Free, Non-DEPC-Treated*, yielding a 0,5 µM ready-to-use primer mix. The qPCR reaction mix was prepared according to the

manufacturer's instruction for the *SYBR Green Master, FastStart Universal (ROX)* with altered primer concentrations and total volume:

Master mix:	SYBR Green Master 10x	10	µl
	Primer mix (0,5 µM)	2	µl
	Water, Nuclease-Free	4	µl
Template:	cDNA	4	µl
Total:		**20**	**µl**

The qPCR layout and protocol were configured using the *QuantStudio Design and Analysis* software. All samples were measured in duplicates. The following qPCR program was applied with subsequent melt curve analysis to indicate amplicon specificity:

1x	Activation	95 °C	10	min
40x	Denaturation:	95 °C	15	s
	Annealing & Elongation:	60 °C	1	min

Gene expression of the housekeeper gene *Hprt* was used as a reference for normalization during analysis.

2.2.5.2 Western Blot Analysis of Total Protein

To semi-quantitatively analyze protein expression in snap-frozen tissue samples, Western blot analysis was performed.

The method comprised size-based protein separation through sodium dodecyl sulfate-polyacrylamide gel electrophoresis (SDS-PAGE), protein transfer to a polyvinylidene fluoride (PVDF) membrane through electrophoresis, and detection of target proteins by using specific primary (1°AB) and horseradish peroxidase (HRP)-linked secondary (2°AB) antibodies together with a luminol-based substrate to obtain a chemiluminescent reaction.

Initially, tissue was homogenized in *Lysis Buffer* using *Ceramic Beads Precellys 1,4 mm* and the *Tissue Homogenizer Fisherbrand Bead Mill 24*, according to the manufacturer's instructions (5,5 m/s, 25-30 s). Depending on tissue texture, 1-3 cycles were performed in-between which, samples were cooled down on ice for at least 5 min. Proteins were

isolated from other cell components by centrifugation at full speed for 20 min. For fatty tissue, multiple centrifugation cycles were performed until the supernatant became clear. The protein-containing supernatant was transferred to a fresh tube and protein concentration was determined according to the manufacturer's instructions for the *Protein Assay Kit, Pierce BCA*.

Next, isolated proteins were separated by molecular mass using the *TGX Stain Free Fast Cast Acrylamide Kit 10 %* or *12 %* gels, according to the manufacturer's instructions. Gel acrylamide percentage was selected depending on the molecular mass of the protein of interest. Sample concentrations were normalized in *Lysis Buffer* before identical volumes of sample were pipetted into the gel pockets. *Sample Buffer 4x* was completed with 25 % (v/v) 2-Mercaptoethanol and then added to each sample at a ratio of 1:4. All such prepared samples were incubated at 98 °C for 10 min in the *Thermal Shaker Thermomixer Comfort 1,5 ml*, placed on ice for 1-2 min, briefly centrifuged, and then loaded into the gel pockets. Gel electrophoresis was carried out at 100 V for 90 min.

SDS-PAGE-separated proteins were transferred ("blotted") from the SDS-PAGE gel to a *PVDF Transfer Membrane* that was previously equilibrated in 100 % methanol for 1 min. Therefore, using the *Western Mini Trans-Blot Module Set*, the blotting sandwich was assembled as instructed by the manufacturer and wet blotting was performed at 100 V for 60 min. Quality of the blot and total protein amount were documented using the *MemCode Reversible Protein Stain Kit* and *Gel Imaging System ChemiDoc Touch* according to the manufacturers' instructions. The obtained images were used as references for normalization during analysis. The MemCode stain was removed according to the manufacturer's instruction and the membrane was washed in *TBS-T 1x*.

For detection of specific protein bands, the membrane was initially blocked in *Blocking Solution 5 %* for 60 min at room temperature (RT), 40 rpm, and a 5° tilt angle, to prevent unspecific binding of antibodies. Next, the membrane was incubated in 1° antibody diluted in *Blocking Solution 5 %*, rolling over night at 4 °C. Then, the membrane was washed in *TBS-T 1x* for 6 x 10 min at RT and 200 rpm, and finally incubated with 2° antibody diluted in *Blocking Solution 5 %*, for 60 min at RT, 40 rpm, and a 5° tilt angle. Another wash with *TBS-T 1x* for 6 x 5 min at RT and 200 rpm was performed. Lastly, the *Western ECL Substrate Clarity Max* was applied to the membrane and images were taken, again, using the *Gel Imaging System ChemiDoc Touch*.

For investigation of further targets, blots were stripped using the *Western Blot Stripping Buffer Restore Plus* to rid them of previous antibodies before incubation with the next.

Analysis was undertaken using the *Image Lab Version 6.1* software.

2.2.5.3 Analysis of Enriched Membrane Proteins

To investigate the expression of membrane receptors DRD1 and DRD2 in iBAT and iWAT, Western blots and liquid chromatography-tandem mass spectrometry (LC-MS/MS) analyses were performed during a research stay with the group of Prof. Dr. Gert Lubec at the University of Vienna (Group of Functional Proteomics, Department of Pharmaceutical Chemistry). All experiments were supervised and instructed by Dr. Fernando Sialana.

2.2.5.3.1 Subcellular Fractionation for Protein Enrichment

Initially, subcellular fractionation was performed to enrich membrane proteins as described by (Sialana *et al*., 2016).
Therefore, samples were homogenized in *Vienna Western Lysis Buffer for Subfractions* (~100 µl/10 mg tissue) and centrifuged in two steps. First, at 1200x *g* and 4 °C for 10 min, yielding a pellet (P1) containing the enriched nuclear fraction. The supernatant was transferred to a fresh 1,5 ml tube and centrifuged at 15000x *g* and 4 °C for 30 min, yielding a second pellet (P2), containing the enriched membrane fraction, and supernatant (SN), containing the enriched cytosolic fraction.

The P2 pellets, containing the enriched membrane fractions, were further processed depending on the analysis to follow.
In preparation for Western blot analyses, the P2 pellets were resuspended in 30-60 µl *Vienna Western SDS Buffer for Subfractions*, for faint and strong pellets, respectively and stored at -80 °C until determination of protein concentration.
In preparation for LC-MS/MS analyses, the P2 pellets were resuspended by vigorous mixing in 30 - 50 µl *Vienna Proteomics Protein Solubilization Buffer* for faint and strong pellets, respectively; then briefly centrifuged to collect all liquid in the cone tip of the tube; incubated at 750 rpm and RT for 1 h; and stored at 4 °C overnight until determination of protein concentration.
Protein concentration for all samples was measured using the *Protein Assay Kit, Pierce BCA*.

The SNs, containing the cytosolic fractions, were further processed depending on the analysis to follow.

For Western blot analysis, 20 % (v/v) SDS were added per sample, yielding a final concentration of 2 % SDS. Samples were then each transferred to a *Filter Column 3K Pierce Protein Concentrator* and centrifuged at 14000x *g* and RT for 10 min. The permeate was discarded, while the retentate was recollected by inserting the column upside down into a fresh 1,5 ml tube and spinning it for 2 min at 1000x *g*. These samples were also stored at -80 °C for potential further processing.

For LC-MS/MS analysis, 10 % (v/v) SDS were added to each sample to reach a final concentration of 2 % (v/v) SDS. Then, ice cold acetone (>99 %) was added very slowly (to prevent precipitation of proteins together with debris) in a 1:5 v/v ratio, mixed vigorously, and stored at -80 °C for 1 hr. Next, samples were centrifuged at 15000x *g* and 4 °C for 10 min. The supernatant was discarded and the same volume of ice-cold acetone was added again, repeating the previously described steps. Pellets were dissolved in 30-50 µl *Vienna Proteomics Protein Solubilization Buffer*, shaken at 750 rpm and RT for 1 hr, and stored at 4 °C until further processing.

2.2.5.3.2 Western Blot Analysis of Enriched Membrane Proteins

Western blot analysis of enriched membrane proteins followed the same principle as described for total protein (2.2.5.2), with some methodological alterations due to the established procedures for this method in the hosting laboratory at the University of Vienna.

Samples were normalized in *Vienna Western SDS Buffer for Subfractions*. *Sample Buffer 4x Laemmli* was completed with 10 % (v/v) 2-Mercaptoethanol and added to samples at a ratio of 1:4.

Samples of the enriched membrane fraction were incubated in the *Thermal Shaker Thermomixer Comfort 1,5 ml* at 37 °C and 300 rpm for 30 min. Incubation at 37 °C (as opposed to 98 °C for total protein samples) was crucial to ensure the integrity of highly glycosylated dopamine receptors in the enriched membrane fractions and therefore adequate migration in the SDS-PAGE gel. Samples were then loaded into the SDS-PAGE gel pockets. Gel electrophoreses was performed in three steps, at 50 V for 30 min, 100 V for 30 min and 150 V for 60 min, for the same reason.

Meanwhile, the *PVDF Transfer Membrane* was equilibrated for about 1 min with 100 % Methanol. Subsequently, blotting was performed using the *Western Semi-Dry Transfer Cell Trans-Blot SD* according to the manufacturer's instructions at 15 V for 70 min. Incubation with antibodies was executed as aforementioned (2.2.5.2). The *Western ECL*

Substrate Clarity was used to initiate the chemiluminescent reaction before imaging. For investigation of further targets on the same membrane, blots were stripped using the *Vienna Western Mild Stripping Buffer* to rid them of previous antibodies before incubation with the next. Analysis was performed in *Image Lab Version 6.1*.

2.2.5.3.3 LC-MS/MS Sample Preparation

Enriched membrane protein samples (2.2.5.3.1) were processed further to prepare them for LC-MS/MS analysis. The procedure has been described previously by (Sialana et al., 2016).

First, proteolytic digestion of proteins was carried out in a filter-aided sample preparation (FASP) procedure (Wiśniewski *et al*., 2009).
Therefore, samples were initially cleaned and concentrated using a *Filter Column 10K Vivacon 500 Protein Concentrator*. The filter was loaded with 200 µl of *Vienna Proteomics Sample Cleaning Buffer* and centrifuged at 12000x *g* and 20 °C for 15 min. The flow-through was discarded. Then, 50-70 µg of protein sample were loaded onto the column (min 30 µl, max 50 µl), 200 µl of *Vienna Proteomics Sample Cleaning Buffer* were added and samples were centrifuged at 12000x *g* and 20 °C for 15 min. The flow-through was discarded. Another wash with 200 µl *Vienna Proteomics Sample Cleaning Buffer* at 12000x *g* and 20 °C for 15 min was carried out and the flow-through was discarded.
Next, samples were alkylated by applying 100 µl of 50 mM Indoacetamide (IAA) (final concentration in *Vienna Proteomics Sample Cleaning Buffer*) to the column, shaking at RT for 1 min, incubating at RT for 30 min in the dark without shaking, and centrifuging at 12000x *g* and 20 °C for 10 min.
Then, samples were washed again three times with 100 µl of *Vienna Proteomics Sample Cleaning Buffer* at 12000x *g* and 20 °C for 15 min. Followed by washing three times with 100 µl of 50 mM TEAB at 12000x *g* and 20 °C for 10 min.
Lastly, samples were proteolytically digested using trypsin. Therefore, filter columns were placed into fresh collection tubes and 20 µl of 50 mM TEAB were added to each column to prevent the filter from drying out. From a trypsin stock solution (0,5 µg/µl trypsin in 1 mM HCl), a trypsin working solution was prepared for an enzyme to protein ratio of 1:100. The according volume of trypsin stock was added to 50 mM TEAB (pH 8,5) to make up a total volume of 40 µl (e.g., for 50 µg protein = 1 µl of 0,5 µg/µl trypsin stock + 39 µl of 50mM TEAB). To each sample, the correctly prepared trypsin working solution was

added and tubes were sealed with parafilm. Samples were incubated on a shaker at 37 °C for 1-2 hr, followed by overnight (~18 hr) incubation at 37 °C without shaking. Peptides were collected by centrifuging the columns at 12000x *g* and 20 °C for 20 min, then adding 70 µl of 50 mM TEAB and centrifuging at 12000x *g* and 20 °C for 10 min, and lastly adding 70 µl of 0,5 M NaCl and centrifuging at 12000x *g* and 20 °C for 10 min. The peptide-containing flow-through was stored in 2 ml brown vials at -20 °C.

All digests were desalted and concentrated by solid phase extraction (SPE) using *MicroSpin Columns 5-60 µg*.
Therefore, samples were first acidified by adding 5 µl of 30 % trifluoroacetic acid (TFA) to every 150 µl of sample in brown glass vials. From there, titration with 30 % TFA was performed in 5 µl steps until pH 3 was reached for each sample. pH levels were continuously tested by applying 1-2 µl of sample to *pH-Indicator Strips MColorpHast*. Additionally, CO_2 bubbles were observed inside the brown glass vials to monitor neutralization of residual TEAB buffer. *MicroSpin Columns 5-60 µg* were labelled, placed into 2 ml tubes, and activated by washing three times with 200 µl acetonitrile (ACN) at 110x *g* and RT for 30 s. The flow-through was discarded and the columns equilibrated twice with 100 µl 2 % (v/v) ACN in 0,1 % (v/v) TFA at 110x *g* and RT for 1 min. The flow-through was discarded. Then, the acidified sample was loaded onto the column (max. 300 µl at once) and centrifuged at 110x *g* and RT for 1-3 min (depending on loading volume). Next, samples were washed with 100 µl 0,1 % TFA and centrifuged at 110x *g* and RT for 1-3 min. The flow-through was discarded and columns put into fresh collection tubes. Lastly, elution was performed with 52,5 µl of 70 % ACN in 0,1 % formic acid (FA) at 110x *g* and RT for 1-3 min and solvent was evaporated down to 0-2 µl remainder in a *Centrifuge Vacuum Concentrator Plus* at 45 °C (~50-100 min). Lyophilized peptides were stored at 4 °C.
Once needed, lyophilized samples were reconstituted in 2% ACN in 0,1% TFA, sonicated for 10-15 min, and peptide concentrations were determined using the *Peptide Assay Kit, Pierce Fluorometric*, according to the manufacturer's instructions.
In preparation for lable-free quantification (LFQ), samples were normalized to a final peptide concentration of 0,2 µg/µl, using 2 % ACN in 0,1 % TFA (5 µg in 25 µl). Additionally, the remainder of each sample was separated into eight subfractions using the *Peptide Fractionation, Pierce High pH Reversed-Phase* kit to increase the dynamic range of protein identifications. Normalized samples were stored at -20 °C until further

use. Approximately 1µg of peptides of each sample was analyzed by LC-MS/MS with two technical replicates.

2.2.5.3.4 LC-MS/MS Analysis of Enriched Membrane Proteins

This method and the following method were carried out by Dr. Fernando Sialana, who kindly contributed the following paragraphs (2.2.5.3.4 - 2.2.5.3.5).

Peptide analyses were performed using a single-shot LC-MS approach with a 4-h gradient using a *LCMS UltiMate 3000 RLSCnano HPLC System* coupled to a *LCMS Q Exactive Plus Hybrid Quadrupol-Orbitrap* mass spectrometer, with LC-MS parameters as described previously (Stojanovic *et al*., 2017).
Samples were injected onto a *LCMS UltiMate 3000 RLSCnano HPLC System* coupled to a *LCMS Q Exactive Plus Hybrid Quadrupol-Orbitrap* mass spectrometer. For data acquisition and operation of the *LCMS Q Exactive Plus Hybrid Quadrupol-Orbitrap* mass spectrometer, the *Tune 2.8.1.2806* and *Xcalibur 4* software were used. HPLC solvents were as follows: solvent A consisted of 0,1 % FA in water and solvent B consisted of 0,1 % FA in 80 % ACN.
From a thermostated autosampler, 10 µl of each sample, which corresponds to 1 µg of peptide mixture, were automatically loaded onto an *LCMS PepMap C18 HPLC Trap Column 3 µm* with a binary pump at a flow rate of 5 µl/min using 2 % ACN in 0.1 % TFA for loading and washing the pre-column. After washing, the peptides were eluted by forward-flushing onto a 50 cm analytical *LCMS PepMap C18 HPLC Trap Column 2 µm* with an inner diameter of 75 µm. Peptides were eluted from the analytical column with a 220 min gradient ranging from 5 to 24 % solvent B, followed by a 20 min gradient from 24 to 38 % solvent B and finally, to 90 % solvent B for 5 min before re-equilibration to 5 % solvent B at a constant flow rate of 300 nl/min.
The *LTQ Velos ESI Positive Ion Calibration Solution, Pierce* was used to externally calibrate the instrument prior to sample analysis and an internal calibration was performed on the polysiloxane ion signal at m/z 445.120024 from ambient air (Olsen *et al*., 2005).

MS^1 scans were performed from m/z 400-2000 at a resolution of 70000. Using a data-dependent acquisition mode, the 20 most intense precursor ions of all precursor ions with +2 to +7 charge were isolated within a 1.6 m/z window and fragmented to obtain the corresponding MS/MS spectra. The fragment ions were generated in a higher-energy

collisional dissociation (HCD) cell at 27 % normalized collision energy and detected in an Orbitrap mass analyzer at a resolution of 17500. The dynamic exclusion for the selected ions was 40 s. Maximal ion accumulation time allowed in MS^1 and MS^2 mode was 30 and 50 ms, respectively. Automatic gain control was used to prevent overfilling of the ion trap and was set to 1×10^6 ions and 5×10^4 ions for a full Fourier transform MS^1 and MS^2 scan, respectively.

2.2.5.3.5 LC-MS/MS Protein Identification and Label-Free Quantification

Protein identification and label-free quantification was performed as previously described by Stojanovic *et al*., 2017. Intensities were normalized, missing values imputed, and the data log-transformed. Two sided t-test was performed and FDR determined using Benjamini-Hochberg. Significance was set at $P < 0.01$ and ratio iBAT/iWAT = 8 (log2=3).

2.2.5.4 Glycogen Assay

To determine the glycogen content in liver, 10-20 mg of liver samples were weighed into 2 ml tubes with screw caps, prefilled with *Ceramic Beads Precellys 1,4 mm*, and homogenized in 1 ml of 5 % Trichloracetic Acid (TCA). The homogenate was transferred to a 1,5 ml tube and incubated at RT for 30 min before it was centrifuged at 16000x *g* and RT for 10 min to precipitate proteins. From each individual sample, 3 x 50 µl of supernatant were transferred to fresh 1,5 ml tubes. Glycogen was precipitated by adding 100 µl ethanol per sample, incubating over night at 4 °C, and centrifuging at 16000x *g* for 30 min. The supernatant was discarded, and the pellet dried at RT in the fume hood. Detection of glycogen was brought about by resuspending each pellet in 80 µl of *Lugol Reaction Mix* through vigorous shaking and incubation at RT for 10 min. Samples were vigorously shaken again, before 75 µl of each sample were pipetted into wells of a *Microplate ELISA 96 Well, Skirted, Flat Base*. The optical density at 600 nm (OD_{600}) was measured in the *Absorption Microplate Reader SPECTROstar Nano* and normalized against tissue weight.

2.2.5.5 Lipase Activity Assay

Lipase activity – an indicator for the extent of lipolysis taking place in tissue samples, and therefore allowing an assumption of the amount of FFA being released from triglycerides through hydrolyzation – was determined in BAT and WAT using the *Lipase Activity Assay Kit, Colorimetric* according to the manufacturer's instructions. Kinetics were measured in

the *Absorption Microplate Reader SPECTROstar Nano*, with a protocol set up as instructed by the manufacturer. All samples were measured in duplicates.

2.2.5.6 Enzyme-Linked Immunosorbent Assay (ELISA)

ELISAs were performed to quantify proteins of interest in tissue samples. Namely, Leptin and cAMP content was assessed, using the *Leptin ELISA Kit 96 Well, Mouse* and *cAMP Direct Biotrak EIA*, respectively, according to the manufacturers' instructions. For cAMP analysis, the instructions for the "Non-Acetylation EIA Procedure" were followed. The *Microplate Washer Wellwash Versa 2x8* performed washing steps for both assays. Absorbance was measured in the *Absorption Microplate Reader SPECTROstar Nano.*

2.2.5.7 Immunohistochemistry (IHC)

IHC was performed to investigate whether treatment with any of the applied substances caused histological changes in iBAT, iWAT, liver and brain.
Therefore, samples were fixated in *Paraformaldehyde Solution 4 % in PBS* in 5 ml tubes at 4 °C for 24 - 48 h, transferred into *Tissue Processing/Embedding Casettes, Histosette*, washed in cold 1x DPBS (2 x 2 min), dehydrated in a row of ascending ethanol concentrations (50 %, 70 %, 95 %, 100 %, 3 x 20 min each) and xylene (3 x 10 min) – all at 4 °C on the *Shaker Orbital Titramax 100* – and subsequently infiltrated with and embedded in *Paraffin Wax, Shandon Histoplast* (3 x 1 h, 60 °C) using the *Tissue Embedding Base Mold, 15x15, Parafree*.
Paraffin sample blocks were cut into 5 µm thin sections at the *Microtome Rotary Electronic Microm HM340E* according to the manufacturer's instructions, using *Microtome Blades, Epredia MB35*. The sections were allowed to relax on the surface of 42 °C warm water before affixing them onto *Microscope Slides SuperFrost Plus*.
Hematoxylin and eosin (H&E) staining on these 5 µm thin histological sections of embedded tissue samples was achieved by first, dewaxing the specimen sections in xylene (2 x 15 min), hydrating them in an ethanol row (100 %, 2 x 5 min; 96 %, 5 min; 80 %, 5 min; 70 %, 10 min), and briefly washing them in de-ionized water (6 min). Then, nuclear staining was attained in a hematoxylin bath (4 min) followed by flowing tab water (15 min). Again, slides were briefly washed in de-ionized water (2 min). Next, non-nuclear staining was achieved in an eosin bath (2 min) and de-ionized water (10 s). Lastly, sections were dehydrated in a row of ascending ethanol concentrations (70 %, 2 x 10 s; 80 %, 15 s;

96 %, 20 s; 100 %, 2 x 30 s) and cleared in xylene (2x15 min). Specimens were mounted with *Mounting Medium Pertex* and covered with a glass cover slip.

2.2.6 Statistical Analyses

Data were gathered, normalized, and processed in *Microsoft Excel* and statistically analyzed in *Prism 6*. Statistical tests applied for each analysis are depicted alongside the figures displaying the results for each method.

3 RESULTS

The here presented study is designed to investigate the direct (i.e., peripheral) effects of DA on iBAT thermogenesis of C57BL/6NCrl mice *ex vivo* and *in vivo*. The results are presented in sections 3.1 and 3.2. In parts, this data has been published in (Raffaelli et al., 2020) before the completion of this thesis. Indications are given in figure subtitles where this is the case.

In addition to the outcome of the planned project work, the results led to further investigations regarding the question whether dopamine receptors truly exist in iBAT of mice. The effort to answer this question brought about a collaboration to conduct LC-MS/MS analyses, resulting in an extensive proteomics data set. In addition to the original aim, this data set lead to the identification of potential new markers for distinction between iBAT and iWAT depots and their respective state of thermogenic activity. The results are presented in section 3.3.

3.1 *Ex Vivo* Studies

This *ex vivo* approach was employed to confirm results generated in an *in vitro* model of brown adipocytes (Kohlie et al., 2017), while, at the same time, omitting the complex, centrally mediated effects of DA and its receptors (Sonne et al., 2023).

To determine immediate peripheral effects of the DRD1-agonist SKF-38393, DRD2-agonist Sumanirole, and DA on iBAT thermogenesis markers, iBAT explants from mice were cultured in 6-well plates and directly treated with various concentrations (10 nM - 500 nM) of each of these substances for 24 h. iBAT explant samples were subsequently analyzed for changes in gene expression and protein content.

3.1.1 Treatment of iBAT explants with the DRD1-agonist, DRD2-agonist, or DA did not affect Ucp1 mRNA expression

The *ex vivo* experimental approach was verified by employing the ADRB3-agonist CL316,243 as a positive control; which significantly increased mRNA expression of thermogenic markers *Ucp1* and *Dio2,* and expectedly decreased mRNA expression of *Adrb3* itself (Figure 3-1) (Bengtsson et al., 1996; Himms-Hagen et al., 1994; Klaus et al., 1995). However, neither the DRD1-agonist, DRD2-agonist, nor DA significantly increased mRNA expression of thermogenesis marker *Ucp1* (Figure 3-1 A, D, G).

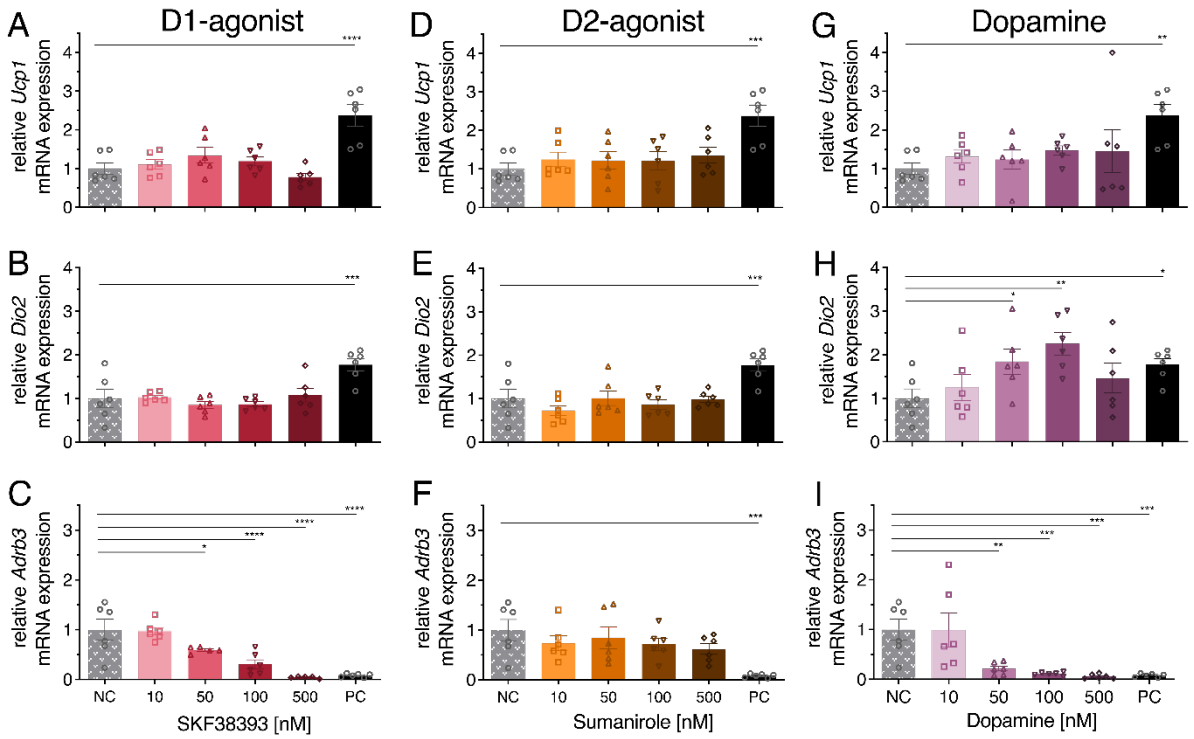

Figure 3-1: Dose-response study in iBAT explant tissue culture.

*mRNA expression of thermogenesis markers uncoupling protein 1 (Ucp1) (top), deiodinase 2 (Dio2) (middle), and adrenoreceptor β3 (Adrb3) (bottom), after direct treatment of iBAT tissue explants from C57BL/6NCrl mice with DRD1-agonist SKF-38393 (left), DRD2-agonist Sumanirole (middle), or DA (right) (each at 10, 50, 100, and 500 nM) for 24 h. NC: negative control (vehicle), PC: positive control (ADRB3-agonist CL316,243; 1 µM). Data are expressed as mean ± SEM and each compared to NC by 1 W ANOVA (uncorrected Fisher's LSD). **P < 0.01; ***P < 0.001; ****P < 0.0001; n = 6; cf. Raffaelli et al., 2020.*

3.1.2 Treatment of iBAT explants with DA increased Dio2 mRNA expression

Treatment with the DRD1-agonist or DRD2-agonist had no significant effect on mRNA expression of thermogenesis marker *Dio2*. However, DA itself significantly increased *Dio2* mRNA expression at concentrations 50 and 100 nM (Figure 3-1 B). Moreover, combined treatment of iBAT explants with DA (10 nM) and T3 (50 nM) increased *Dio2* mRNA expression significantly (P < 0,0001), while neither of these substances alone at these concentrations did. Given that *Dio2*-mediated conversion of thyroxin (T4) to T3 is essential for BAT thermogenesis activation (de Jesus et al., 2001), and *Dio2* mRNA expression is highly feedback-regulated by thyroid hormones (Bianco et al., 2002), this result serves as proof of principle for potential crosstalk between DA and T3 in the regulation of BAT thermogenesis, independently of dopamine receptors.

3.1.3 Treatment of iBAT explants with the DRD1-agonist and DA decreased Adrb3 mRNA expression

Down-regulation of *Adrb3* mRNA expression in iBAT explants treated with the ADRB3-agonist CL316,243 proved agonist-related receptor downregulation (Figure 3-1 C, F, I). Interestingly, the DRD1-agonist and DA also significantly decreased *Adrb3* mRNA expression (50, 100, and 500 nM) (Figure 3-1 C, I), while the DRD2-agonist did not decrease *Adrb3* mRNA expression at any of the tested concentrations (Figure 3-1 F).

In sum, the presented *ex vivo* study suggests no relevant immediate and direct effect of either agonist or DA on iBAT thermogenesis, thus, contrasting the aforementioned *in vitro* study in immortalized brown adipocytes that showed thermogenic effects of the DRD1-agonist and DA (Kohlie et al., 2017).

3.2 *In Vivo* Studies

Since the lack of effects *ex vivo* could be accounted to a lack of sympathetic signaling, peripheral effects of the DRD1-agonist, DRD2-agonist, and DA on iBAT thermogenesis and metabolic parameters were studied in three different approaches in mice *in vivo*.
Firstly, acute effects, one hour after a single i.p. injection, were investigated (3.2.1). Secondly, effects of daily i.p. injections for one week were analyzed (3.2.2). And lastly, effects of constant release of active substances through an i.p.-implanted osmotic minipump were examined over a period of one week (3.2.3).
Study design timelines for each approach are illustrated in the appendix (Figure 6-1).

3.2.1 Single Injection In Vivo Study (1 h)

3.2.1.1 Single i.p. injection of the DRD1-agonist, DRD2-agonist, or DA had no lasting effect on iBAT temperature within 1 h post treatment

IRT videography for the duration of 1 h after the injection of mice with the DRD1-agonist (10 mg/kg), DRD2-agonist (3,2 mg/kg), or DA (100 µg/kg), revealed no lasting effects on iBAT temperature (Figure 3-2). The DRD1-agonist only briefly increased iBAT temperature (min 36 to 45) (Figure 3-2 A), whereas the DRD2-agonist very briefly decreased iBAT temperature (min 16 to 20) (Figure 3-2 B). Injection with DA did not lead to significant changes compared with saline injection at any time point (Figure 3-2 C). The experimental approach was validated by injection of NE (1 mg/kg) in one animal as positive control.

Of note, IRT photos, taken 24 h after single injections, showed a significant increase in iBAT temperature (normalized to rectally measured core temperature) in DA-treated compared to saline-treated animals (Figure 6-2 C). This was not the case with DRD1- or DRD2-agonist-treatment, which suggests the possibility of indirect or off-target effects of DA despite its extremely short halflife (Sturgill et al., 2011).

3.2.1.2 Single i.p. injection of the DRD1-agonist or DRD2-agonist affected locomotor activity during 1 h post treatment

Most mice (5/6), injected with the DRD1-agonist, appeared to move more actively inside their individual cage during the 1 h post-injection period, compared to animals treated with saline, the DRD2-agonist, or DA. This observation was visualized retrospectively for qualitative comparison, by generating overlay images from the acquired IRT video sequences (1 image/sec for 7x10 min: 1x10 min baseline and 6x10 min post-injection; n=6). The overlay images for one of the six animals are shown in Figure 3-3, while those for the remaining five animals are presented in the appendix (Figure 6-3 - Figure 6-7).
While treatment with the DRD1-agonist appeared to cause an increase in locomotor activity compared to the saline control – especially in the second half of the hour, treatment with the DRD2-agonist was followed by a noticeable and distinct period of inactivity from min 11 to 20 (Figure 3-3) in all, and minutes 11 to 30, or even 11 to 40 in some of the six animals (Figure 6-3 - Figure 6-7), followed by increased activity thereafter. Contrarily, treatment with DA or saline control, had most animals (5/6) gradually calm down and become less active with the progression of the 1 h-experiment (Figure 3-3; Figure 6-3 - Figure 6-7).

3.2.1.3 Single i.p. injection of the DRD1-agonist or DA decreased tail root temperature within 1 h post treatment

IRT photos taken 1 h post-injection (after completion of the IRT video), revealed a significant decrease in tail root temperature (normalized to rectal core body temperature) in DRD1-agonist- and DA-treated animals (Figure 6-2 B), likely caused by the vasoconstrictive actions of the compounds (Vasse et al., 1990; Wiglusz & Jedrzejak, 2011). Meanwhile, treatment with the DRD2-agonist appeared to increase heat emittance from the tail during IRT videography, as visible in overlay images from three of the six animals Figure 6-3; Figure 6-5; Figure 6-6), but could not be quantified in IRT photos subsequently (Figure 6-2 B, D).

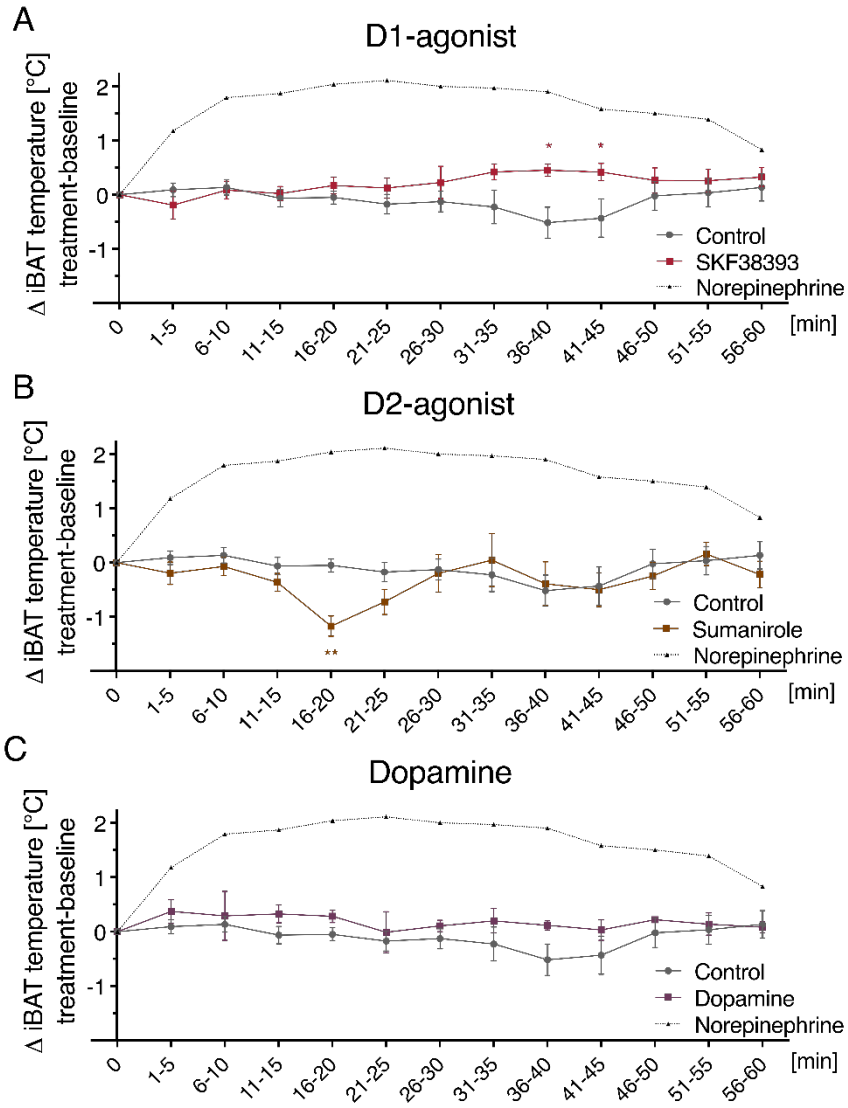

Figure 3-2: iBAT temperature after a single injection (1 h).

*iBAT temperature changes in C57BL/6NCrl mice, determined by infrared thermography (IRT) videography, during 1 h after injection of DRD1-agonist SKF-38393 (10 mg/kg) (A), DRD2-agonist Sumanirole (3,2 mg/kg) (B), or DA (100 µg/kg) (C). iBAT temperature in each 5 min timeslot was normalized to iBAT temperature during a 10 min baseline measurement. Injection with saline (0,9 %) served as negative control (Control) (n=6). Injection of one animal with norepinephrine (1 mg/kg) served as positive control (n=1). Data are presented as mean ±SEM. Groups were compared using 2 W RM ANOVA with Holm-Sidak's multiple comparison test. *P < 0.05; **P < 0.01; n = 6; cf. Raffaelli et al., 2020.*

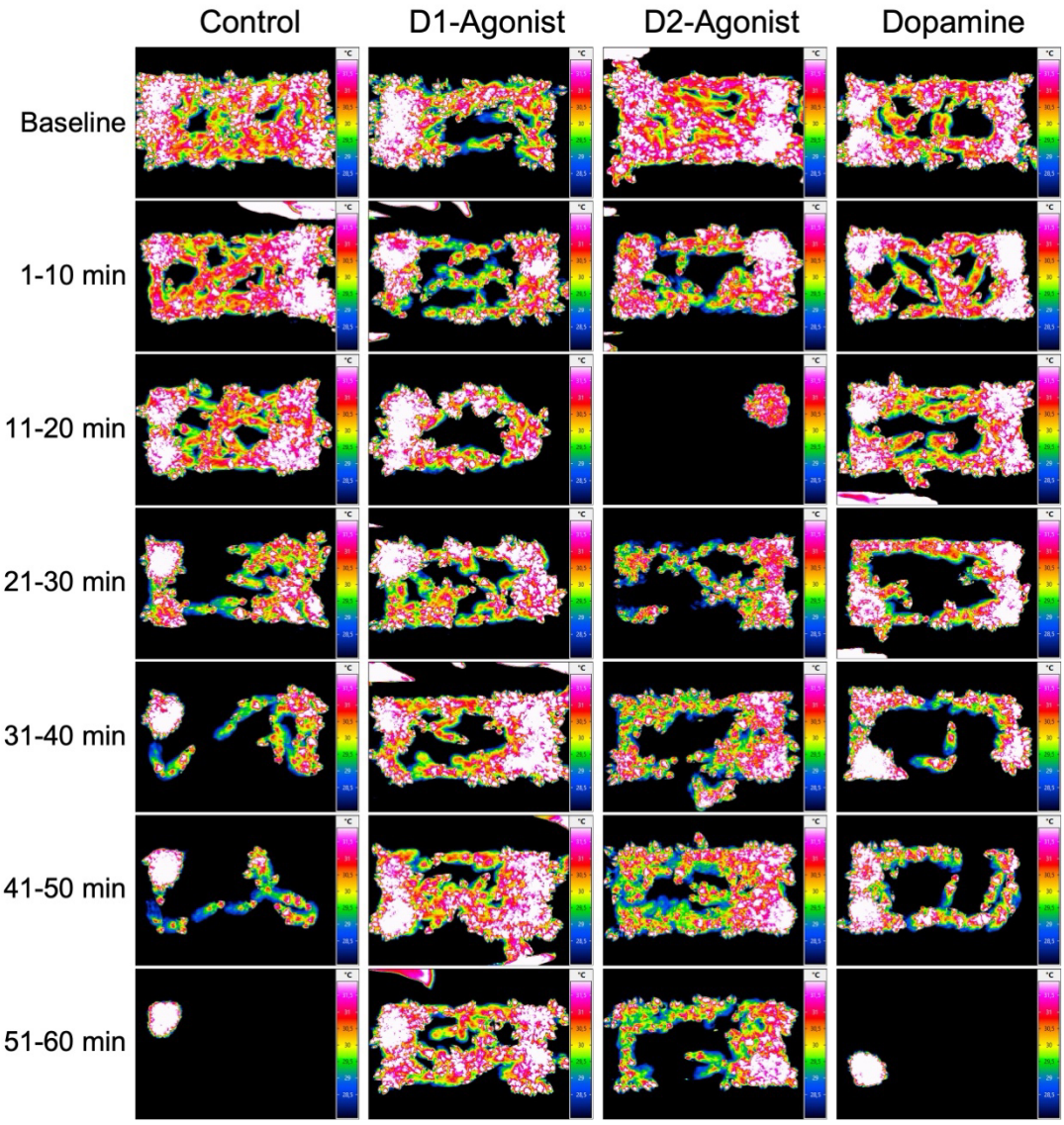

Figure 3-3: Overlay images of infrared thermography (IRT) videos after single injections in vivo. 1/6

Overlay images (10 min/image) of IRT videos (1 frame/s), taken within 1 h after a single injection of 0,9 % saline (control), DRD1-agonist SKF-38393 (10 mg/kg), DRD2-agonist Sumanirole (3,2 mg/kg), or DA (100 µg/kg) to illustrate locomotion of a single C57BL/6NCrl mouse inside its cage. Recovery time in-between treatments: three days. Animal 1/6. For animals 2-6, see appendix (Figure 6-3 - Figure 6-7). n=6

3.2.2 Repeated Injection In Vivo Study (1 week)

To test whether repeated administrations would reveal stronger effects, we treated mice with the DRD1-agonist or DRD2-agonist by daily i.p. injections, compared to respective saline groups. Due to its pronounced first pass effect (Sturgill et al., 2011), DA was not included in this study design.

3.2.2.1 Daily i.p. injections of the DRD1-agonist and DRD2-agonist for 1 week did not affect iBAT temperature

In concordance with results of the *ex vivo* and single injection *in vivo* studies (3.1 - 3.2.1), iBAT temperature did not sustainably change in mice receiving daily i.p. injections of the DRD1-agonist or DRD2-agonist for one week (Figure 3-4 D, E, I, J). Additionally, neither treatment had an effect on the assessed physiological parameters body weight (Figure 3-4 A, F), food intake (Figure 3-4 B, G), or core body temperature (Figure 3-4 C, H).
A significant increase in tail root temperature of DRD1-treated animals compared to the control group was seen, contrarily to the results of the single injection *in vivo* study; while the slight increase in DRD2-treated animals was in accordance with it (Figure 3-4 D, E, I, J).

3.2.2.2 Daily i.p. injections of the DRD1-agonist for 1 week decreased adipose depot weight and increased cAMP protein in iBAT

Analysis of adipose tissue homeostasis showed significantly decreased weight of all three collected adipose depots – iBAT, inguinal, and gonadal white adipose tissue (iWAT and gWAT) – after daily DRD1-agonist i.p. injections for one week (Figure 3-5 A). DRD1-treatment did not alter *Ucp1* mRNA expression or UCP1 protein in iBAT (Figure 3-5 B, C), or *Dio2* mRNA expression in any of the three analyzed adipose depots (Figure 3-5 D). Interestingly, DRD1-treatment significantly increased cAMP in iBAT (Figure 3-5 E), suggesting a $G_{\alpha s}$ protein-mediated molecular effect of the DRD1-agonist. Despite lipase activity in iWAT being unaltered by the DRD1-agonist (Figure 3-5 F), histological analyses showed smaller adipocytes in iWAT and a more pronounced multilocular appearance of adipocytes in iBAT (Figure 3-5 G). The DRD2-agonist had no effect on adipose tissue homeostasis, except for an increase in Ucp1 mRNA expression in iBAT that did reflect on protein level or iBAT temperature (Figure 3-5 I, J). Interestingly, leptin mRNA expression was increased in iBAT tissue of DRD1-agonist treated animals (Figure 6-8 A), while concentration of circulating leptin in serum was not affected (Figure 6-8 B).

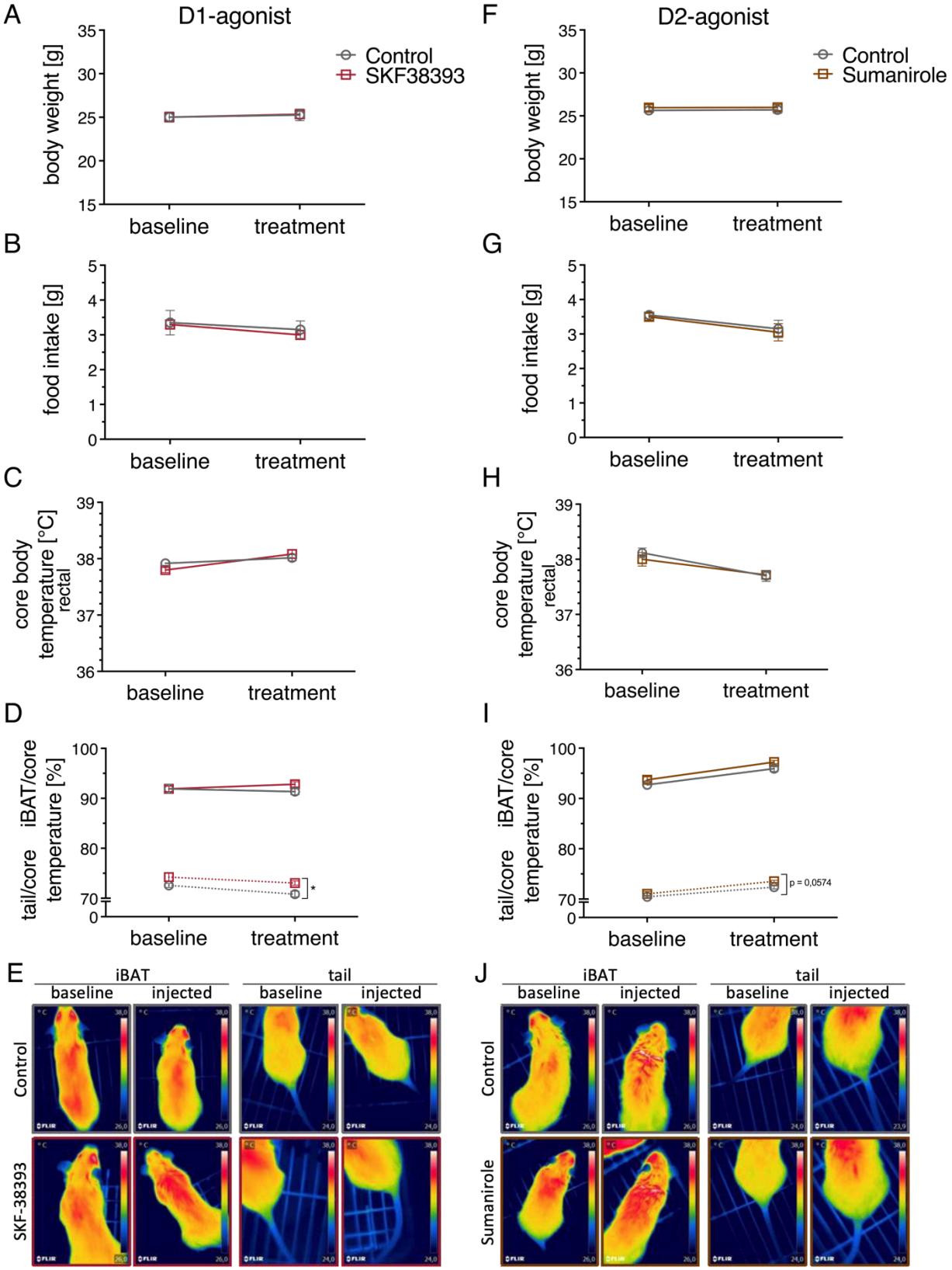

Figure 3-4: Physiological parameters during the repeated injections in vivo-study (1 week).

*Body weight (A, F), food intake (B, G), core temperature (C, H), iBAT and tail temperature (D, I), and representative infrared thermography (IRT) photos of mice treated with DRD1-agonist SKF-38393 (10 mg/kg) (left) or DRD2-agonist Sumanirole (3,2 mg/kg) (right) daily for 1 week via i.p. injections, and respective saline-injected (0,9 %) control groups. Data are presented as mean ± SEM. Groups were compared using 2WA with Bonferroni's multiple comparison test. *P < 0.05; n = 6; cf. Raffaelli et al., 2020.*

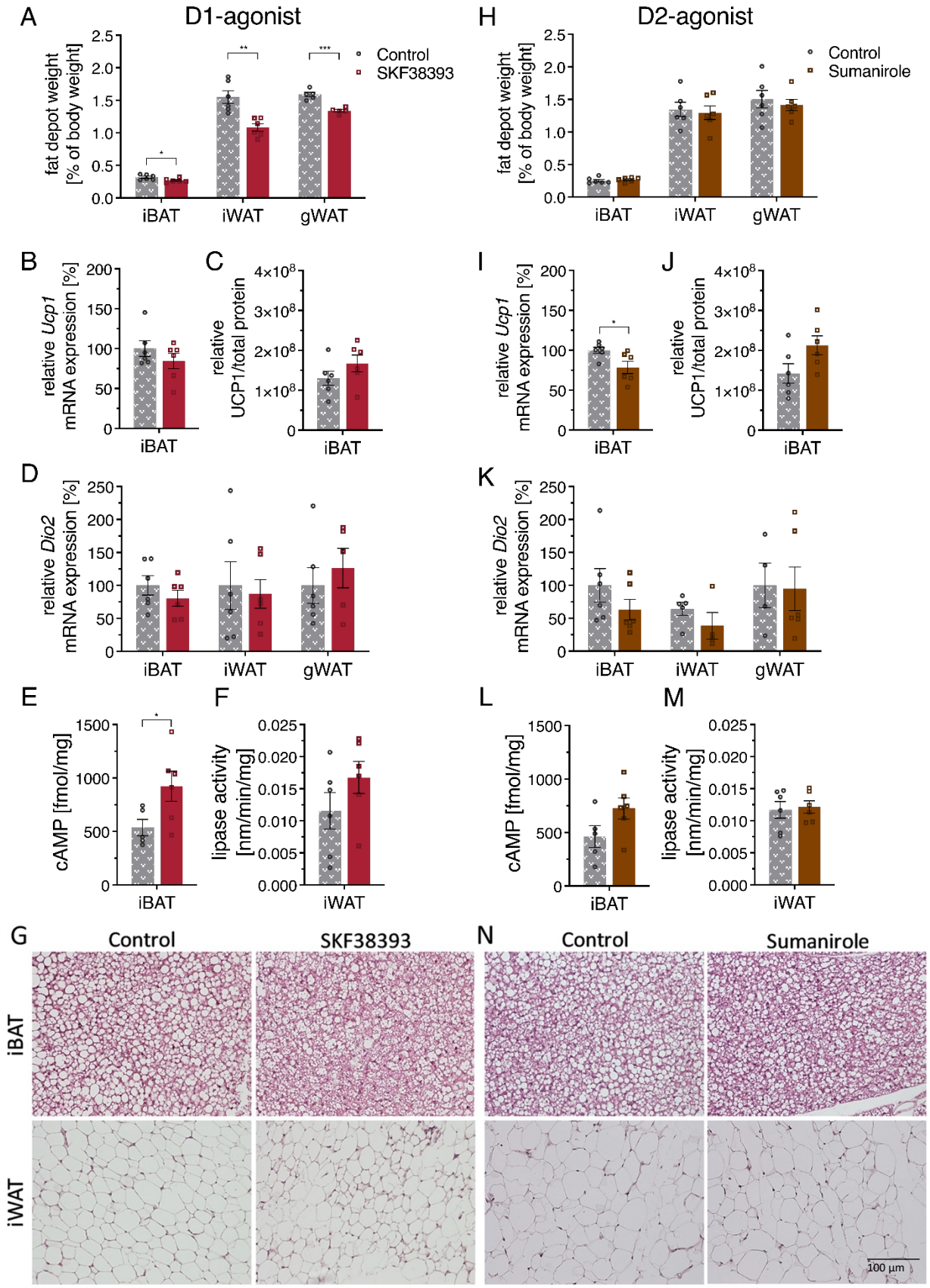

Figure 3-5: Adipose tissue analyses following repeated injections in vivo (1 week).

Fat depot weight of iBAT, iWAT, and gWAT (A, H), Ucp1 mRNA expression (B, I) and UCP1 protein (C, J) in iBAT, Dio2 mRNA expression in iBAT, iWAT, and gWAT (D, K), cAMP in iBAT (E, L), lipase activity in iWAT (F, M), and histological H&E images of iBAT and iWAT (G, N) of C57BL/6NCrl mice treated with DRD1-

*agonist SKF-38393 (10 mg/kg) (left) or DRD2-agonist Sumanirole (3,2 mg/kg) (right) daily for 1 week via i.p. injections, and respective saline-injected (0,9 %) control groups. Data are presented as mean ± SEM. Groups were compared using two-tailed t-tests. *P < 0,05; **P < 0,01; n = 6; cf. Raffaelli et al., 2020.*

3.2.2.3 *Daily i.p. injections of the DRD1-agonist or DRD2-agonist for 1 week had no significant effect on the abundance of protein complexes I-V in the oxidative phosphorylation (OXPHOS) cascade*

Additionally, oxidative capacity of iBAT collected from mice repeatedly treated with the DRD1-agonist or DRD2-agonist was analyzed. No major changes in the abundance of protein complexes I-V of the oxidative phosphorylation cascade could be detected.

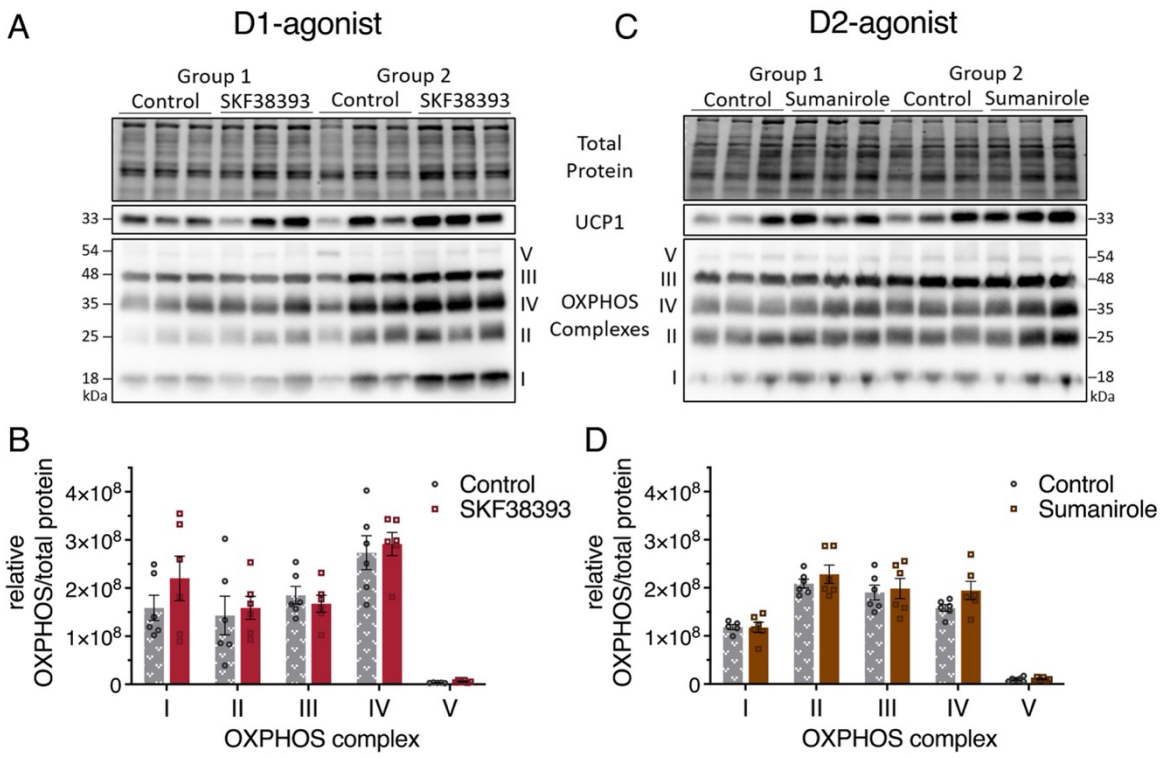

Figure 3-6: OXPHOS and UCP1 protein in iBAT following repeated injections in vivo (1 week).

Western blot images (A, C) and semi-quantitative analysis (B, D) of protein complexes I-V in the oxidative phosphorylation (OXPHOS) cascade in iBAT of C57BL/6NCrl mice treated with DRD1-agonist SKF-38393 (10 mg/kg) (left) or DRD2-agonist Sumanirole (3,2 mg/kg) (right) daily for 1 week via i.p. injections, and respective saline-injected (0,9 %) control groups. Furthermore, UCP1 Western blot images (A, C) of which semi-quantitative analysis is displayed in Figure 3-5. Data in B and D are presented as mean ± SEM. Groups were compared using two-tailed t-tests; n=6; cf. Raffaelli et al., 2020.

3.2.2.4 *Daily i.p. injections of the DRD1-agonist for 1 week decreased hepatic glycogen and increased mRNA expression of hepatic energy homeostasis marker Pyrk*

In addition to metabolic analyses in adipose tissue depots, markers for energy homeostasis were studied in liver samples of animals repeatedly treated with the DRD1-agonist or DRD2-agonist for one week.

Treatment with the DRD1-agonist caused a significant decrease in hepatic glycogen content (Figure 3-7 A), as well as a significant increase in pyruvate kinase (*Pyrk*) mRNA expression (Figure 3-7 B). Both markers suggest an increase in energy expenditure compared to the saline control group, which is in concordance with decreased weight of adipose tissue depots while food intake did not change.

Treatment with the DRD2-agonist had no significant effect on any of the analyzed hepatic parameters.

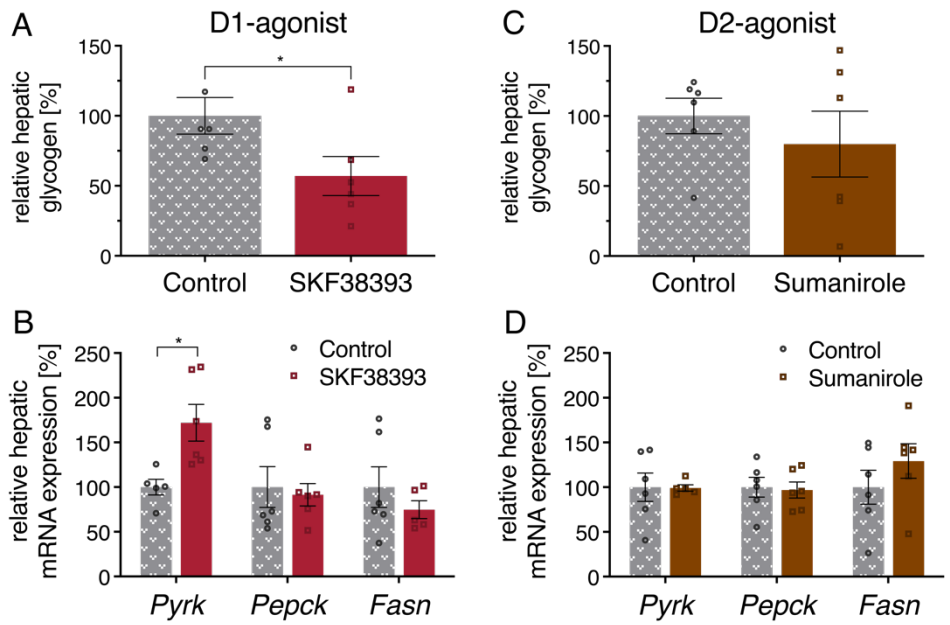

Figure 3-7: Hepatic analyses following repeated injections in vivo (1 week).

*Relative hepatic glycogen content (A, C) and mRNA expression of metabolic markers pyruvate kinase (Pyrk), phosphoenolpyruvate carboxykinase 1 (Pepck), and fatty acid synthase (Fasn) (B, D) in liver of C57BL/6NCrl mice treated with DRD1-agonist SKF-38393 (10 mg/kg) (left) or DRD2-agonist Sumanirole (3,2 mg/kg) (right) daily for 1 week via i.p. injections, and respective saline-injected (0,9 %) control groups. Data are presented as mean ± SEM. Groups were compared using two-tailed t-tests. *P < 0,05; n = 6; cf. Raffaelli et al., 2020.*

3.2.2.5 *Daily i.p. injections of the DRD1-agonist or DRD2-agonist for 1 week had no significant effect on further vital parameters and organ weights*

Given the prominent role of DA signaling in cardiovascular function, we recorded blood pressure and heart weight in the animals. Interestingly, neither was affected by repetitive treatment of mice with the DRD1-agonist or DRD2-agonist for one week (Figure 3-8 A, B, D, E).

Furthermore, neither liver nor kidney weights were significantly altered (Figure 3-8 B, E). Likewise, weight of various collected muscles was indifferent between saline control- and DRD1-agonist- or DRD2-agonist-treated groups (Figure 3-8 C, F).

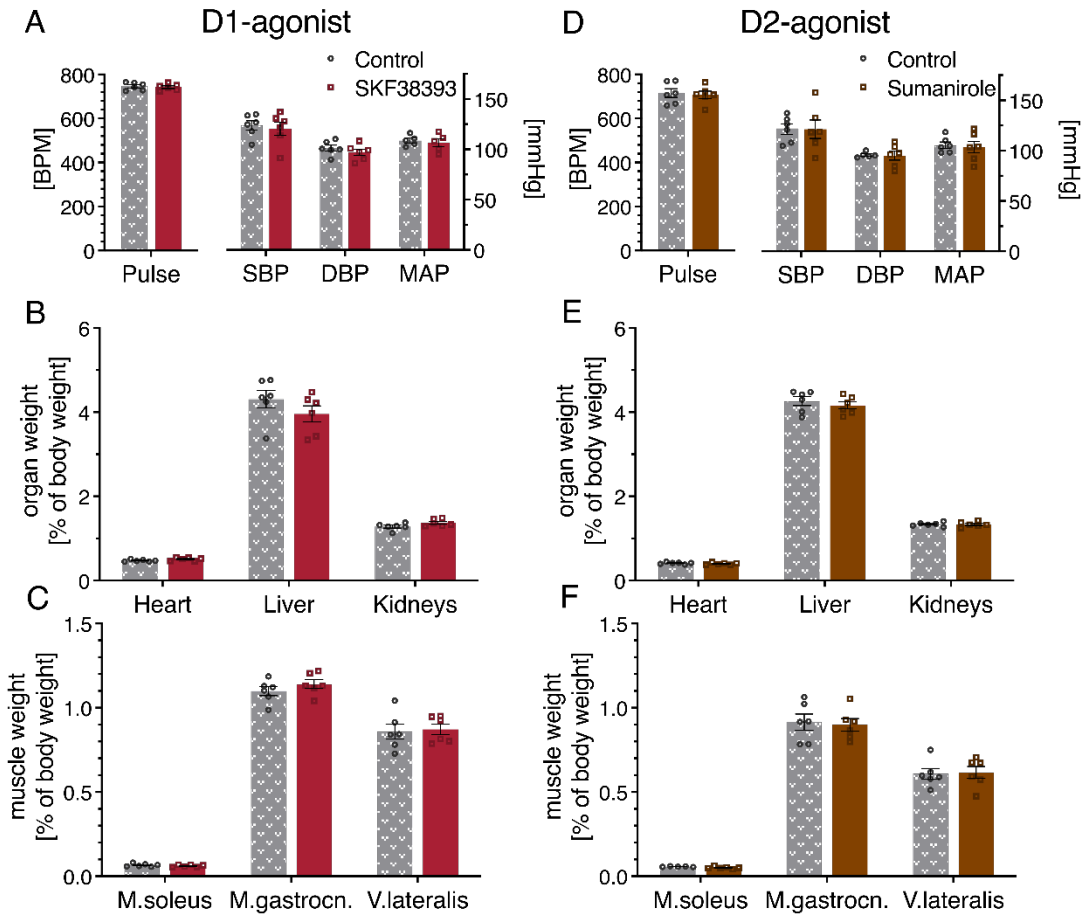

Figure 3-8: Vital parameters and organ weight analyses following repeated injections in vivo (1 week).

Pulse, systolic blood pressure (SBP), diastolic blood pressure (DBP), and mean arterial pressure (MAP) (A, D), weight of heart, liver and kidneys (B, E), and weight of musculus soleus, musculus gastrocnemius and vastus lateralis (C, F) in C57BL/6NCrl mice treated with DRD1-agonist SKF-38393 (10 mg/kg) (left) or DRD2-agonist Sumanirole (3,2 mg/kg) (right) daily for 1 week via i.p. injections, and respective saline-injected (0,9 %) control groups. Data are presented as mean ± SEM. Groups were compared using two-tailed t-tests. n = 6; cf. Raffaelli et al., 2020

3.2.2.6 *Daily i.p. injections of the DRD1-agonist or DRD2-agonist for 1 week did not affect markers of alternative thermogenesis activation or dopamine clearance in iBAT*

As UCP1-independent thermogenesis has been reported previously (Ikeda et al., 2017), markers of alternative BAT thermogenesis activation and dopamine metabolism were analyzed in iBAT to determine potential modes of action that led to the observed changes in iBAT weight, histology, and cAMP protein under DRD1-agonist treatment.

Neither the DRD1-agonist nor the DRD2-agonist had significant effects on mRNA expression of alternative thermogenesis activation markers or SERCA2 protein (Figure 3-9 A, B, D, E). Moreover, neither treatment had a significant effect on relative protein abundance of dopamine metabolism markers, namely dopamine transporter (DAT) (dopamine recycling) and monoamine oxidase A (MAO-A) (dopamine degradation) in iBAT (Figure 3-9) (Graves et al., 2020).

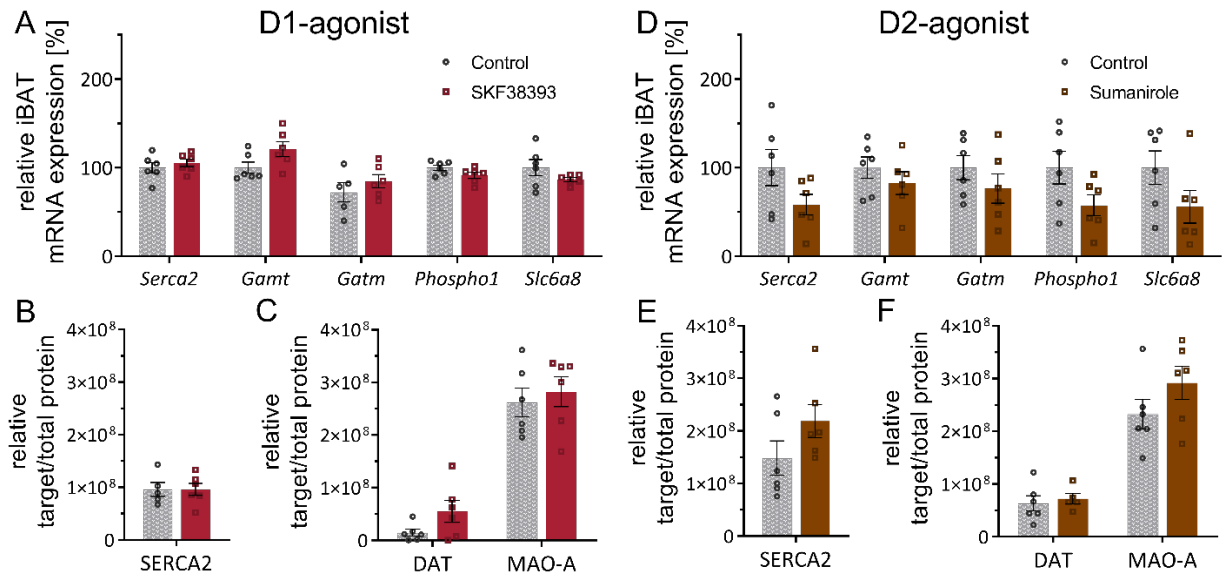

Figure 3-9: Alternative thermogenesis activation and dopamine metabolism markers in iBAT following repeated injections in vivo (1 week).

mRNA expression of alternative (Ucp1-independent) thermogenesis activation marker genes (A, D), relative abundance of alternative thermogenesis activation marker protein SERCA2 (B, E), and dopamine clearance-associated proteins DAT and MAO-A (C, F) in iBAT of C57BL/6NCrl mice treated with DRD1-agonist SKF-38393 (10 mg/kg) (left) or DRD2-agonist Sumanirole (3,2 mg/kg) (right) daily for 1 week via i.p. injections, and respective saline-injected (0,9 %) control groups. Data are presented as mean ± SEM. Groups were compared using two-tailed t-tests. n = 6; cf. Raffaelli et al., 2020

3.2.3 Constant Release In Vivo Study (1 week)

To assess the effects of prolonged application of DA, despite its pronounced first-pass effect and short half-life, i.p.-implanted osmotic minipumps were used to achieve a constant release-treatment for the duration of one week. In this study, the DRD1-agonist and DA were investigated and compared to a common saline control group. The DRD2-agonist was not employed in this study, since it showed little to no effect in previous experiments (3.1; 3.2.1; 3.2.2), with respect to iBAT thermogenesis activation.

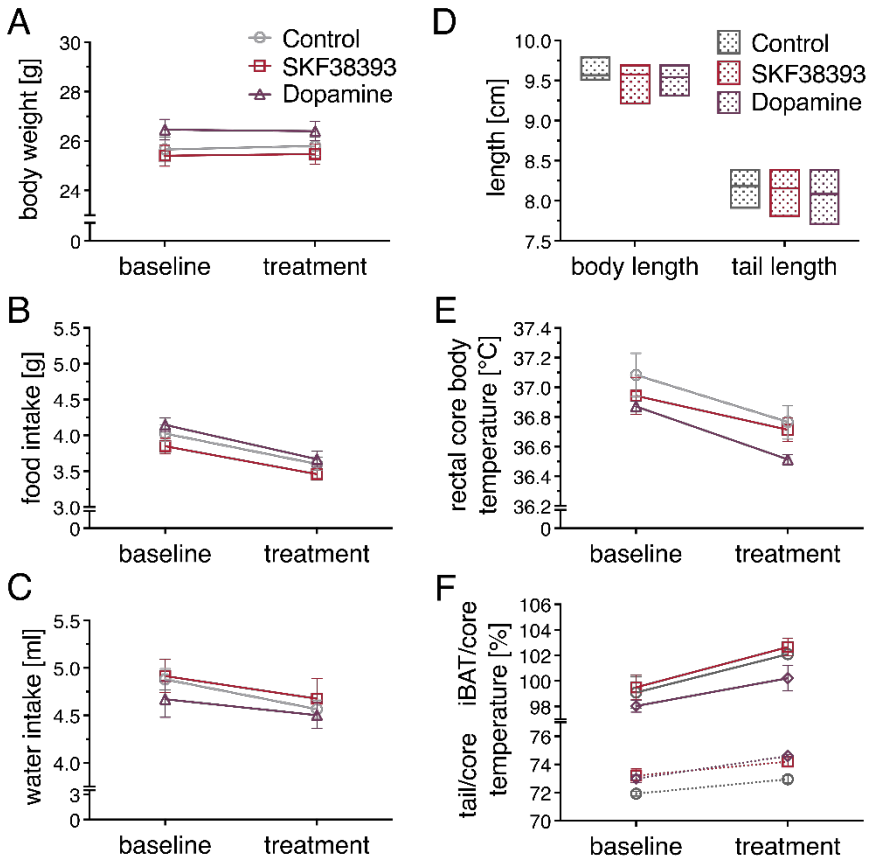

Figure 3-10: Physiological parameters during constant release in vivo (1 week).

Body weight (A), food intake (B), water intake (C), body and tail length (D), core body temperature (E), iBAT and tail temperature (F) of C57BL/6NCrl mice treated with DRD1-agonist SKF-38393 (10 µg/kg/min) or DA (7 µg/kg/min) for 1 week via i.p.-implanted osmotic minipumps, and a respective saline-filled minipump (0,9 %)-control group. Data are presented as mean ±SEM. Groups were compared using 2WA with Bonferroni's multiple comparison test. n = 6.

3.2.3.1 Constant release of the DRD1-agonist or DA did not affect physiological parameters over the course of 1 week

The physiological parameters documented in this experimental setting – body weight, body length, tail length, core body temperature, food intake, and water intake – were not affected by constant release of the DRD1-agonist or DA over the course of one week. Neither parameter showed a significant difference between the treated and control groups (Figure 3-10 A-E). Interestingly, iBAT and tail root temperature were not affected by either treatment when determined by IRT photography on d5 and d7 during the week of constant release-treatment (Figure 3-10; Figure 6-1). However, when iBAT temperature was determined by IRT videography on d3 of the treatment week, a significant increase in iBAT temperature in the DRD1-agonist-treated group was detected (Figure 6-9). DA treatment did not affect iBAT temperature by either means of IRT recording.

3.2.3.2 Constant release of the DRD1-agonist or DA did not affect iBAT thermogenesis marker mRNA expression or adipose tissue weights

The collected adipose depots were analyzed for potential changes in iBAT thermogenesis mRNA expression markers and adipose tissue weights. No effect of either treatment was observed (Figure 3-11 A, B, C), supporting the findings of the physiological parameter analysis in 3.2.3.1, and suggesting that neither the DRD1-agonist nor DA have a lasting peripheral effect on iBAT thermogenesis in this experimental framework.
Additionally, no difference between histological samples of iBAT and iWAT of DRD1- or DA-treated animals and saline controls was observed (Figure 3-11 D), further supporting the previous findings.

3.2.3.3 Constant release of the DRD1-agonist or DA increased mRNA expression of hepatic energy homeostasis marker Fasn

Investigation of effects of DRD1- and DA-treatment on non-adipose tissue consisted of vital parameter analysis, organ weight determination of muscle, heart, liver, and kidney, as well as metabolic marker mRNA expression analysis in liver.
Cardiovascular parameters (Pulse, SBP, DBP, MAP), measured on d4 and d6 during the constant release experiment (Figure 6-1), were not affected by either treatment (Figure 3-11 E). Also, muscle and organ weights did not differ between each treatment and their

saline control groups (Figure 3-11 F, G). However, both treatments led to a significant increase in mRNA expression of fatty acid synthase (*Fasn*) in liver (Figure 3-11 H).
Taken together, no significant DRD1- or DRD2-mediated effects were observed on iBAT thermogenesis in mice, by peripheral treatment with respective agonists.

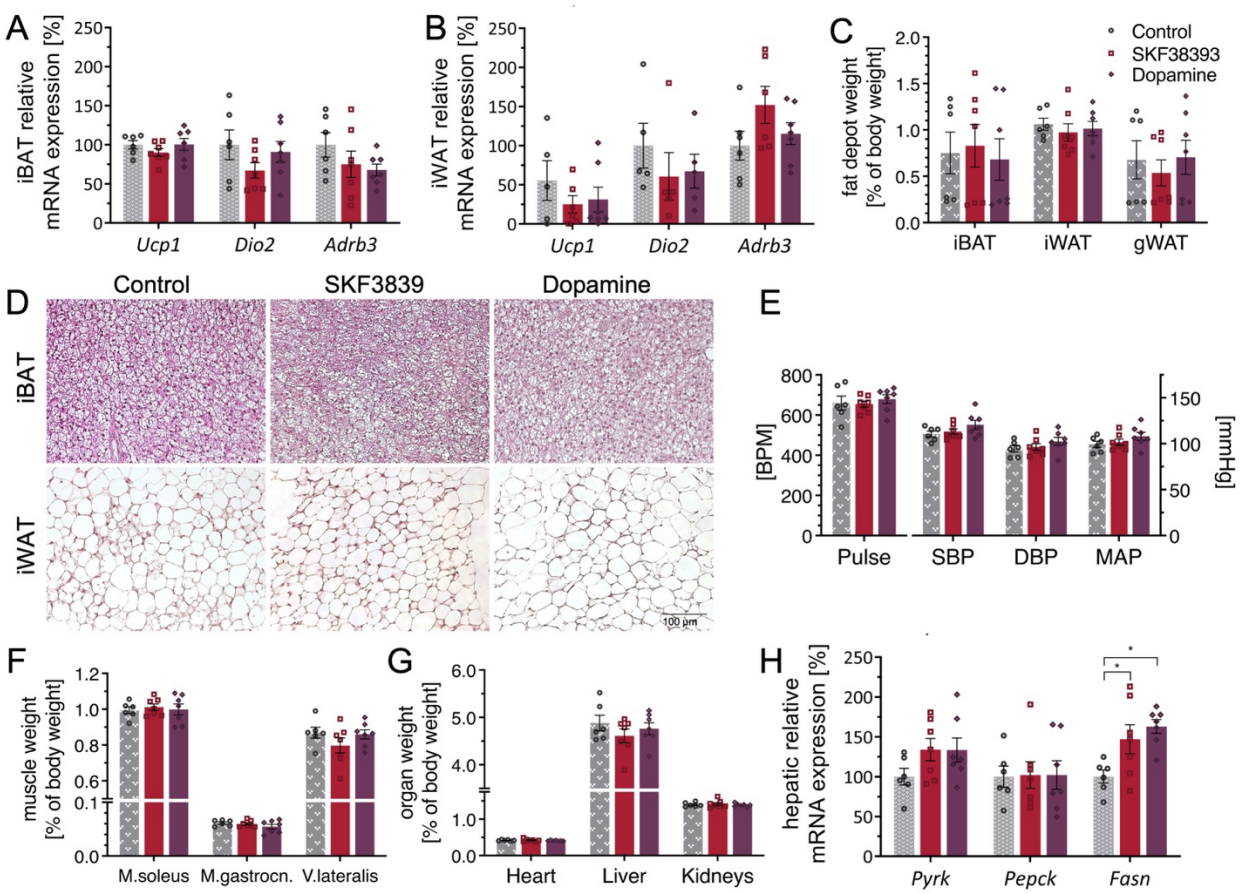

Figure 3-11: Adipose tissue thermogenesis markers, hepatic energy homeostasis markers, organ weight, and vital parameters following constant release in vivo (1 week).

*Thermogenic marker mRNA expression in iBAT (A) and iWAT (B), hepatic energy homeostasis marker mRNA expression (C), fat depot weight of iBAT, iWAT, and gWAT (D), weight of heart, liver, and kidneys (F), and weight of musculus soleus, musculus gastrocnemius and vastus lateralis (G) in C57BL/6NCrl mice treated with DRD1-agonist SKF-38393 (10 µg/kg/min) or DA (7 µg/kg/min) for 1 week via i.p.-implanted osmotic minipumps, and a respective saline-filled minipump (0,9 %)-control group. Data are presented as mean ±SEM. Groups were compared using two-tailed t-tests. *P < 0,05; n = 6.*

3.3 LC-MS/MS Analysis of Enriched Membrane Protein Fraction of iBAT and iWAT

The lack of effects of the DRD1- and DRD2-agonist in the *ex vivo* model, followed by only minor effects on thermogenesis in iBAT and iWAT *in vivo*, seriously questioned whether dopamine receptors are indeed present in adipose tissues, despite previous *in vitro* and *ex vivo* studies showing their presence in iBAT and immortalized brown adipocytes, by performing immunoblots with respective antibodies (Kohlie et al., 2017). To help answer this question beyond qRT-PCR analysis and Western blotting, and therefore independently of inherent technical problems such as unspecific antibodies, enriched membrane fractions of iBAT and iWAT samples were analyzed by LC-MS/MS.

3.3.1 DRD1 and DRD2 could not be detected in enriched membrane protein fractions of iBAT or iWAT

On one hand, DA was confirmed to be abundantly present in iBAT of C57BL/6NCrl mice and also, to a lesser extent, in iWAT (Figure 3-12 A) (executed by Dr. Kornelia Johann in collaboration with Prof. Dr. Jeffrey W. Dalley, Department of Psychology, University of Cambridge, UK (Johann *et al*., 2019)).
On the other hand, mRNA expression of dopamine receptors DRD1 and DRD2 in iBAT and iWAT was inconclusive (Figure 3-12 B), and DRD1 protein could not be detected unequivocally by Western blot analysis either, while no specific DRD2-antibodies were available to begin with, as proven by knockout-validation experiments (Figure 3-12 B; Stojanovic *et al*., 2017). Whole brain samples and striatum served as positive control in qRT-PCR and Western blot, respectively (Figure 3-12 B, C).
Ultimately, dopamine receptors DRD1 and DRD2 could also not be identified in iBAT or iWAT by LC-MS/MS analysis. Interestingly, DRD2 could not be detected in striatum control samples by LC-MS/MS either (Figure 3-12 C, D).
Furthermore, DAT was also not detected in iBAT or iWAT by qRT-PCR (Table 3-1), Western blot (not shown), or LC-MS/MS (Figure 3-12 D).
However, the abundant detection of adrenergic receptor ADRB3 by LC-MS/MS in iBAT and iWAT, showed the integrity of the investigated adipose tissue samples and the experimental procedure (Figure 3-12 D).

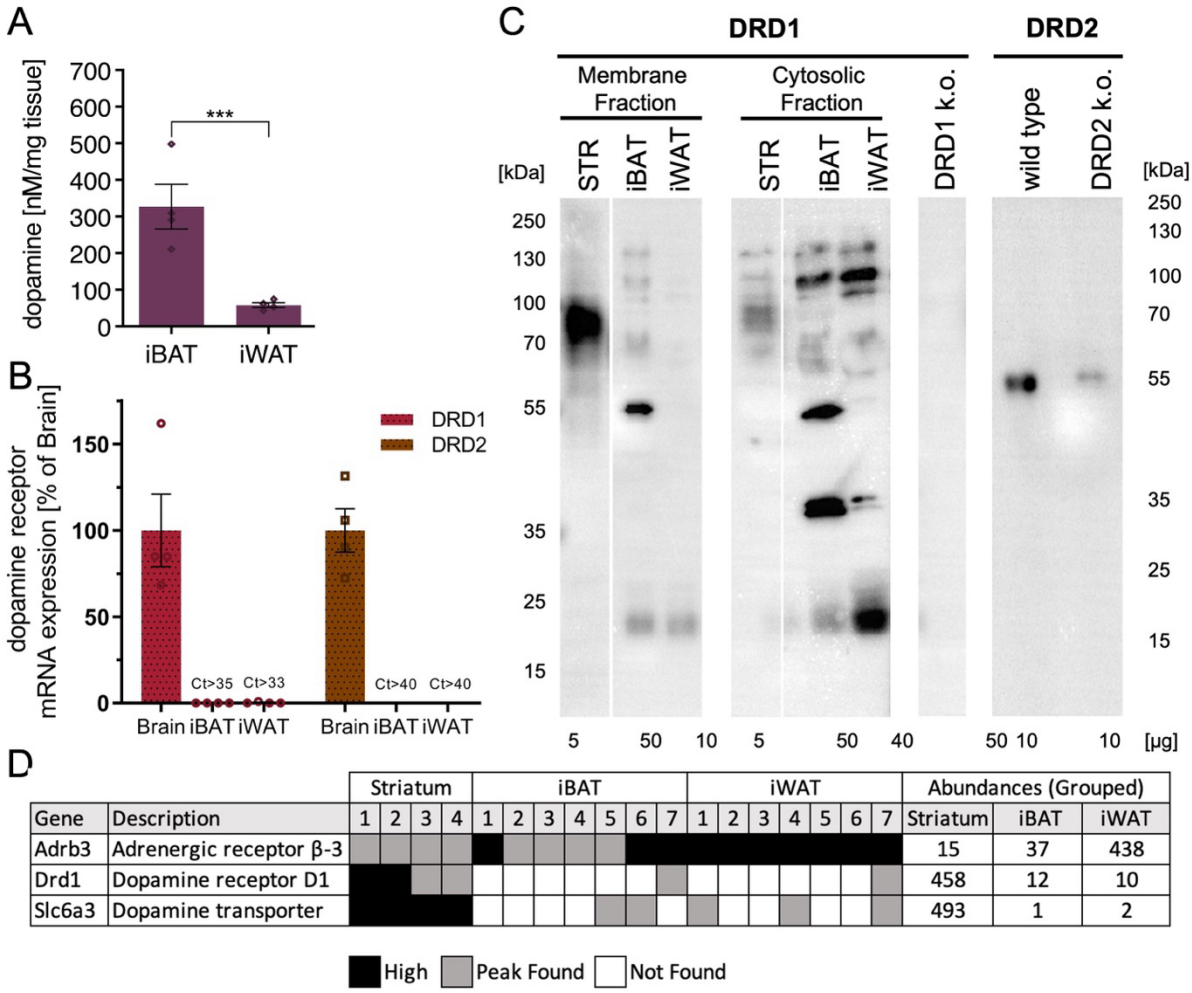

Gene	Description	Striatum 1	2	3	4	iBAT 1	2	3	4	5	6	7	iWAT 1	2	3	4	5	6	7	Abundances (Grouped) Striatum	iBAT	iWAT
Adrb3	Adrenergic receptor β-3																			15	37	438
Drd1	Dopamine receptor D1																			458	12	10
Slc6a3	Dopamine transporter																			493	1	2

Figure 3-12: Dopamine and dopamine receptor (DRD1, DRD2) analysis in enriched membrane fraction of iBAT and iWAT.

*Dopamine content in iBAT and iWAT of C57BL/6NCrl mice (n=4) (A), mRNA expression of dopamine receptors DRD1 and DRD2 in whole brain, iBAT, and iWAT (n=4) (B), Western blot analysis of DRD1 (left) and DRD2 (right) (C), and LC-MS/MS analysis of DRD1 and dopamine transporter (DAT) protein in striatum (n=4), iBAT (n=7), and iWAT (n=7) of C57BL/6NCrl mice. Brain tissue samples of DRD1 k.o. (DRD1 (-/-)) mice was collected from animals bought from and developed by Prof. em. Motoya Katsuki (National Institutes of Natural Sciences, Medical Institute of Bioregulation, Kyushu University Japan) by the group of Prof. Gert Lubec (Functional Proteomics, Department of Pharmaceutical Chemistry, University of Vienna). Data are presented as mean ± SEM. Groups were compared using two-tailed t-tests. ***P < 0,001.*

Additionally, qRT-PCR analysis of iBAT and iWAT was inconclusive for all dopamine receptors (DRD1-DRD5) and DAT as shown by late (Ct > 30) or lack of (Ct > 40) amplification (Table 3-1).

Table 3-1: Dopamine receptors (DRD1-DRD5) and dopamine transporter (DAT) mRNA expression (Ct values) in whole Brain, iBAT, and iWAT (n=4), n.d. - not determined.

Tissue	DRD1	DRD2	DRD3	DRD4	DRD5	DAT
Brain	~27	~29	~31	~30	>34	~29
iBAT	>35	>40 (n.d.)	>40 (n.d.)	>39	>40 (n.d.)	>40 (n.d.)
iWAT	>33	>40 (n.d.)	>40 (n.d)	>37	>40 (n.d.)	>40 (n.d.)

3.3.2 Identification of potential new markers for distinction between iBAT and iWAT, and their respective state of thermogenic activity

Preparation of enriched membrane protein samples from striatum, iBAT, and iWAT, followed by LC-MS/MS analysis, generated a set of about 6300 identified master proteins. This dataset is valuable far beyond the investigation of whether dopamine receptors are present in the analyzed tissue samples.

Accordingly, targeted sorting and filtering of the dataset in *Proteome Discoverer* (versions 2.3 - 3.0), as exemplarily depicted in the screenshots below, allowed to identify a list of "top hits" of proteins that occurred highly abundant in iBAT, while, at the same time, lowly abundant in iWAT (Figure 3-13); and vice versa (Figure 3-14). Then, primers were designed for ten hits of each "top 20" list, that were used in qRT-PCR analyses. This allowed to explore the potential of these putative markers when it comes to distinction between iBAT and iWAT, and even between the different states of thermogenic activity of these tissues. The list of potential markers, for which primers were designed and a description of selection criteria, is shown in Table 3-2 and its subtitle, respectively.

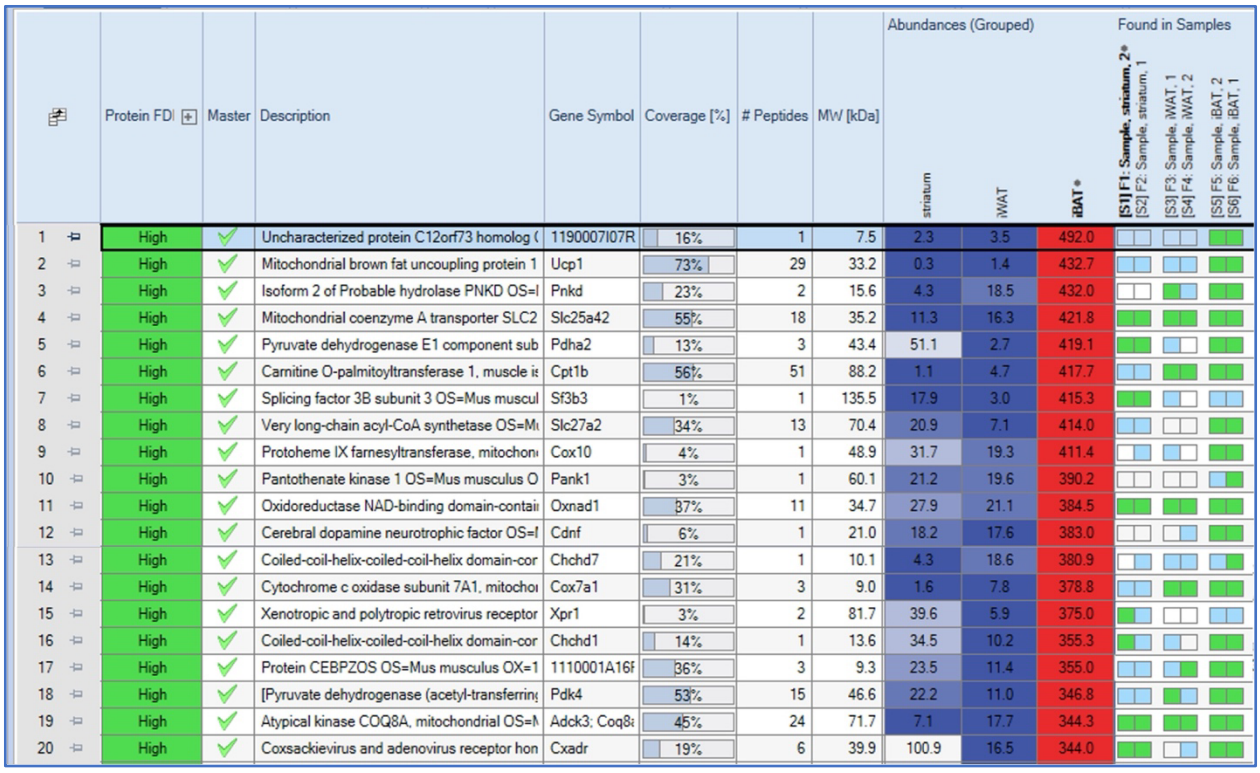

	Protein FDI	Master	Description	Gene Symbol	Coverage [%]	# Peptides	MW [kDa]	Abundances (Grouped) striatum	Abundances (Grouped) iWAT	Abundances (Grouped) iBAT*	Found in Samples [S1] F1: Sample, striatum, 2* [S2] F2: Sample, striatum, 1	Found in Samples [S3] F3: Sample, iWAT, 1 [S4] F4: Sample, iWAT, 2	Found in Samples [S5] F5: Sample, iBAT, 2 [S6] F6: Sample, iBAT, 1
1	High	✓	Uncharacterized protein C12orf73 homolog (	1190007I07R	16%	1	7.5	2.3	3.5	492.0			
2	High	✓	Mitochondrial brown fat uncoupling protein 1	Ucp1	73%	29	33.2	0.3	1.4	432.7			
3	High	✓	Isoform 2 of Probable hydrolase PNKD OS=I	Pnkd	23%	2	15.6	4.3	18.5	432.0			
4	High	✓	Mitochondrial coenzyme A transporter SLC2	Slc25a42	55%	18	35.2	11.3	16.3	421.8			
5	High	✓	Pyruvate dehydrogenase E1 component sub	Pdha2	13%	3	43.4	51.1	2.7	419.1			
6	High	✓	Carnitine O-palmitoyltransferase 1, muscle is	Cpt1b	56%	51	88.2	1.1	4.7	417.7			
7	High	✓	Splicing factor 3B subunit 3 OS=Mus muscul	Sf3b3	1%	1	135.5	17.9	3.0	415.3			
8	High	✓	Very long-chain acyl-CoA synthetase OS=M	Slc27a2	34%	13	70.4	20.9	7.1	414.0			
9	High	✓	Protoheme IX farnesyltransferase, mitochon	Cox10	4%	1	48.9	31.7	19.3	411.4			
10	High	✓	Pantothenate kinase 1 OS=Mus musculus O	Pank1	3%	1	60.1	21.2	19.6	390.2			
11	High	✓	Oxidoreductase NAD-binding domain-contai	Oxnad1	37%	11	34.7	27.9	21.1	384.5			
12	High	✓	Cerebral dopamine neurotrophic factor OS=I	Cdnf	6%	1	21.0	18.2	17.6	383.0			
13	High	✓	Coiled-coil-helix-coiled-coil-helix domain-cor	Chchd7	21%	1	10.1	4.3	18.6	380.9			
14	High	✓	Cytochrome c oxidase subunit 7A1, mitochor	Cox7a1	31%	3	9.0	1.6	7.8	378.8			
15	High	✓	Xenotropic and polytropic retrovirus receptor	Xpr1	3%	2	81.7	39.6	5.9	375.0			
16	High	✓	Coiled-coil-helix-coiled-coil-helix domain-cor	Chchd1	14%	1	13.6	34.5	10.2	355.3			
17	High	✓	Protein CEBPZOS OS=Mus musculus OX=1	1110001A16F	36%	3	9.3	23.5	11.4	355.0			
18	High	✓	[Pyruvate dehydrogenase (acetyl-transferrin	Pdk4	53%	15	46.6	22.2	11.0	346.8			
19	High	✓	Atypical kinase COQ8A, mitochondrial OS=M	Adck3; Coq8a	45%	24	71.7	7.1	17.7	344.3			
20	High	✓	Coxsackievirus and adenovirus receptor hon	Cxadr	19%	6	39.9	100.9	16.5	344.0			

Figure 3-13: Top 20 proteins highly abundant in iBAT (sorted highest to lowest) while lowly abundant in iWAT (grouped abundance <22,22). Exemplary analysis output for 2/7 membrane enriched protein samples of iBAT and iWAT (Proteome Discoverer 3.0. screenshot).

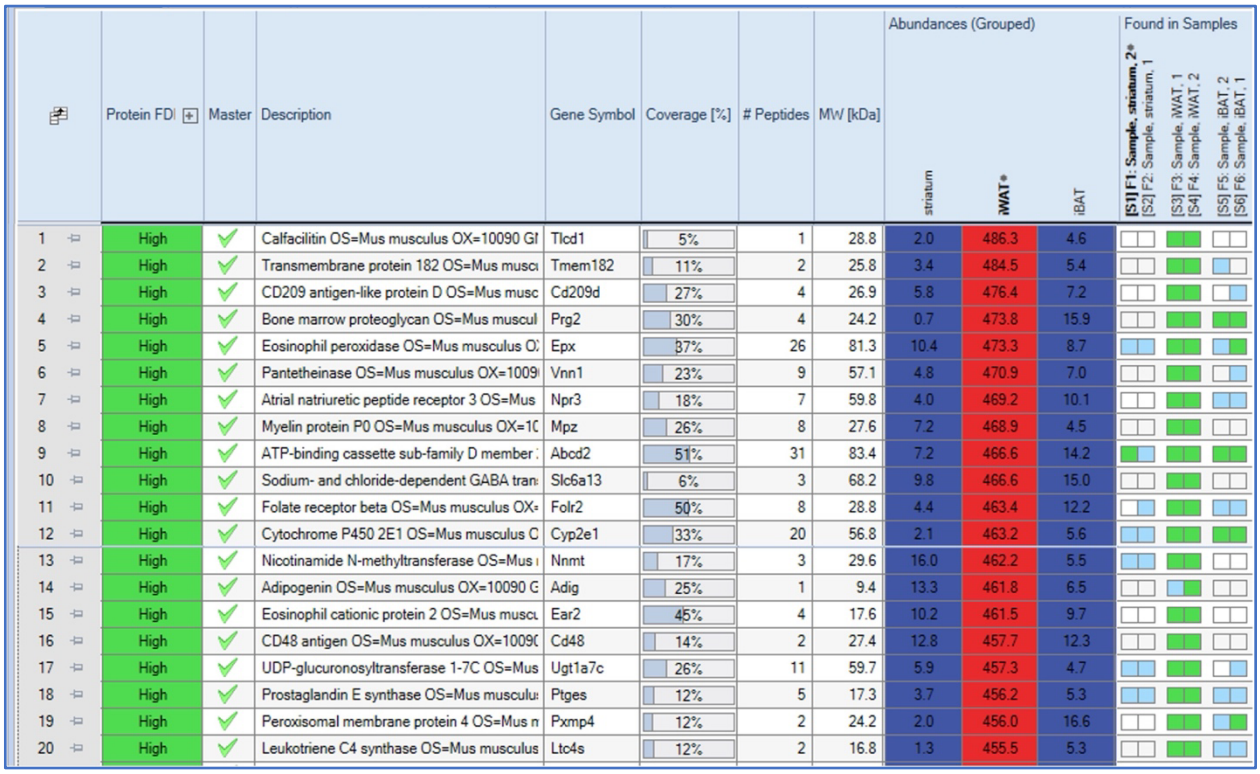

	Protein FDI	Master	Description	Gene Symbol	Coverage [%]	# Peptides	MW [kDa]	Abundances (Grouped) striatum	Abundances (Grouped) iWAT*	Abundances (Grouped) iBAT	Found in Samples [S1] F1: Sample, striatum, 2* [S2] F2: Sample, striatum, 1	Found in Samples [S3] F3: Sample, iWAT, 1 [S4] F4: Sample, iWAT, 2	Found in Samples [S5] F5: Sample, iBAT, 2 [S6] F6: Sample, iBAT, 1
1	High	✓	Calfacilitin OS=Mus musculus OX=10090 GI	Tlcd1	5%	1	28.8	2.0	486.3	4.6			
2	High	✓	Transmembrane protein 182 OS=Mus musc	Tmem182	11%	2	25.8	3.4	484.5	5.4			
3	High	✓	CD209 antigen-like protein D OS=Mus musc	Cd209d	27%	4	26.9	5.8	476.4	7.2			
4	High	✓	Bone marrow proteoglycan OS=Mus muscul	Prg2	30%	4	24.2	0.7	473.8	15.9			
5	High	✓	Eosinophil peroxidase OS=Mus musculus O	Epx	37%	26	81.3	10.4	473.3	8.7			
6	High	✓	Pantetheinase OS=Mus musculus OX=1009	Vnn1	23%	9	57.1	4.8	470.9	7.0			
7	High	✓	Atrial natriuretic peptide receptor 3 OS=Mus	Npr3	18%	7	59.8	4.0	469.2	10.1			
8	High	✓	Myelin protein P0 OS=Mus musculus OX=1C	Mpz	26%	8	27.6	7.2	468.9	4.5			
9	High	✓	ATP-binding cassette sub-family D member	Abcd2	51%	31	83.4	7.2	466.6	14.2			
10	High	✓	Sodium- and chloride-dependent GABA tran	Slc6a13	6%	3	68.2	9.8	466.6	15.0			
11	High	✓	Folate receptor beta OS=Mus musculus OX=	Folr2	50%	8	28.8	4.4	463.4	12.2			
12	High	✓	Cytochrome P450 2E1 OS=Mus musculus C	Cyp2e1	33%	20	56.8	2.1	463.2	5.6			
13	High	✓	Nicotinamide N-methyltransferase OS=Mus	Nnmt	17%	3	29.6	16.0	462.2	5.5			
14	High	✓	Adipogenin OS=Mus musculus OX=10090 G	Adig	25%	1	9.4	13.3	461.8	6.5			
15	High	✓	Eosinophil cationic protein 2 OS=Mus muscu	Ear2	45%	4	17.6	10.2	461.5	9.7			
16	High	✓	CD48 antigen OS=Mus musculus OX=1009(	Cd48	14%	2	27.4	12.8	457.7	12.3			
17	High	✓	UDP-glucuronosyltransferase 1-7C OS=Mus	Ugt1a7c	26%	11	59.7	5.9	457.3	4.7			
18	High	✓	Prostaglandin E synthase OS=Mus musculu	Ptges	12%	5	17.3	3.7	456.2	5.3			
19	High	✓	Peroxisomal membrane protein 4 OS=Mus n	Pxmp4	12%	2	24.2	2.0	456.0	16.6			
20	High	✓	Leukotriene C4 synthase OS=Mus musculus	Ltc4s	12%	2	16.8	1.3	455.5	5.3			

Figure 3-14: Top 20 proteins highly abundant in iWAT (sorted highest to lowest) while lowly abundant in iBAT (grouped abundance <22,22). Exemplary analysis output for 2/7 membrane enriched protein samples of iBAT and iWAT (Proteome Discoverer 3.0. screenshot).

Table 3-2: List of potential marker genes for iBAT and iWAT distinction (depot and thermogenic state).

iBAT marker candidates:	*Aldh2*	**iWAT marker candidates:**	*Abcd2*
	*C12orf73**		*Adig**
	Cox7a		*Cd209d*
	Cpt1b		*Epx*
	Letmd1		*Mpz*
	Mtfp1		*Npr3*
	Mtg1		*Prg2*
	Pnkd		*Prx*
	Slc25a42		*Ugt1a6*
	Slc27a2		*Vnn1*

*Criteria for selected markers included: had to be among top 20 list when grouped abundance in iBAT or iWAT was sorted highest to lowest; protein = master; protein FDR confidence = high; contaminant = false; coverage >10 %; #peptides >1; grouped abundance <27 in iWAT (for iBAT candidates) or iBAT (for iWAT candidates). *For iBAT marker candidate C12orf73 and iWAT marker candidate Adig, primers were designed, despite #peptides = 1. Grey: did not amplify.*

To determine, whether primer design was successful, qRT-PCR was performed in iBAT (for iBAT candidates) or iWAT (for iWAT candidates) of C57BL/6NCrl mice that were housed at 23°C. Successful primer design was determined by amplification of the according target sequences and melting curve analysis. Subsequently, mRNA expression of potential new iBAT markers was cross-validated in iWAT (Figure 3-15 A), and vice versa (Figure 3-16 A). Moreover, mRNA expression in iBAT and iWAT from animals housed at different temperatures (iBAT 10°C, iBAT 30°C, iWAT 10°C) was analyzed, representing increased (10°C) or decreased (30°C) thermogenic activity (Johann et al., 2019).

Out of 10 pursued marker candidates for iBAT, nine successfully amplified in qRT-PCR (Table 3-2), all of which showed significantly less mRNA expression in iWAT 23°C (Figure 3-15 A), as indicated previously by the LC-MS/MS data.
Moreover, all nine of these marker candidates showed significantly reduced mRNA expression in iBAT 30°C compared to iBAT 23°C, reflecting less gene expression in less thermogenically active iBAT. Six of these marker candidates additionally showed significantly increased mRNA expression in iBAT 10°C compared to iBAT 23°C, reflecting more gene expression in more thermogenically active iBAT (Figure 3-15 B).
All but one (*Mtg1*) of the nine potential iBAT markers also showed significantly less mRNA expression in iWAT 10°C, compared to iBAT 23°C, expectedly reflecting less thermogenic capacity of cold-induced beige adipose tissue compared to regular BAT.

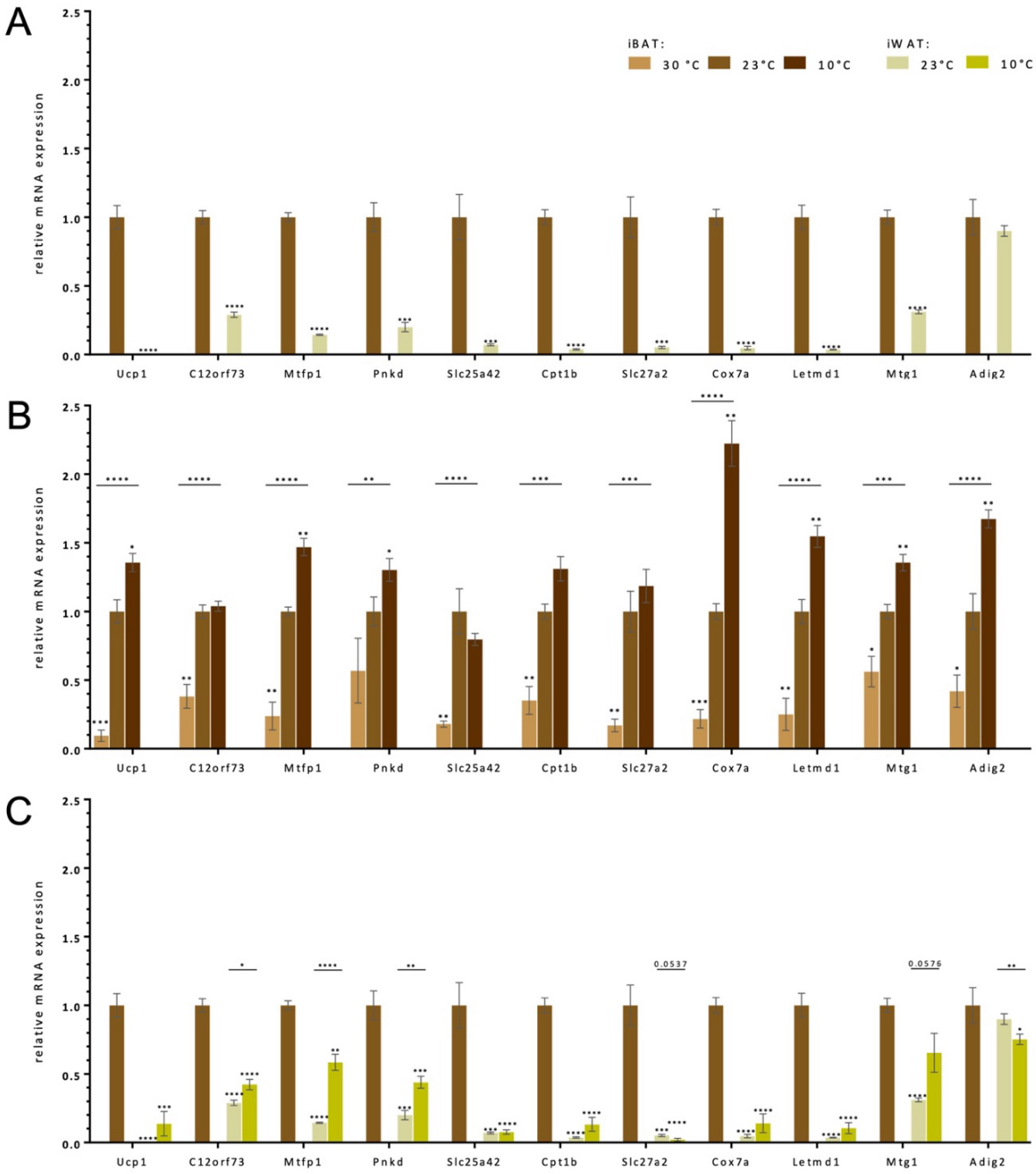

Figure 3-15: mRNA expression validation of marker candidates for iBAT and its state of thermogenic activity, that were previously identified by LC-MS/MS analysis in iBAT and iWAT.

*Cross validation between iBAT collected from C57BL/6NCrl mice housed at 23°C (iBAT 23°C) and iWAT 23°C (A), between iBAT 23°C, iBAT 10°C, and iBAT 30°C, which represent different states of thermogenic activity in iBAT (B), and iBAT 23°C, iWAT 23°C, and iWAT 10°C, which represents a different state of thermogenic activity in iWAT (C). Data are presented as mean ± SEM. Groups were compared by multiple t-test analysis (Holm-Sidak method). *P < 0,05; **P < 0.01; ***P < 0.001; ****P < 0.0001; n≥4.*

At the same time, three of these potential markers (*C12orf73*, *Mtfp1*, *Pnkd*) were significantly increased in iWAT 10°C compared to iWAT 23°C, and therefore additionally qualify for distinguishing between more (10°C) and less (23°C) thermogenically active WAT. Meanwhile, one of these markers (*Adig2*) was significantly decreased in iWAT 10°C compared to iWAT 23°C (Figure 3-15 C). This same marker candidate was originally recognized as a potential iWAT marker according to the LC-MS/MS analysis. However, on mRNA expression level, no significant difference in expression between iBAT 23°C and iWAT 23°C was seen (Figure 3-15 A). If anything, it is even slightly higher expressed in iBAT 23°C than iWAT 23°, and therefore not a fit marker to distinguish between these adipose depots per se. Surprisingly, it appears to be well suited to distinguish between more and less thermogenically active iBAT (Figure 3-15 B), as well as more and less thermogenically active iWAT (Figure 3-15 C), only that it does so in opposite expression patterns in the two tissues. Increased thermogenic activity in iBAT is accompanied by an *Adig2* increase, while increased thermogenic activity in iWAT is accompanied by an *Adig2* decrease.

Out of 10 pursued marker candidates for iWAT, five amplified in qRT-PCR (Table 3-2), four of which showed significantly less mRNA expression in iBAT 23°C (Figure 3-16 A), as indicated previously by the LC-MS/MS data.
Moreover, three of these marker candidates showed significantly reduced mRNA expression in iWAT 10°C compared to iWAT 23°C, reflecting less gene expression in more thermogenically active iWAT. Additionally, one of the marker candidates (*Vnn1*) showed significantly increased mRNA expression in WAT 30°C compared to iWAT 23°C, reflecting higher gene expression in less thermogenically active iWAT (Figure 3-16 B). Therefore, it appears to be a well suited marker to distinguish sensitively between both, iWAT and iBAT depots and thermogenic states of activity of iWAT.

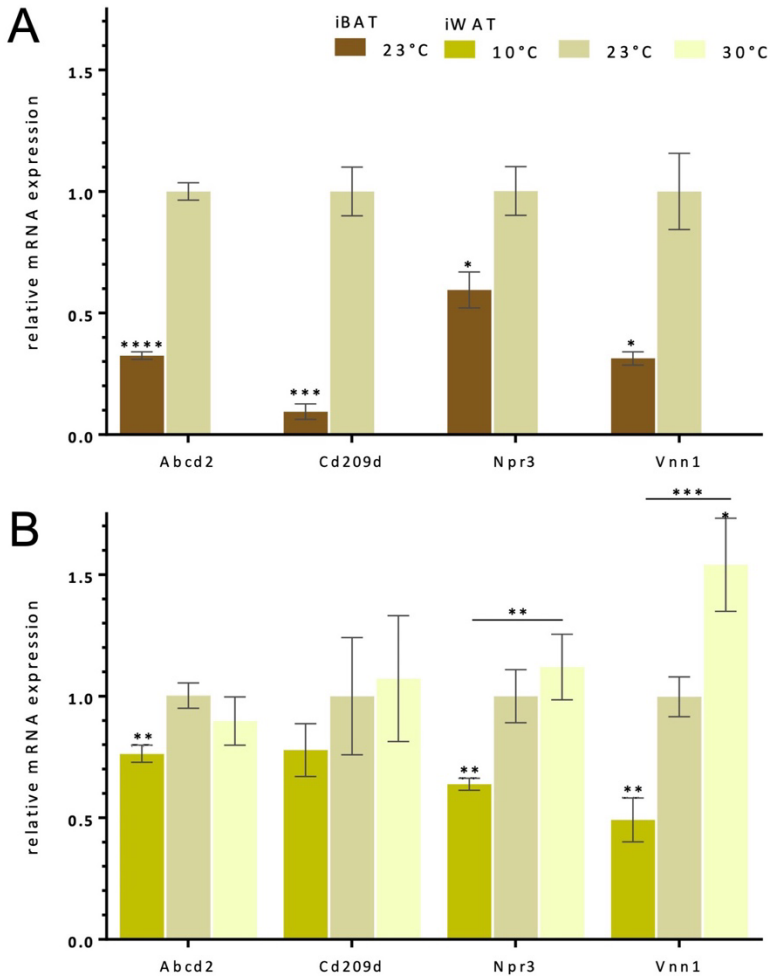

Figure 3-16: mRNA expression validation of marker candidates for iWAT and its state of thermogenic activity, that were previously identified by LC-MS/MS analysis in iBAT and iWAT.

*Cross validation between iWAT collected from C57BL/6NCrl mice housed at 23°C (iWAT 23°C) and iBAT 23°C (A), and between iWAT 23°C, iWAT 10°C, and iWAT 30°C, which represent a different state of thermogenic activity in iWAT (B). Data are presented as mean ± SEM. Groups were compared by multiple t-test analysis (Holm-Sidak method). *P < 0,05; **P < 0.01; ***P < 0.001; ****P < 0.0001; n≥4.*

Of all tested and amplified iBAT marker candidates, *Cox7a*, *Letmd1*, *Mtfp1*, and *Mtg1* were at least as capable of distinguishing between iBAT and iWAT depots and their different stages of thermogenic activity, as *Ucp1*; while *Mtfp1* superseded the capabilities of *Ucp1*, in that it additionally allowed for distinction between thermogenically more (iWAT 10°C) and less active (iWAT 23°C) iWAT (Table 3-3 iBAT).

Of all tested and amplified iWAT marker candidates, Vnn1 was superior to the remaining candidates, in that it allowed distinguishing not only between iBAT and iWAT depots, but also between both, more (10°C) and less thermogenically active (30°C) iWAT, compared to iWAT 23°C (Table 3-3 iWAT).

Table 3-3: Summary of potential markers' ability to distinguish between iBAT and iWAT depots and/or their thermogenic states of activity.

iBAT	*C12orf73*	*Cox7a*	*Cpt1b*	*Letmd1*	*Mtfp1*	*Mtg1*	*Pnkd*	*Slc25a42*	*Slc27a2*	*Adig*	***Ucp1***
Depots	X	X	X	X	X	X	X	X	X		**X**
iBAT ON		X		X	X	X	X			X	**X**
iBAT OFF	X	X	X	X	X	X		X	X	X	**X**
iWAT ON	X				X	X	X		1/X	1/X	
iWAT	*Abcd2*	*Cd209d*	*Npr3*	*Vnn1*							
Depots	X	X	X	X							
iWAT ON	X		X	X							
iWAT OFF				X							

3.3.3 KEGG analysis of membrane enriched proteins that are differentially expressed in iBAT compared to iWAT confirms expected pathway clusters

Lastly, proteins that are significantly differently expressed in iBAT compared to iWAT (ratio iBAT/iWAT = 8) were identified by normalizing and log-transforming the generated LC-MS/MS data. The resulting list of proteins was run in a KEGG (Kyoto Encyclopedia of Genes and Genomes) analysis by Dr. Fernando Sialana.

The identified membrane enriched proteins differentially expressed in iBAT are enriched, first and foremost, in pathways associated with thermogenesis. This validates the approach in which marker candidates were selected according to an abundance-based, cross-filtering sorting scheme. It further verifies the procedures of sample collection, preparation, and analysis. Other pathways highly associated with proteins identified to be significantly higher abundant in iBAT than iWAT are PPAR signaling, citrate cycle, fatty acid metabolism, and fatty acid degradation, among others.

KEGG Pathways			
pathway	*description*	*count in gene set*	*false discovery rate*
mmu04714	Thermogenesis	9 of 223	4.16e-05
mmu01200	Carbon metabolism	6 of 118	0.00051
mmu03320	PPAR signaling pathway	5 of 85	0.00096
mmu00020	Citrate cycle (TCA cycle)	3 of 32	0.0080
mmu00620	Pyruvate metabolism	3 of 38	0.0103
mmu01100	Metabolic pathways	14 of 1296	0.0129
mmu01212	Fatty acid metabolism	3 of 51	0.0156
mmu00071	Fatty acid degradation	3 of 50	0.0156

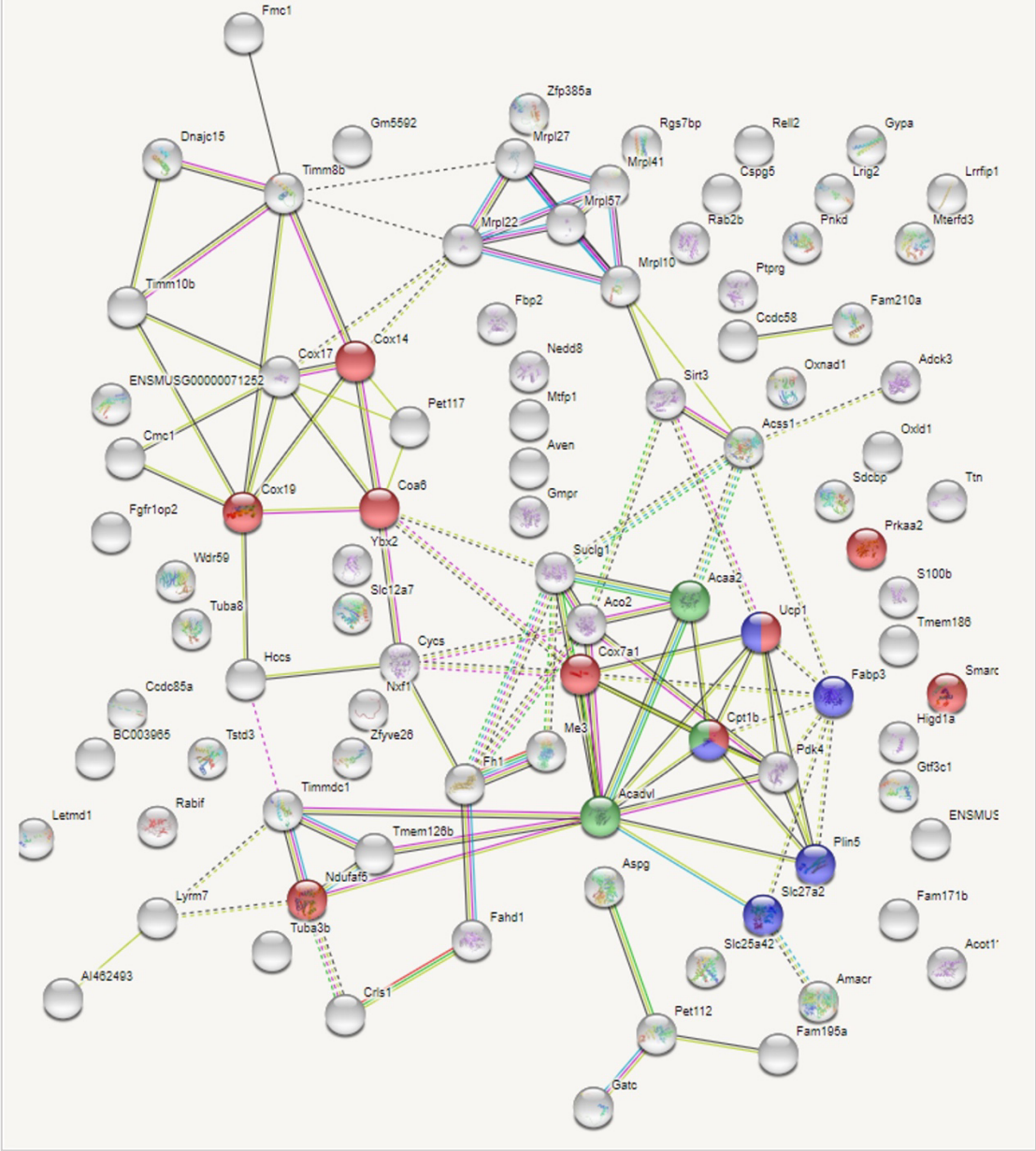

Figure 3-17: KEGG (Kyoto Encyclopedia of Genes and Genomes) analysis of proteins identified to be significantly more abundant in iBAT compared to iWAT.

The LC-MS/MS data set strongly suggests that dopamine receptors are not present in iBAT and iWAT of C57BL/6NCrl mice, therefore supporting the *ex vivo* and *in vivo* results of this study, which showed that peripheral administration of DRD1- and DRD2-agonists as well as DA had no significant effects on iBAT thermogenesis.

In addition to this finding, the data set allowed to identify potential new markers for the distinction between brown and white adipose depots, as well as their state of thermogenic activity.

4 DISCUSSION

The role of NE as a regulator of iBAT thermogenesis is well established (Cannon & Nedergaard, 2004).
The role of DA, on the other hand, has only recently been started to be investigated on a molecular level (Folgueira et al., 2019; Kohlie et al., 2017), despite the fact that first indications for its partake were published back in the 1980s (Maxwell et al., 1985; Rothwell et al., 1982).
While more recent *in vivo* studies focus on the role of central dopaminergic effects on iBAT thermogenesis (Folgueira et al., 2019), this thesis study appears to be the first study designed to investigate the direct (i.e., peripheral) effects of DA on iBAT thermogenesis *ex vivo* and *in vivo*.

The presented *ex vivo* and *in vivo* results strongly suggest that, in mice, DA plays only a negligible role in iBAT thermogenesis activation directly via dopamine receptors in peripheral tissue. Nevertheless, *in vivo* minor changes in energy homeostasis were observed.
Furthermore, an LC-MS/MS dataset, generated from enriched membrane protein samples of iBAT and iWAT from mice, supports this finding. Even with this highly sensitive method, the presence of dopamine receptors (DRD1-DRD5) could not be confirmed in the analyzed adipose depots. Dopamine receptors are therefore either lacking in these tissues or present only below detection limit in this experimental approach.
Additionally, the LC-MS/MS dataset allowed for the identification of potential new markers for the distinction between the iBAT and iWAT depots, as well as their thermogenic activity state.

4.1 *Ex Vivo* Effects

The lack of effects of DRD1-agonist SKF-38393 and DRD2-agonist Sumanirole on mRNA expression of key thermogenesis markers *Ucp1* and *Dio2*, *ex vivo* in iBAT explants from C57BL/6NCrl mice, is in contradiction with previous *in vitro* results in immortalized brown adipocytes (Kohlie et al., 2017), which showed an increase in UCP1 protein in brown adipocytes treated with DA or the DRD1-agonist. The discrepancy could be due to the following:

On one hand, it can be accounted to the different models employed. For instance, *in vitro*, preadipocytes undergo proliferation and differentiation in defined culture media to obtain synchronized cells presenting brown adipocyte-like characteristics, while the *ex vivo* model provides a closer representation of the physiological milieu in which adipocytes reside *in vivo*, consisting, mainly, of adipocytes, pre-adipocytes, and adipose-derived stromal stem cells, but also of, e.g., macrophages and endothelial cells (Esteve Ràfols, 2014).

On the other hand, different readouts were analyzed. The mentioned *in vitro* study analyzed effects on UCP1 protein levels and oxygen consumption, among others; while the presented *ex vivo* study investigated effects on gene expression. However, it appears that model differences are more likely to be decisive for the different results, since the *in vivo* results presented here showed that UCP1 protein was not significantly increased by the DRD1-agonist. Also, total UCP1 protein in the immortalized brown adipocytes was extremely low compared to BAT.

Moreover, dopamine effects *in vitro* were reported using 1-100 nM treatment concentrations, which, except for the lowest dose of 1 nM is similar to what was used here *ex vivo*. Nevertheless, it would be interesting to investigate this low dose of DA *ex vivo* too, since DA is known to excert fundamentally different effects at low, medium and high doses (see 4.2.3).

Proof of concept for the *ex vivo* model was provided by treatment with the ADRB3-agonist CL316,243, which mimics NE exposure in terms of β3-adrenergic stimulation of BAT thermogenesis and, expectedly, increased mRNA expression of both thermogenesis markers, *Ucp1* and *Dio2*, significantly and, in the sense of agonist related homologous receptor desensitization, decreased *Adrb3* mRNA expression (Himms-Hagen et al., 1994; Valentine et al., 2021).

Interestingly, the DRD1-agonist and DA also caused significantly decreased *Adrb3* mRNA expression in iBAT explants, suggesting possible off-target effects of these substances via adrenergic receptors – which have previously been reported in various tissues (El-Mas et al., 2005; Habuchi et al., 1997).

Lastly, DA caused a significant increase in *Dio2* mRNA expression at 50 nM and 100 nM, and in combination with T3 (50 nM) even at 10 nM, which neither of these substances at these concentrations achieved on their own, suggesting synergistic effects. This underlines potential off-target effects of DA by, again, hinting at β-adrenergic action, since thyroid hormones have been previously shown to alter the β-adrenergic response

to catecholamines in the various tissues, including iBAT and the heart, i.e., enhancing β-adrenergic activity and increasing the number of β-adrenergic receptors (ADRB1 in iBAT), and therefore sensitivity to catecholamines (Weiner et al., 2016; Whybrow & Prange, 1981; Williams et al., 1977) Therefore, *Dio2* may potentially be increased as a result of positive feedback regulation caused by DA effects on β-adrenergic receptors.

4.2 *In Vivo* Effects

Explantation of iBAT tissue essentially goes along with denervation – the cutoff from the SNS, which, in the live animal, transmits hypothalamic signals to brown adipocytes to induce BAT thermogenesis (L. T. Tran et al., 2022). With BAT thermogenesis being strongly dependent on SNS signalling in live organisms (Hsieh et al., 1957; Hsieh & Carlson, 1957), the lack of effects of DA and the DRD1- and DRD2-agonist on thermogenesis markers *ex vivo* could potentially be due to the lack of the complex systemic SNS activity in this model. Accordingly, *in vivo* experiments were conducted to further investigate the direct effects of dopamine receptor agonists and DA on iBAT, since potential effects may co-depend on intact SNS-signalling or other physiological co-regulation.

4.2.1 Single Injection In Vivo Study (1 h)

Acute interventions with single injections of either the DRD1- or DRD2-agonist, or DA in C57BL/6NCrl mice showed no lasting effects on iBAT thermogenesis. Interestingly though, the very brief and transient increase in iBAT temperature caused by the DRD1-agonist, and the very brief and transient decrease in iBAT temperature caused by the DRD2-agonist, coincide with the timeframes of changes in locomotor activity in treated animals, compared to the control group.

Effects of DRD1- and DRD2-agonists on movement in rodents have been described in previous studies. For instance, it has been reported that DRD1 knockout mice showed significantly reduced forward locomotor activity (A. H. Tran et al., 2005). Furthermore, very similar patterns of locomotor activity changes in response to DRD1- and DRD2-agonists, as were described here, have been observed previously in rats within the same timeframes. For example, a DRD1-agonist (6-Br-APB) significantly increased forward locomotor activity 20-40 min after intracerebroventricular (i.c.v.) injection, while a DRD2-agonist (LY 163502) i.c.v. significantly decreased locomotor activity in the first 20 min and then significantly increased locomotor activity between 20-40 min (Boulay et al., 2000). Another study showed, that i.p. injection of DRD2-agonist quinpirole, at concentrations

0,5-10 mg/kg, also lead to suppression of locomotor activity early in the recording session and a subsequent increase compared to controls, after about 40 min (Horvitz et al., 2001), which is in astounding concordance with the results presented here. Additionally, DRD1-agonist SKF-38393 injected i.p. at 1-10 mg/kg has been reported to significantly increase locomotor activity at all concentrations starting about 20 min post injection in C57BL/6J mice, while DRD2-agonist quinpirole increased locomotor activity at 5-10 mg/kg between 20-40 min, but not at 1 mg/kg (Jung & Shim, 2011). In sum, the locomotor response of rodents to DRD1- and DRD2-agonists appears to align over quite a number of studies. However, effects may be subject to type of agonist, concentration, rout of administration, timepoint of measurement, and species. As, for instance, DRD1-agonist SKF-38393 has been reported to decrease locomotor activity in common marmosets (Löschmann et al., 1992), which contradicts the findings discussed in rodents and underlines the limitations regarding conclusions for translational relevance.

Further, effects of DRD1- and DRD2-agonists on thermoregulation in rodents have been reported previously. For example, it was shown in mice that DRD2-agonist quinpirole caused hypothermia when injected both i.p. (0,3-3 mg/kg) or i.c.v. (0,1 mg/kg) and that the effect was reversed by DRD2-antagonists i.p. and i.c.v. that readily cross the blood brain barrier, while it could not be reversed by a DRD2-antagonist i.p. that does not cross the blood brain barrier. Which suggests a centrally mediated DRD2-dependent mechanism in the hypothermia response to DRD2-agonists (Nunes et al., 1991). Moreover, DRD1-agonist SKF-38393 i.p. injection at a high dose (10 mg/kg) was shown to mildly attenuate DRD2-induced hypothermia, while the same dose i.c.v. injected potentiated DRD2-induced hypothermia (Nunes et al., 1991), suggesting a modulating role of DRD1, potentially both, peripherally and centrally.

With regards to iBAT temperature, it was shown in rats, that 0,5 mg/kg of s.c. DRD2-agonist quinpirole reversed cold-induced iBAT thermogenesis, and i.v. quinpirole inhibited cold-induced sympathetic nerve discharge into iBAT, suggesting, that activation of DRD2 in the CNS inhibits SNS-mediated iBAT thermogenesis (Ootsuka et al., 2007).

Additionally, in rodents, vasoregulation in the tail is a major thermoregulatory mechanism (Gordon, 1990; Warner & Mittag, 2014). Taking together the discussed observations, and the observed drop in tail temperature upon acute treatment with the DRD1-agonist or DA 1 hr after injection, and the observed “lighting-up” (heat dissipation in IRT images) of the tail upon treatment with the DRD2-agonist, one could speculation that, when administered peripherally, the DRD1- and DRD2-agonist simulate coping mechanisms

that originally serve to counter cold or heat-exposure, respsectively. A cold stimulus would be expected to lead to increased BAT thermogenesis to prevent diversion of the body temperature below the setpoint, which in rodents would typically be accompanied by heat conservation through constriction of the tail vasculature. Both we see, even if only very briefly and mildly, with the DRD1-agonist. Meanwhile, heat stimulation would be expected to decrease BAT thermogenesis to prevent body temperature from exceeding the setpoint, which would be accompanied by heat dissipation through vasodilation in the tail. Again, both of which is seen in the single injection *in vivo* study very briefly and mildly, with the DRD2-agonist. However, the effects appear to be so very mild and transient, that it seems unlikely they are of significant physiological impact.

Also, it remains unclear, if and how these thermoregulatory effects are linked to the changes in locomotor activity and whether any of the seen effects result from direct peripheral action of the treatments on any of the tissues of interest, or if they may be due to direct or indirect (e.g. via feedback regulation) effects on the CNS.

On the one hand, dopamine receptors DRD1 and DRD2 are present in numerous peripheral tissues (e.g., heart, kidney, lung) (Amenta et al., 2002), including endothelial cells (Bhattacharya et al., 2008). On the other hand, central effects, despite i.p. injection, can not be excluded, since both agonists readily cross the blood brain barrier (Barone et al., 2007; Kamien & Woolverton, 1985) (see 4.2.3).

4.2.2 Repeated Injection In Vivo Study (1 week)

To investigate whether the minimal effects seen in the single injection *in vivo* study would persist or potentially intensify if treatments were repeated over a longer period, an *in vivo* experiment was performed with daily injections for one week.

However, no significant effect of the DRD1- or DRD2-agonist on iBAT thermogenesis was observed – neither in terms of iBAT temperature and UCP1 expression, nor expression of markers of alternative activation of thermogenesis and complexes I-V of oxidative phosphorylation.

Nevertheless, the DRD1-agonist had significant impact on parameters that suggest its participation in the regulation of metabolic processes. Firstly, cAMP protein was found to be increased. This effect would be expected during BAT thermogenesis activation; yet, no significant effects on core or iBAT temperature were observed. However, cAMP as a second messenger is, of course, utilized in many different biological processes apart from BAT thermogenesis activation, including metabolic processes (Patra et al., 2023). A

correlation between cAMP and lipase activity, as well as their induction by catecholamine stimulation has been described before (Huttunen & Steinberg, 1971; Shepherd et al., 1981). Moreover, cAMP/PKA signalling has been shown to alter energy metabolism by ultimately increasing β-oxidation of fatty acids (Manerba et al., 2019). Therefore, elevated cAMP is in concordance with elevated lipase activity, which was indeed somewhat increased after one week of daily DRD1-agonist injections, even if not significant. Together with decreased tissue weight of iBAT and iWAT, a reduction in the size of individual white adipocytes in histological samples, as well as increased *Pyrk* mRNA expression and decreased glycogen storage in liver samples of DRD1-agonist treated animals, the results quite clearly point towards increased metabolic activity and energy expenditure. In fact, it has been shown before, that DRD1-agonism decreases fat storage through β-oxidation (Barros et al., 2014), and that DRD1-signalling stimulates lipolysis (J. Yu et al., 2022). Interestingly, catecholamine neurotransmitter adrenaline, to whom DA is a metabolic precursor (Blaschko, 1942), is also known to induce glycogenolysis via cAMP and PKA during exercise (Kjær et al., 2000). Increasded catabolism, in turn, would align with the observed and previously described effect of the DRD1-agonist on locomotor activity. The increased locomotor activity, and therefore likely increased energy expenditure after DRD1-agonist injections, could potentially be causal for the described effects on metabolic parameters. Eventhough, body weight and muscle weights were not affected in this experiment, which could be due to the duration of the experiment of only one week.

Additionally, an increase in tail temperature was observed with the DRD1-agonist when comparing treated animals to control animals, which would be contradicting the results of the single injection *in vivo* study. However, the increase between treatment groups was not concurrent with an increase from baseline to treatment timepoint within each group. In fact, within each group tail temperature was decreased when comparing baseline to treatment measurments. This result is not very clear and would need further investigation to better tie into the overall results. For instance, tail temperature measurments could be taken at multiple timepoints after each treatment injection to obtain more precise insight into the pattern of regulation. After all, the DRD1-agonist and DA have been described to , if anything, possess vasocontrictive effects (Vasse et al., 1990; Wiglusz & Jedrzejak, 2011).

4.2.3 Constant Injection In Vivo Study (1 week)

To rule out that the lack of effects of the agonists and DA on BAT thermogenesis was potentially due to their rather short half-life and high susceptibility to oxidation (Baker et al., 2008; Jackson et al., 1988; McCall et al., 2005b; Sturgill et al., 2011), an experimental setup was designed that ensured constant release of the treatment substances in the intraperetonial cavity over one week. This was achieved by implanting osmotic minipumps filled with the according treatment substance. Also, under these conditions, the risk of potentially missing the timeframe during which effects on BAT temperature could occur after individual injections was minimized. Due to the, so far, even lesser effects seen with the DRD2-agonist, only the DRD1-agonist and DA were included in this study.

However, no significant effects were observed on body or iBAT temperature when IRT photos from day 5 and 7 post-operation were analyzed, supporting the results of the previously discussed experiments. Although, during IRT videography on day 3 post-operation a significant increase in iBAT temperature was detected in the DRD1-agonist treated group, suggesting a potentially short and transient effect, as previously seen in the single injection *in vivo* study. However, compared to effects commonly seen with, e.g. NE (Himms-Hagen, 1990; Johann et al., 2019; Reed & Fain, 1968), the peripheral effect of the DRD1-agonist on BAT thermogenesis appears to be rather negligible. Nevertheless, it can not be fully excluded, that an overall lack of effects in this experimental setup may be due to the continuous secretion of a lower dose of the treatment substances or their quick oxidation, despite containment in an osmotic minipump. This is supported by the observation, that only one metabolic parameter was significantly altered upon treatment with either substance – the hepatic mRNA expression of Fasn. At first glance this could be thought of as contradictory to the results of the repeated injection *in vivo* study, where multiple parameters point towards an involvement of the DRD1-agonist in metabolic regulation in a way that suggests increased energy expenditure, since *Fasn* is commonly associated with liponeogenesis and even steatosis (Dorn et al., 2010). However, *Fasn* has been suggested to function as both, a catalyst to *de novo* synthesis of fatty acids (even a housekeeper gene in liver) when nutrients are abundantly present, and a signalling factor for fat catabolism through PPARα induced β-oxidation of FFA derived from peripheral tissues or lipid droplets stored in hepatocytes under fasting conditions (Jensen-Urstad & Semenkovich, 2012). The latter of which fits well into the results seen throughout the presented project, since an overall decrease in adipocyte and fat depot size, metabolic

changes hinting at increased energy expenditure and increased locomotor activity were observed in different DRD1 and DA treatment scenarios *in vivo*. Arguably, the effects are not all present under one single experimental setting, which may be due to differences in measurement timepoints, treatment concentration, application, frequency, and continuity of treatment. However, this line of interpretation is also backed by the many reports of DA causing weight loss (Simonds & Cowley, 2019) and alterations in glucose homeostasis by, e.g., reducing insulin secretion and increasing circulating glucose levels, likely as part of a stress response that requires availability of energy substrates (Lelou et al., 2022; Underland et al., 2018). All the while DRD-antagonism has been associated with weight gain and obesity, as has the discontinuation of DA after chronic overstimulation due to subsequent, compensatory overeating (Gangopadhyay et al., 2022; Reinholz et al., 2008).

Taken together, the *ex vivo* and *in vivo* experiments presented here have demonstrated that peripheral administration of DA or specific DRD1- and DRD2-agonists have very little to no effect on BAT thermogenesis. Nevertheless, hypothalamic dopaminergic signalling via DRD2 has been reported to regulate BAT thermogenesis upon central administration (Folgueira et al., 2019). Moreover, dopamine-β-hydroxylase, the enzyme converting DA into NE, has been described to be present in BAT of rats, suggesting centrally initiated dopaminergic effects may ultimately affect BAT thermogenesis through conversion to NE (Behrens & Depocas, 1977). Eventhough the agonists used here do potentially cross the blood brain barrier, they may, e.g., be metabolized, oxidized or else modified before reaching the brain or simply arrive at much lower concentration, and therefore not show effects comparable to when centrally administered. Additionally, it is important to note, that DA has been described to predominantly act on different receptor types depending on the applied dosis. For example, at low doses (0,5-2 µg/kg/min) DA preferably binds to DRDs, at medium doses (2-10 µg/kg/min) β-adrenergic receptors are favored, and at high doses (>10 µg/kg/min) binding to α-adrenergic receptors predominates (MacGregor et al., 2000; Sonne et al., 2022). Whereby stimulation of the first two receptor types has been associated with weight loss through lipolytic effects, while agonism on the latter has been shown to excert antilipolytic effects (Hellström et al., 1997). A role of DA in BAT thermogenesis can therefore still not be fully excluded and dose response experiments *in vivo* with longterm IRT observation of BAT temperature would be helpful to further determine whether a contribution in this key mechanism of energy homeostasis is likely – both centrally and peripherally. Further, species differences must be considered, since,

e.g., the effects of DA on BAT described in studies in the 1980s were observed in rats (Maxwell et al., 1985; Rothwell et al., 1982). Also, in humans, BAT thermogenesis has been shown to be driven by β2-adrenergic receptor (ADRB2) stimulation as opposed to ADRB3 in mice (Blondin et al., 2020), which underlines that, regaredless of the results shown here, an implication of DA in other species, including humans, can not be ruled out.

Aside from effects of DA, which can act unspecifically on different receptor types other than DRDs, the peripheral effects of the DRD1- and DRD2-agonists (or lack thereof) leave the question whether or not DRD1 and DRD2 are actually present in BAT and WAT.

4.3 LC-MS/MS Analysis

To ascertain the fundamental possibility of a direct and dopamine receptor-mediated effect of the DRD1- and DRD2-agonist on adipoise tissue thermogenesis, it was expedient to investigate whether dopamine receptors are indeed present in iBAT and iWAT. Leading up to the presented project, preliminary studies *in vitro* and *ex vivo* were undertaken, which nicely demonstrated the presence of DRD1 and DRD2 in iBAT (Kohlie et al., 2017). The study also showed a DRD1-mediated increase in UCP1 protein, cAMP, and oxygen consumption *in vitro* in brown adipocytes upon treatment with DA or the DRD1-agonist. However, during analysis of the data presented here, both *ex vivo* and *in vivo* results did not confirm these preliminary findings – therefore, raising the question of dopamine receptor presence in iBAT and iWAT, again.

Surprisingly, upon researching the quality of antibodies available for DRD1 and DRD2, including those that were used in previous studies, it was discovered, very recently at the time, that a knockout study found the majority of commonly used DRD1- and DRD2-antibodies to be unspecific (Stojanovic et al., 2017). In fact, out of all DRD1 and DRD2 antibodies tested, only one of each kind (Anti-DRD1: D2944, monoclonal, Sigma; Anti-DRD2: AB5084P, polyclonal, Millipore) were proven specific, yet these were not used by Kohlie et al., 2017. Remarkably, the specificity of the polyclonal DRD2-antibody AB5084P varied greatly inbetween batches and could not be confirmed to be specific when tested in two further batches for the presented study.

Nevertheless, immunoblots, even with the proven specific DRD1-antibody D2944, were inconclusive in the presented experiments. Moreover, qRT-PCR did not yield detectable amplification of DRD1 or DRD2 in iBAT or iWAT. Therefore, an LC-MS/MS approach was used as a method of higher sensitivity in the attempt to detect receptors of potentially

very low abundance in adipose tissues. Yet, neither receptor subtype emerged in the proteomics data readout in either adipose depot, leading to the conclusion, that DRD1 and DRD2 in iBAT and iWAT are either present in extremely low abundance, or not at all. Since DRD2 was also not detected in striatum samples, it must be considered that proteins of comparatively low abundance were not detected in this approach, and that DRDs in adipose tissues are among them. During sample preparation, a total of eight subfractions of enriched membrane proteins of each sample was prepared. For this thesis, the first fraction of each sample was run by LC-MS/MS. It would be of great interest to analyze the remaining samples in the future to identify proteins of even lower abundance – potentially including DRDs – in adipose tissue.
Interestingly, DRD1 and DRD2 have been reported to be present in human pre-adipocytes and mature adipocytes (Borcherding et al., 2011), which was determined using qRT-PCR and immunoblotting. However, neither information about Ct values is available, nor could knockout validation studies for the used antibodies be found. Therefore, the results may be handled with caution.

Nevertheless, the resulting proteomics data set gave ample insight into the differences in composition of BAT and WAT, which were further investigated. The resulting list of potential marker candidates may be of great use in future studies in order to not only help distinguish between adipose depots, but potentially also between single cells in approaches to determine the cellular heterogeneity of adipose tissue samples; and aid lineage determination *ex vivo* and *in vitro*. Moreover, these markers may help establish differentiation protocols for white, beige, or brown adipocytes *in vitro* for immortalized pre-adipocyte cell lines, primary adipose-derived stem cells, or even induced pluripotent stem cells. Furthermore, some of these markers additionally bear the potential to evaluate the state of thermogenic activity of each cell type, which makes them helpful tools in the validation process in a vast array of experimental approaches regarding adipose tissue biology in general, and BAT thermogenesis in particular.

Besides, three markers stood out for different reasons: Firstly, *C12orf73*, which allowed for distinction between iBAT and iWAT and was significantly lower expressed in less thermogenically activated samples (iBAT 23°C > iBAT 30°C > iWAT 10°C > iWAT 23°C), but not higher expressed in activated BAT (BAT 10°C = BAT 23°C). This marker presented as a completely unidentified membrane protein at the time of analysis (2018). Very recently,

on May 17 2023 information about the identification and functionality of the according (human) gene (Gene ID 728568) was uploaded to the "NIH- Gene" website. An entry for the mouse ortholog followed on August 5 2023 (Gene ID 544717). In these entries, the gene is introduced under two new names, *Uqcc6* and *Brawnin*. At the time of search (August 14 2023, 06:32:00, GMT+1), PubMed retrieved 22 entries for "C12orf73", 38 for "BRAWNIN", as first named in 2020 (S. Zhang et al., 2020), 2 for "Uqcc6", both published in 2023, 11 for "id: 728568", and 14 for "id: 544717". While in one of these studies, "*Brawnin*" was shown to be present in BAT but not WAT of mice using a custom antibody, in supplementary material (S. Zhang et al., 2020), the presented results of this thesis, independently of these findings, are the first to demonstrate that a) *C12orf73* is the number one most abundant peptide, as identified by LC-MS/MS of enriched membrane protein samples, in iBAT from C57BL/6NCrl mice, followed by UCP1 as the second most abundant, while lowly abundant in iWAT; and b) *C12orf73* mRNA expression significantly correlates with the temperature induced state of thermogenic activity of iBAT and iWAT from C57BL/6NCrl mice; therefore being the first to truly validate the implicit new name "BRAWNIN". Our results, taken together with published functional studies that showed BRAWNIN to be required for the assembly of mitochondrial respiratory chain complex III (Dennerlein et al., 2021; S. Zhang et al., 2020), validate this peptide to be a solid marker for BAT distinction, BAT whitening, as well as browning of WAT, which may be very useful in future studies on BAT thermogenesis.

Secondly, *Adig2* was seen to be regulated in exact opposite ways in iBAT thermogenesis activation (upregulation) and iWAT thermogenesis activation or "browning" (downregulation). This phenomenon seems quite unique but needs to be investigated further to potentially be exploited in future studies. So far, it is known that *Adig2* (or "small adipocyte factor 1", *Smaf1*) is predominantly expressed in mature adipocytes, not in the stromal vascular fraction, and that expression is induced during adipocyte differentiation and declines again under TNFα-induced dedifferentiation (Kim et al., 2004). Moreover, mRNA expression is upregulated in subcutaneous and visceral fat of mice on a high fat diet and the protein is localized in membranes and not cytosol (Hong et al., 2005). Also, *Adig2* has been found in fatty liver caused by PPARγ1-overexpression (S. Yu et al., 2003). Most interestingly though, *Adig2* has been proposed to regulate leptin expression in humans (Kilpeläinen et al., 2016), and studies in *Adig*$^{-/-}$ mice revealed that mutant mice showed a leaner phenotype, reduced plasma leptin and impaired leptin secretion compared to wild-type (Alvarez-Guaita et al., 2021). All of which make it a highly

interesting target to consider when investigating adipocyte biology in general, and adipose tissue thermogenesis in particular.

Lastly *Vnn1* was identified as the only WAT specific marker candidate that could also distinguish well between all tested thermogenic activity states of iWAT (iWAT 30°C > iWAT 23°C > iWAT 10°C > iBAT 23°C), making it appear to be a true white marker. *Vnn1* codes for the enzyme pantetheinase, which trasforms D-pantethein into pantothenic acid (vitamin B5) by hydrolysis (Maras et al., 1999). Besides implications in inflammation, oxidative stress, and cell migration, VNN1 has been suggested to play a role in key metabolic processes, including hepatic lipid metabolism and glucose metabolism, e.g., increased *Vnn1* expression has been observed in steatotic livers of obese mice (Motomura et al., 2012; van Diepen et al., 2016). Interestingly, it has recently been demonstrated, that pantothenic acid – the product of the reaction catalyzed by VNN1 – protects against obesity via brown adipose tissue activation (Zhou et al., 2022). This finding, together with the presented results, leads to the speculation, that VNN1 may potentially act as part of a regulatory feedback mechanism to white fat mass accumulation and thermogenic inactivity, to prevent further metabolic dysbalances by activating counter mechanisms, e.g., browning and BAT thermogenesis activation.

5 CONCLUSION

Overall, our experiments showed that neither the DRD1- or DRD2-agonists, nor DA had a significant impact on iBAT thermogenesis upon peripheral treatment. These findings do, however, not rule out an effect of either substance on BAT thermogenesis entirely. Different routes of application, duration of treatment, dosage, and measurement timepoints could potentially lead to different results; as could application in different species. Also, a peripheral effect of DA on BAT thermogenesis can explicitly not be ruled out entirely, since different concentrations of DA evidentially have different effects *in vivo*.

Nevertheless, our study strongly raises the question about wether or not DRDs are present in BAT and WAT, since every effort to detect them was in vain. If at all present, their abundance must be extremely low and, moving forward, could be tried to be unravelled in an isotope-labelled LC-MS/MS approach.

All these results taken together lead to the assumption that peripheral DA has no significant and physiologically relevant effect on BAT thermogenesis via DRDs in mice.

However, the limitations of the presented experiments regarding translational relevance must be born in mind, since mechanisms of catecholamine action in, e.g., humans can vary greatly from that in rodents, as discussed. Therefore, it would be highly interesting to investigate potential central and peripheral dopaminergic effects on BAT thermogenesis in humans moving forward.

Perhaps the most exciting finding of this study is the list of potential new markers for the distinction between adipose depots and their respective state of thermogenic acitivity. The generated proteomics dataset of enriched membrane proteins of iBAT and iWAT is – to our knowledge – the first of its kind, and its analysis reveals promising new insight into lesser known players in adipose tissue regulation. This data poses a meaningful resource for future studies.

Moreover, initial (cross-) validation of a short list of candidates was successful and identified interesting candidates, one of which has not been described before in the context of BAT-thermogenesis regulation and – strikingly – was the most abundant protein in the membrane enriched fraction of iBAT, ahead of UCP1, that is only sparsely abundant in iWAT at the same time. Gene expression validation of this marker in adipose tissues of different states of thermogenic activity presents the first approach to truly justify the previously published, implicit new name of this candidate – BRAWNIN.

6 APPENDIX

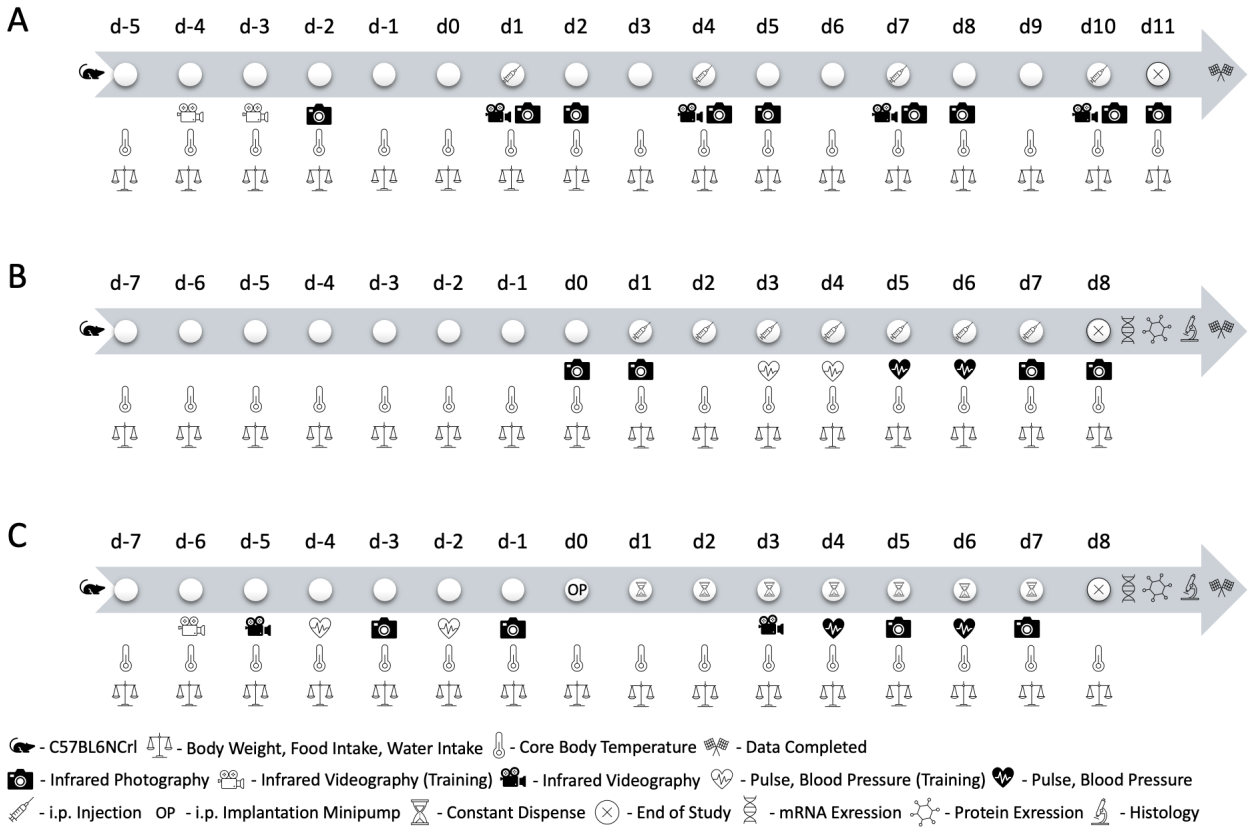

Figure 6-1: Study design overview.

Single injection in vivo study (1 h) (A). Repeated injection in vivo study (1 week) (B). Constant release in vivo study (1 week) (C).

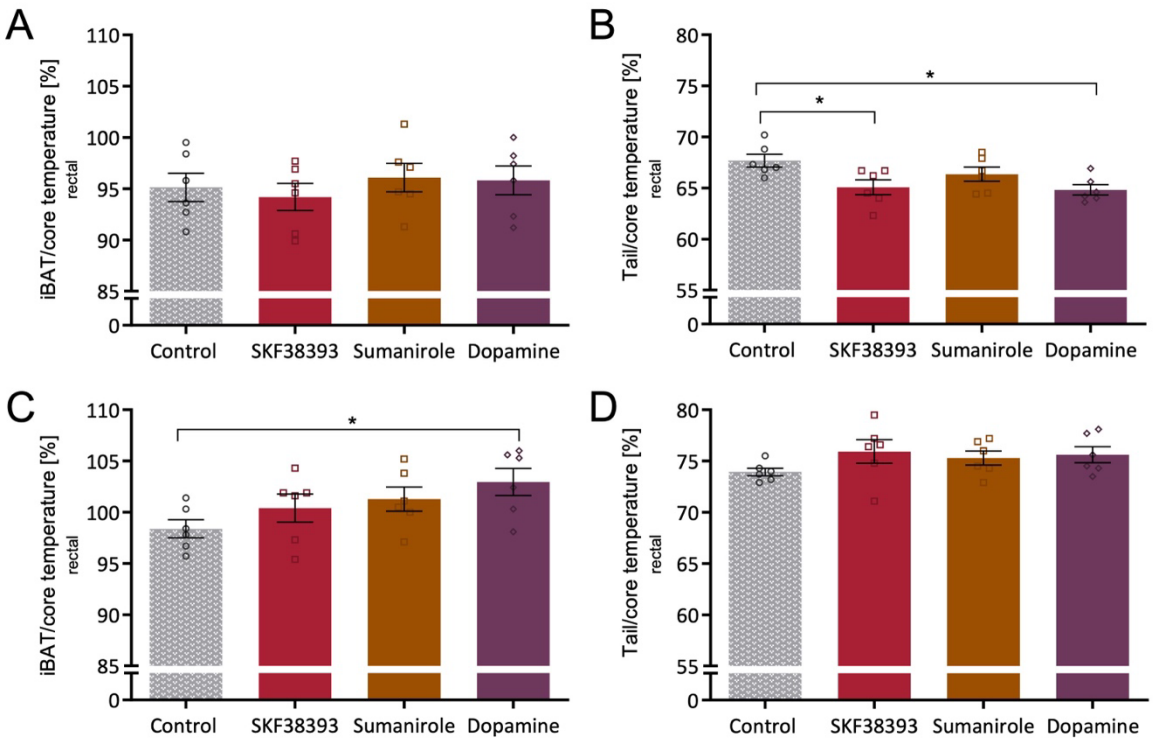

*Figure 6-2: Analysis of iBAT and tail temperature from infrared thermography (IRT) photographs taken 1 h (A, B) or 24 h (C, D) post injection of C57BL/6NCrl mice with the DRD1-agonist, DRD2-agonist, or DA. Data are expressed as mean ± SEM and compared to control by 1 W ANOVA (uncorrected Fisher's LSD). *P < 0.05; n = 6.*

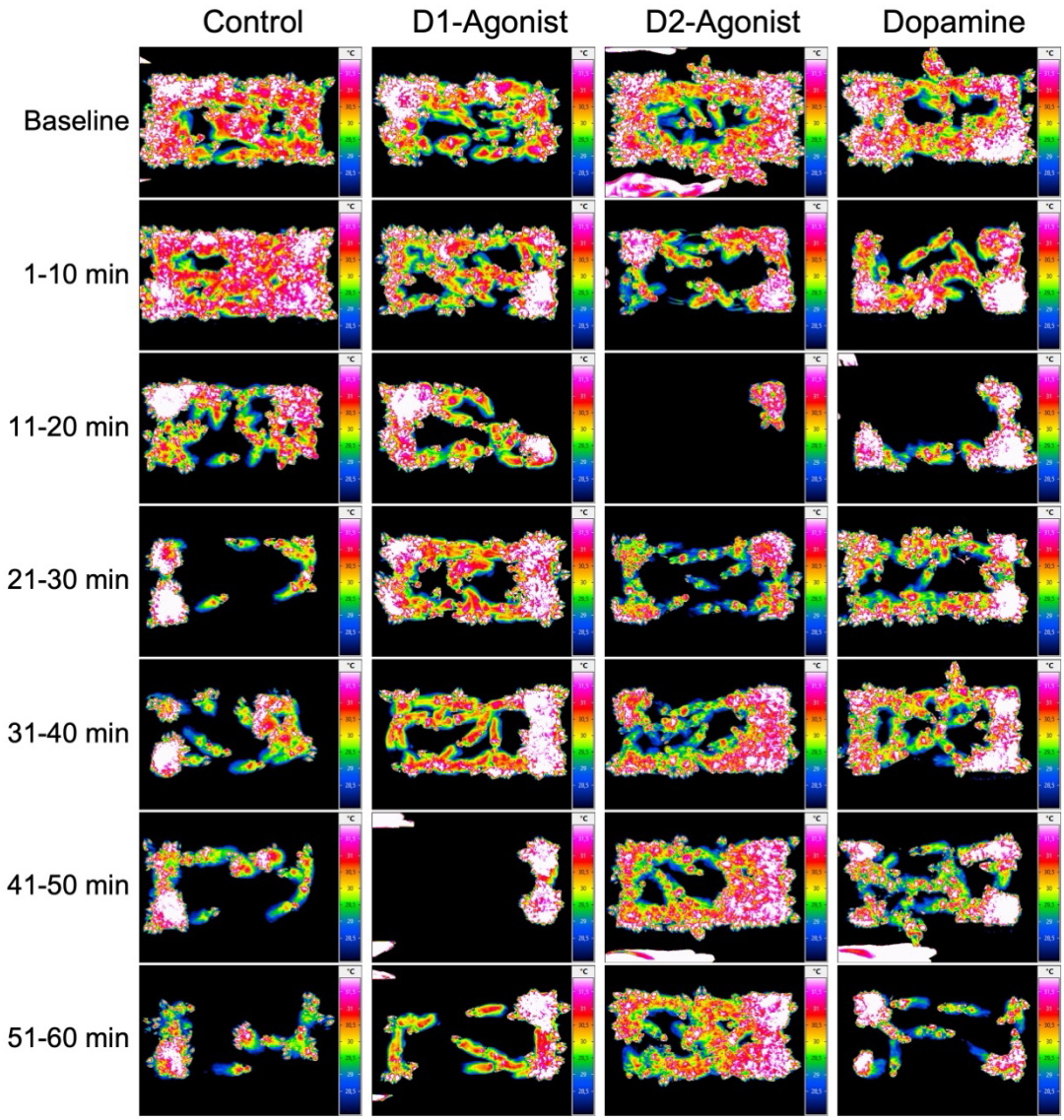

Figure 6-3: Overlay images of infrared thermography (IRT) video after single injections in vivo. 2/6

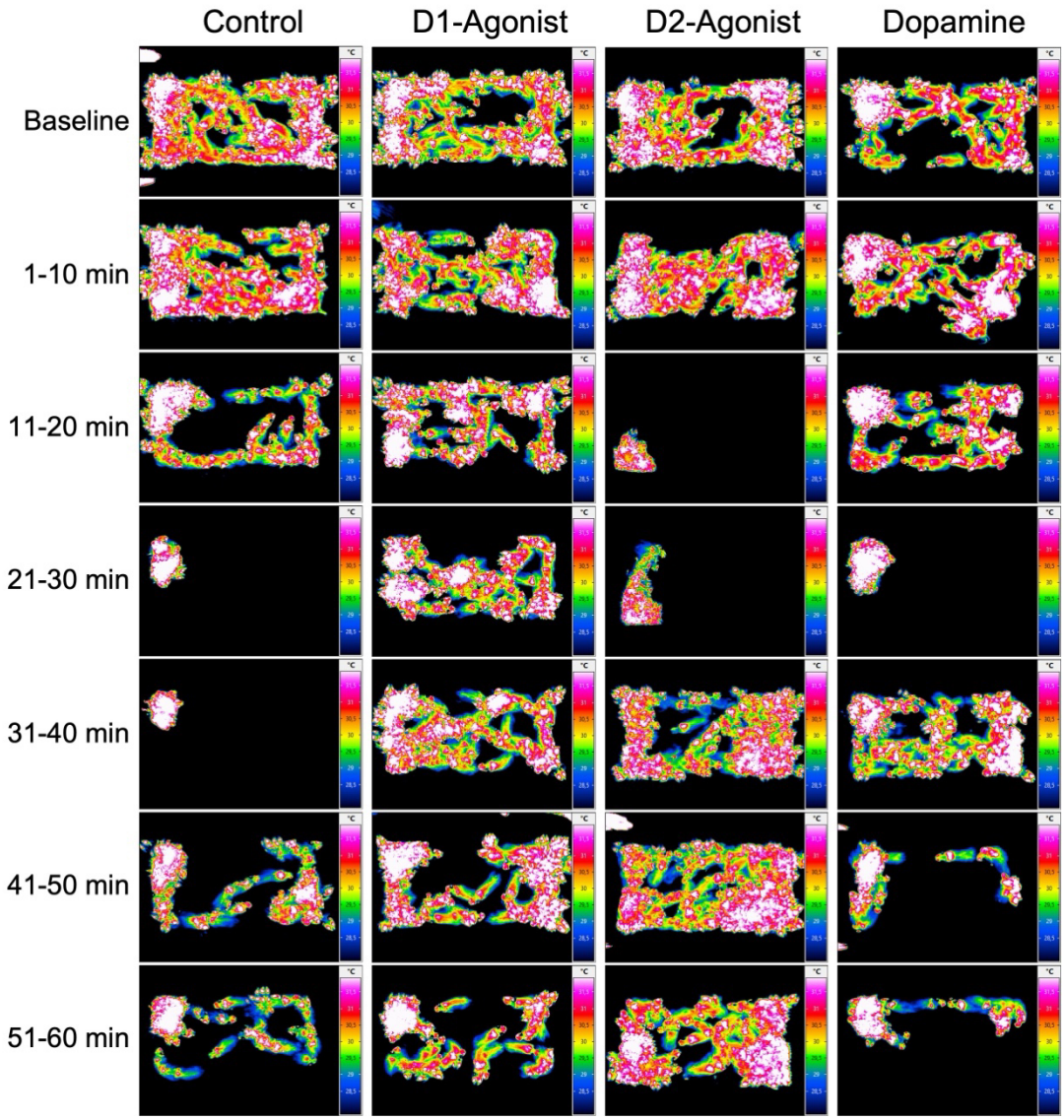

Figure 6-4: Overlay images of infrared thermography (IRT) video after single injections in vivo. 3/6

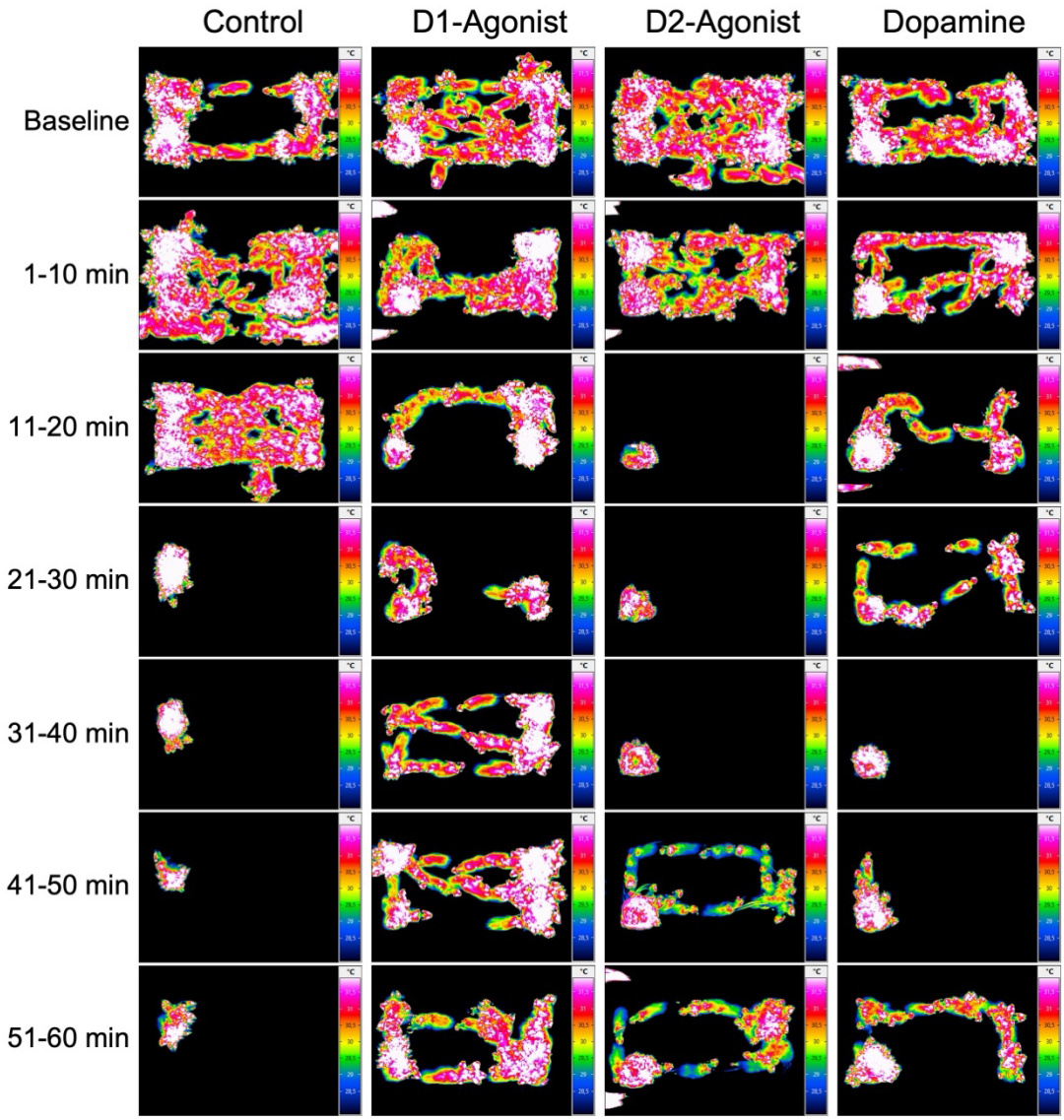

Figure 6-5: Overlay images of infrared thermography (IRT) video after single injections in vivo. 4/6

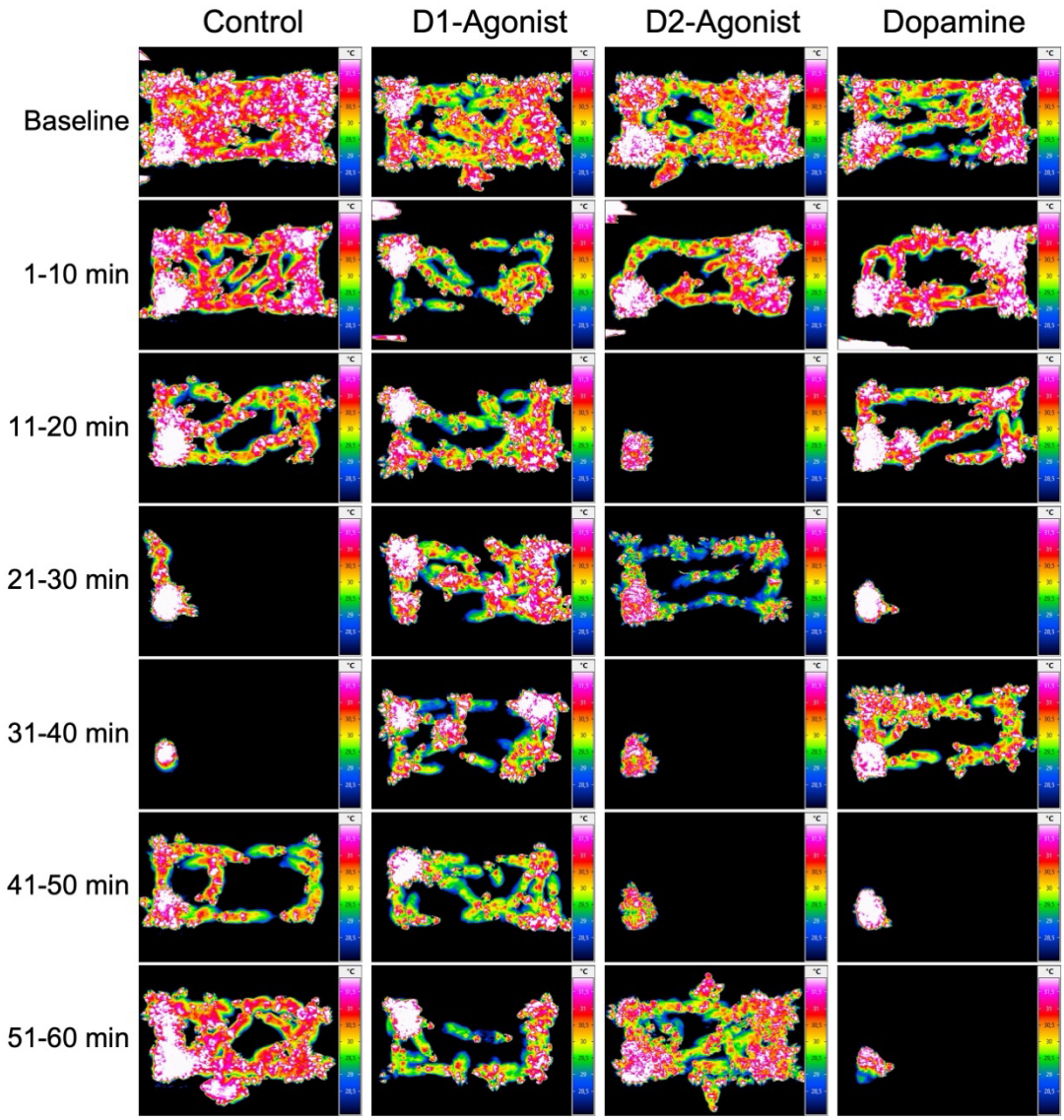

Figure 6-6: Overlay images of infrared thermography (IRT) video after single injections in vivo. 5/6

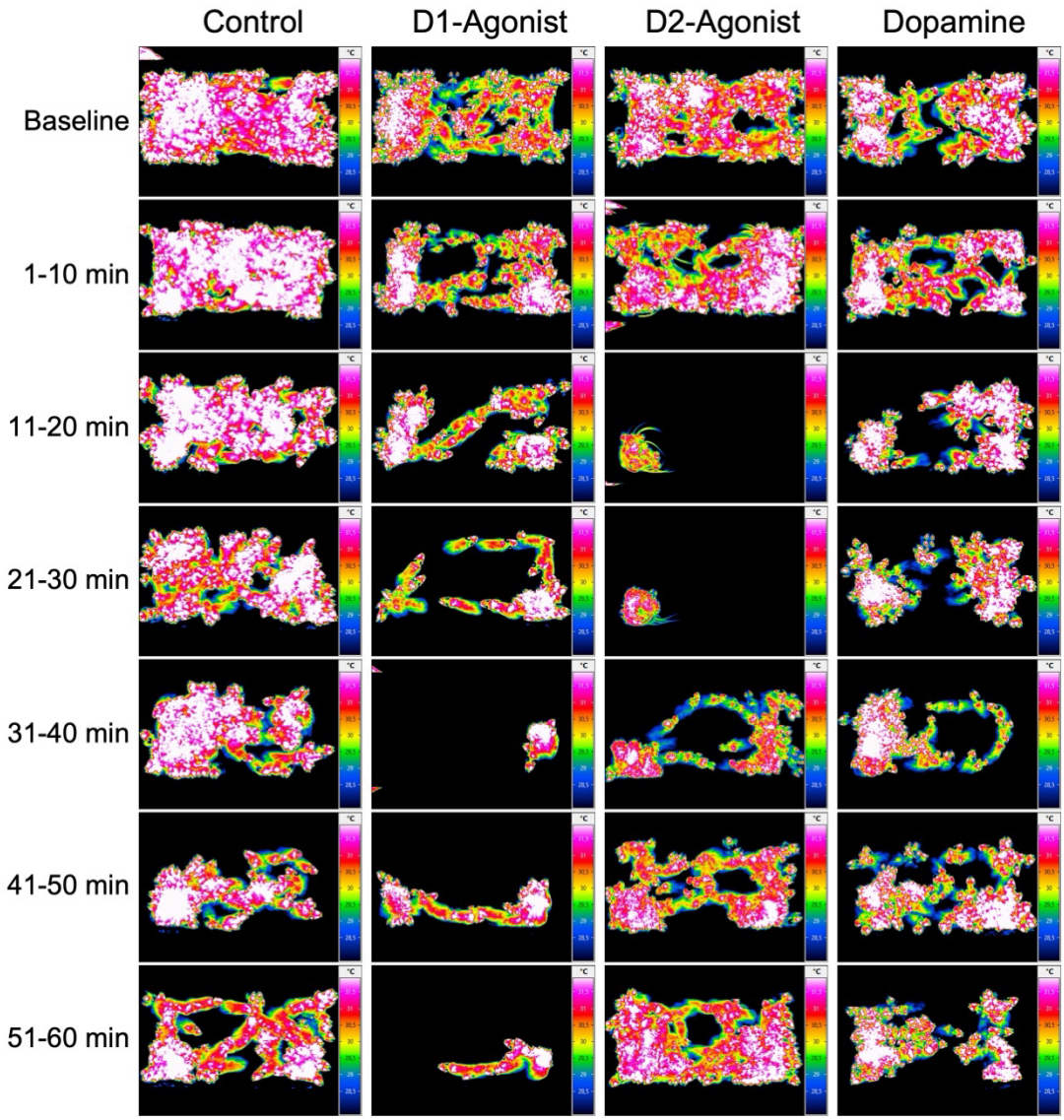

Figure 6-7: Overlay images of infrared thermography (IRT) video after single injections in vivo. 6/6

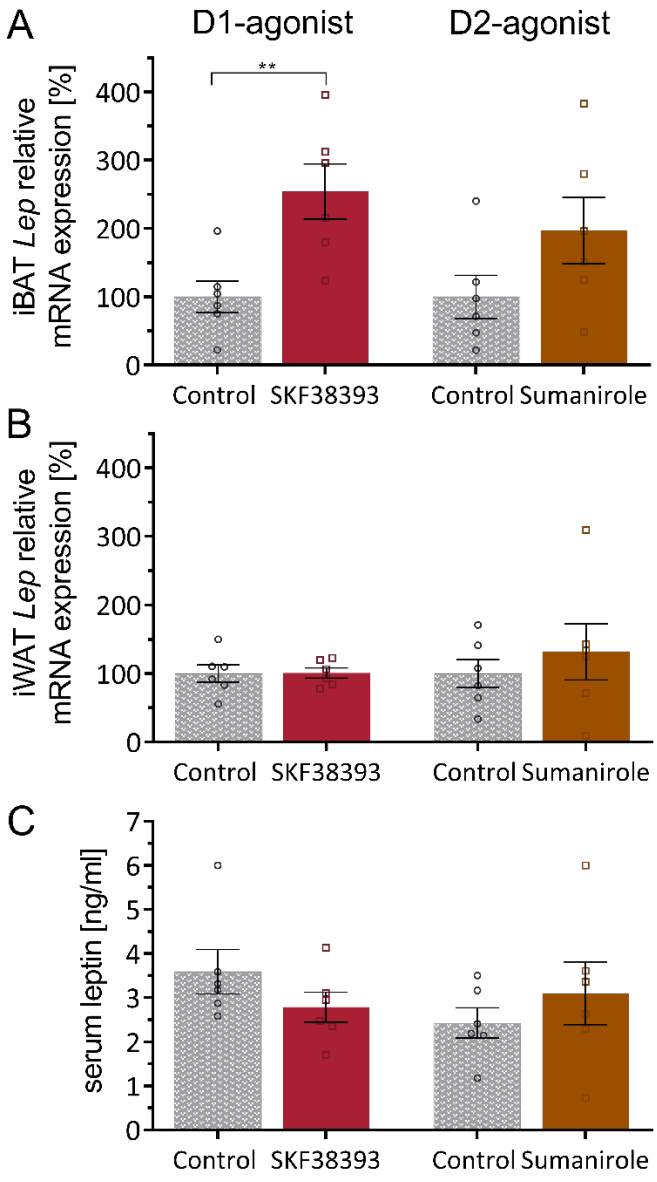

Figure 6-8: Leptin mRNA expression in adipose depots and serum leptin protein after treatment of C57BL/6NCrl mice with the DRD1- or DRD2-agonist for 1 week.

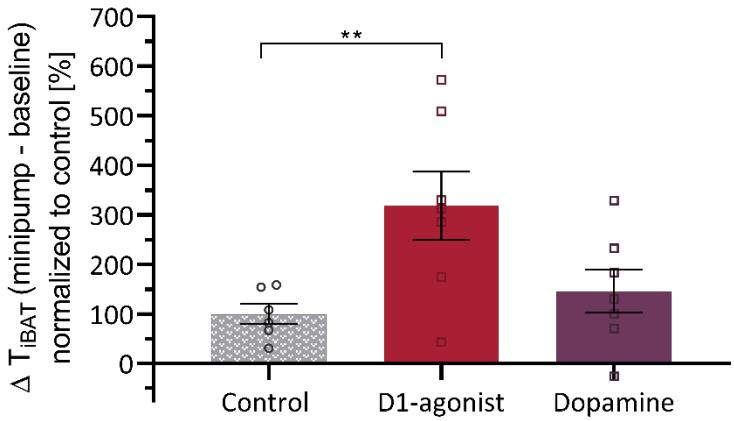

Figure 6-9: iBAT temperature analysis by IRT videography in C57BL/6NCrl mice implanted with minipumps secreting the DRD1-agonist or DA.

7 REFERENCES

Aherne, W., & Hull, D. (1966). Brown adipose tissue and heat production in the newborn infant. *The Journal of Pathology and Bacteriology*, *91*(1), 223–234.

Alvarez-Guaita, A., Patel, S., Lim, K., Haider, A., Dong, L., Conway, O. J., Ma, M. K. L., Chiarugi, D., Saudek, V., O'Rahilly, S., & Savage, D. B. (2021). Phenotypic characterization of Adig null mice suggests roles for adipogenin in the regulation of fat mass accrual and leptin secretion. *Cell Reports*, *34*(10), 108810.

Amenta, F., Ricci, A., Tayebati, S. K., & Zaccheo, D. (2002). The peripheral dopaminergic system: Morphological analysis, functional and clinical applications. *Italian journal of anatomy and embryology = Archivio italiano di anatomia ed embriologia*, *107*(3), 145–167.

Bachmann, K., Chupka, J., Erhardt, P., & White, D. (2007). Application of simple mathematical expressions to relate half-lives of drugs in mice to those in humans. *Drug Metabolism Letters*, *1*(2), 127–129.

Baker, W. L., White, C. M., & Coleman, C. I. (2008). Effect of nonergot dopamine agonists on symptoms of restless legs syndrome. *Annals of Family Medicine*, *6*(3), 253–262.

Barone, P., Lamb, J., Ellis, A., & Clarke, Z. (2007). Sumanirole versus placebo or ropinirole for the adjunctive treatment of patients with advanced Parkinson's disease. *Movement Disorders*, *22*(4), 483–489.

Barros, A. G. de A., Bridi, J. C., de Souza, B. R., de Castro Júnior, C., de Lima Torres, K. C., Malard, L., Jorio, A., de Miranda, D. M., Ashrafi, K., & Romano-Silva, M. A. (2014). Dopamine Signaling Regulates Fat Content through β-Oxidation in Caenorhabditis elegans. *PLoS ONE*, *9*(1), e85874.

Bartness, T. J., Liu, Y., Shrestha, Y. B., & Ryu, V. (2014). Neural innervation of white adipose tissue and the control of lipolysis. *Frontiers in Neuroendocrinology*, *35*(4), 473–493.

Bartness, T. J., Vaughan, C. H., & Song, C. K. (2010a). Sympathetic and sensory innervation of brown adipose tissue. *International Journal of Obesity*, *34*, S36–S42. https://doi.org/10.1038/ijo.2010.182

Bartness, T. J., Vaughan, C. H., & Song, C. K. (2010b). Sympathetic and sensory innervation of brown adipose tissue. *International Journal of Obesity*, *34*(1), S36–S42. https://doi.org/10.1038/ijo.2010.182

Behrens, W. A., & Depocas, F. (1977). Dopamine β-hydroxylase and cytochrome oxidase activities in brown adipose tissue of newborn rats following sympathectomy with 6-hydroxydopamine. *Canadian Journal of Physiology and Pharmacology*, *55*(3), 695–699.

Bengtsson, T., Redegren, K., Strosberg, A. D., Nedergaard, J., & Cannon, B. (1996). Down-

regulation of β3 adrenoreceptor gene expression in brown fat cells is transient and recovery is dependent upon a short-lived protein factor. *Journal of Biological Chemistry*, *271*(52), 33366–33375.

Bhatia, A., Lenchner, J. R., & Saadabadi, A. (2024). Biochemistry, Dopamine Receptors. In *StatPearls*. StatPearls Publishing.

Bhattacharya, R., Sinha, S., Yang, S.-P., Patra, C., Dutta, S., Wang, E., & Mukhopadhyay, D. (2008). The neurotransmitter dopamine modulates vascular permeability in the endothelium. *Journal of Molecular Signaling*, *3*, 14.

Bianco, A. C., & McAninch, E. A. (2013). The role of thyroid hormone and brown adipose tissue in energy homoeostasis. *The Lancet Diabetes and Endocrinology*, *1*(3), 250–258.

Bianco, A. C., Salvatore, D., Gereben, B. Z., Berry, M. J., & Larsen, P. R. (2002). Biochemistry, Cellular and Molecular Biology, and Physiological Roles of the Iodothyronine Selenodeiodinases. *Endocrine Reviews*, *23*(1), 38–89.

Bianco, A. C., & Silva, J. E. (1987). Intracellular conversion of thyroxine to triiodothyronine is required for the optimal thermogenic function of brown adipose tissue. *Journal of Clinical Investigation*, *79*(1), 295–300.

Blaschko, H. (1942). The activity of l(—)-Dopa decarboxylase. *The Journal of Physiology*, *101*(3), 337–349.

Blondin, D. P., Nielsen, S., Kuipers, E. N., Severinsen, M. C., Jensen, V. H., Miard, S., Jespersen, N. Z., Kooijman, S., Boon, M. R., Fortin, M., Phoenix, S., Frisch, F., Guérin, B., Turcotte, É. E., Haman, F., Richard, D., Picard, F., Rensen, P. C. N., Scheele, C., & Carpentier, A. C. (2020). Human Brown Adipocyte Thermogenesis Is Driven by β2-AR Stimulation. *Cell Metabolism*, *32*(2), 287-300.e7.

Borcherding, D. C., Hugo, E. R., Idelman, G., De Silva, A., Richtand, N. W., Loftus, J., & Ben-Jonathan, N. (2011). Dopamine Receptors in Human Adipocytes: Expression and Functions. *PLoS ONE*, *6*(9), e25537.

Boulant, J. A. (2000). Role of the Preoptic-Anterior Hypothalamus in Thermoregulation and Fever. *Clinical Infectious Diseases*, *31*(Supplement_5), S157–S161.

Boulay, D., Depoortere, R., Perrault, G., & Sanger, D. J. (2000). Decreased locomotor activity after microinjection of dopamine D2/D3 receptor agonists and antagonists into lobule 910 of the cerebellum: A D3 receptor mediated effect? *Progress in Neuro-Psychopharmacology and Biological Psychiatry*, *24*(1), 39–49.

Cannon, B., & Nedergaard, J. (2001). Cultures of adipose precursor cells from brown adipose tissue and of clonal brown-adipocyte-like cell lines. *Methods in molecular biology (Clifton, N.J.)*, *155*, 213–224.

Cannon, B., & Nedergaard, J. (2004). Brown Adipose Tissue: Function and Physiological Significance. *Physiological Reviews*, *84*(1), 277–359.

Cao, W.-H., & Morrison, S. F. (2006). Glutamate receptors in the raphe pallidus mediate brown adipose tissue thermogenesis evoked by activation of dorsomedial hypothalamic neurons. *Neuropharmacology*, *51*(3), 426–437.

Cedikova, M., Kripnerová, M., Dvorakova, J., Pitule, P., Grundmanova, M., Babuska, V., Mullerova, D., & Kuncova, J. (2016). Mitochondria in White, Brown, and Beige Adipocytes. *Stem Cells International*, *2016*, 6067349.

Chen, Y., Siegel, F., Kipschull, S., Haas, B., Fröhlich, H., Meister, G., & Pfeifer, A. (2013). MiR-155 regulates differentiation of brown and beige adipocytes via a bistable circuit. *Nature Communications*, *4*(1), 1–13.

Cho, Y. K., Lee, S., Lee, J., Doh, J., Park, J.-H., Jung, Y.-S., & Lee, Y.-H. (2023). Lipid remodeling of adipose tissue in metabolic health and disease. *Experimental & Molecular Medicine*, *55*(9), 1955–1973.

Contreras, C., Nogueiras, R., Diéguez, C., Rahmouni, K., & López, M. (2017). Traveling from the hypothalamus to the adipose tissue: The thermogenic pathway. *Redox Biology*, *12*, 854–863.

Cornil, C. A., & Ball, G. F. (2008). Interplay among catecholamine systems: Dopamine binds to α 2-adrenergic receptors in birds and mammals. *Journal of Comparative Neurology*, *511*(5), 610–627.

de Jesus, L. A., Carvalho, S. D., Ribeiro, M. O., Schneider, M., Kim, S. W., Harney, J. W., Larsen, P. R., & Bianco, A. C. (2001). The type 2 iodothyronine deiodinase is essential for adaptive thermogenesis in brown adipose tissue. *The Journal of Clinical Investigation*, *108*(9), 1379–1385.

De Meis, L., Ketzer, L. A., Da Costa, R. M., De Andrade, I. R., & Benchimol, M. (2010). Fusion of the Endoplasmic Reticulum and Mitochondrial Outer Membrane in Rats Brown Adipose Tissue: Activation of Thermogenesis by Ca2+. *PLoS ONE*, *5*(3), e9439.

Dennerlein, S., Poerschke, S., Oeljeklaus, S., Wang, C., Richter-Dennerlein, R., Sattmann, J., Bauermeister, D., Hanitsch, E., Stoldt, S., Langer, T., Jakobs, S., Warscheid, B., & Rehling, P. (2021). Defining the interactome of the human mitochondrial ribosome identifies SMIM4 and TMEM223 as respiratory chain assembly factors. *eLife*, *10*, e68213.

Dorn, C., Riener, M.-O., Kirovski, G., Saugspier, M., Steib, K., Weiss, T. S., Gäbele, E., Kristiansen, G., Hartmann, A., & Hellerbrand, C. (2010). Expression of fatty acid synthase in nonalcoholic fatty liver disease. *International Journal of Clinical and Experimental Pathology*, *3*(5), 505–514.

El-Mas, M. M., El-Din, M. M. M., El-Gowilly, S. M., & Sharabi, F. M. (2005). The alpha1-

adrenergic receptor not the DA(1)-dopaminergic receptor mediates cyclosporine-SKF38393 renovascular interaction. *Canadian Journal of Physiology and Pharmacology*, *83*(12), 1129–1136.

Esteve Ràfols, M. (2014). Adipose tissue: Cell heterogeneity and functional diversity. *Endocrinologia Y Nutricion: Organo De La Sociedad Espanola De Endocrinologia Y Nutricion*, *61*(2), 100–112. https://doi.org/10.1016/j.endonu.2013.03.011

Ezquerra-Romano, I., & Ezquerra, A. (2017). Highway to thermosensation: A traced review, from the proteins to the brain. *Reviews in the Neurosciences*, *28*(1), 45–57.

Fedorenko, A., Lishko, P. V., & Kirichok, Y. (2012). Mechanism of Fatty-Acid-Dependent UCP1 Uncoupling in Brown Fat Mitochondria. *Cell*, *151*(2), 400–413.

Folgueira, C., Beiroa, D., Porteiro, B., Duquenne, M., Puighermanal, E., Fondevila, M. F., Barja-Fernández, S., Gallego, R., Hernández-Bautista, R., Castelao, C., Senra, A., Seoane-Collazo, P., Gómez-Lado, N., Aguiar, P., Guallar, D., Fidalgo, M., Romero-Pico, A., Adan, R., Blouet, C., … Nogueiras, R. (2019). Hypothalamic dopamine signalling regulates brown fat thermogenesis. *Nature Metabolism*, *1*(8), 811–829.

Fryar, C. D. (2018). *Prevalence of Overweight, Obesity, and Severe Obesity Among Adults Aged 20 and Over: United States, 1960–1962 Through 2015–2016*.

Gangopadhyay, A., Ibrahim, R., Theberge, K., May, M., & Houseknecht, K. L. (2022). Non-alcoholic fatty liver disease (NAFLD) and mental illness: Mechanisms linking mood, metabolism and medicines. *Frontiers in Neuroscience*, *16*, 1042442.

Geerling, E., Hameed, M., Weger-Lucarelli, J., & Pinto, A. K. (2022). Metabolic syndrome and aberrant immune responses to viral infection and vaccination: Insights from small animal models. *Frontiers in Immunology*, *13*.

Goldgof, M., Xiao, C., Chanturiya, T., Jou, W., Gavrilova, O., & Reitman, M. L. (2014). The Chemical Uncoupler 2,4-Dinitrophenol (DNP) Protects against Diet-induced Obesity and Improves Energy Homeostasis in Mice at Thermoneutrality. *The Journal of Biological Chemistry*, *289*(28), 19341–19350.

Gordon, C. J. (1990). Thermal biology of the laboratory rat. *Physiology and Behavior*, *47*(5), 963–991.

Grandbois, J., Khurana, S., Graff, K., Nguyen, P., Meltz, L., & Tai, T. C. (2016). Phenylethanolamine N-methyltransferase gene expression in adrenergic neurons of spontaneously hypertensive rats. *Neuroscience Letters*, *635*, 103–110.

Graves, S. M., Xie, Z., Stout, K. A., Zampese, E., Burbulla, L. F., Shih, J. C., Kondapalli, J., Patriarchi, T., Tian, L., Brichta, L., Greengard, P., Krainc, D., Schumacker, P. T., & Surmeier, D. J. (2020). Dopamine metabolism by a monoamine oxidase mitochondrial shuttle activates the electron transport chain. *Nature neuroscience*, *23*(1), 15–20.

Grundlingh, J., Dargan, P. I., El-Zanfaly, M., & Wood, D. M. (2011). 2,4-Dinitrophenol (DNP): A Weight Loss Agent with Significant Acute Toxicity and Risk of Death. *Journal of Medical Toxicology*, *7*(3), 205–212.

Habuchi, Y., Tanaka, H., Nishio, M., Yamamoto, T., Komori, T., Morikawa, J., & Yoshimura, M. (1997). Dopamine stimulation of cardiac β-adrenoceptors: The involvement of sympathetic amine transporters and the effect of SKF38393. *British Journal of Pharmacology*, *122*(8), 1669–1678.

Hein, L., & Kobilka, B. K. (1995). Adrenergic receptor signal transduction and regulation. *Neuropharmacology*, *34*(4), 357–366.

Hellström, L., Rössner, S., Hagström-Toft, E., & Reynisdottir, S. (1997). Lipolytic catecholamine resistance linked to alpha 2-adrenoceptor sensitivity—A metabolic predictor of weight loss in obese subjects. *International Journal of Obesity and Related Metabolic Disorders: Journal of the International Association for the Study of Obesity*, *21*(4), 314–320.

Hepatology, T. L. G. &. (2021). Obesity: Another ongoing pandemic. *The Lancet Gastroenterology & Hepatology*, *6*(6), 411.

Himms-Hagen, J. (1990). Brown adipose tissue thermogenesis: Interdisciplinary studies. *The FASEB Journal*, *4*(11), 2890–2898.

Himms-Hagen, J., Cui, J., Danforth, E., Taatjes, D. J., Lang, S. S., Waters, B. L., & Claus, T. H. (1994). Effect of CL-316,243, a thermogenic β3-agonist, on energy balance and brown and white adipose tissues in rats. *American Journal of Physiology - Regulatory Integrative and Comparative Physiology*, *266*(4 35-4).

Hong, Y.-H., Hishikawa, D., Miyahara, H., Tsuzuki, H., Nishimura, Y., Gotoh, C., Choi, K.-C., Hokari, Y., Takagi, Y., Lee, H.-G., Cho, K., Roh, S.-G., & Sasaki, S. (2005). Up-regulation of adipogenin, an adipocyte plasma transmembrane protein, during adipogenesis. *Molecular and Cellular Biochemistry*, *276*(1), 133–141.

Horvitz, J. C., Williams, G., & Joy, R. (2001). Time-dependent actions of D2 family agonist quinpirole on spontaneous behavior in the rat: Dissociation between sniffing and locomotion. *Psychopharmacology*, *154*(4), 350–355.

Houtz, J., Liao, G.-Y., An, J. J., & Xu, B. (2021). Discrete TrkB-expressing neurons of the dorsomedial hypothalamus regulate feeding and thermogenesis. *Proceedings of the National Academy of Sciences of the United States of America*, *118*(4), e2017218118.

Hsieh, A. C. L., & Carlson, L. D. (1957). Role of Adrenaline and Noradrenaline in Chemical Regulation of Heat Production. *American Journal of Physiology-Legacy Content*, *190*(2), 243–246.

Hsieh, A. C. L., Carlson, L. D., & Gray, G. (1957). Role of the Sympathetic Nervous System

in the Control of Chemical Regulation of Heat Production. *American Journal of Physiology-Legacy Content*.

Huttunen, J. K., & Steinberg, D. (1971). Activation and phosphorylation adipose tissue hormone-sensitive lipase by cyclic AMP-dependent protein kinase. *Biochimica et Biophysica Acta (BBA) - Lipids and Lipid Metabolism*, *239*(3), 411–427.

Ikeda, K., Kang, Q., Yoneshiro, T., Camporez, J.P., Maki, H. (2017). UCP1-independent signaling involving SERCA2b-mediated calcium cycling regulates beige fat thermogenesis and systemic glucose homeostasis. *Nature Medicine*, *23*(12), 1454-1465.

Jackson, D. M., Ross, S. B., & Hashizume, M. (1988). Further studies on the interaction between bromocriptine and SKF38393 in reserpine and alpha methyl-para-tyrosine-treated mice. *Psychopharmacology*, *94*(3), 321–327.

Jensen-Urstad, A. P. L., & Semenkovich, C. F. (2012). Fatty acid synthase and liver triglyceride metabolism: Housekeeper or messenger? *Biochimica et Biophysica Acta*, *1821*(5), 747–753.

Johann, K., Cremer, A. L., Fischer, A. W., Heine, M., Pensado, E. R., Resch, J., Nock, S., Virtue, S., Harder, L., Oelkrug, R., Astiz, M., Brabant, G., Warner, A., Vidal-Puig, A., Oster, H., Boelen, A., López, M., Heeren, J., Dalley, J. W., … Mittag, J. (2019). Thyroid-Hormone-Induced Browning of White Adipose Tissue Does Not Contribute to Thermogenesis and Glucose Consumption. *Cell Reports*, *27*(11), 3385-3400.e3.

Jung, E.-Y., & Shim, I. (2011). Differential DAergic Control of D1 and D2 Receptor Agonist Over Locomotor Activity and GABA Level in the Striatum. *Experimental Neurobiology*, *20*(3), 153–157.

Kamien, J. B., & Woolverton, W. L. (1985). The D1 dopamine agonist SKF 38393 functions as a discriminative stimulus in rats. *Psychopharmacology*, *87*(3), 368–370.

Kilpeläinen, T. O., Carli, J. F. M., Skowronski, A. A., Sun, Q., Kriebel, J., Feitosa, M. F., Hedman, Å. K., Drong, A. W., Hayes, J. E., Zhao, J., Pers, T. H., Schick, U., Grarup, N., Kutalik, Z., Trompet, S., Mangino, M., Kristiansson, K., Beekman, M., Lyytikäinen, L.-P., … Loos, R. J. F. (2016). Genome-wide meta-analysis uncovers novel loci influencing circulating leptin levels. *Nature Communications*, *7*(1), Article 1.

Kim, J. Y., Tillison, K., & Smas, C. M. (2004). Cloning, expression, and differentiation-dependent regulation of SMAF1 in adipogenesis. *Biochemical and Biophysical Research Communications*, *326*(1), 36–44.

Kjær, M., Howlett, K., Langfort, J., Zimmerman-Belsing, T., Lorentsen, J., Bülow, J., Ihlemann, J., Feldt-Rasmussen, U., & Galbo, H. (2000). Adrenaline and glycogenolysis in skeletal muscle during exercise: A study in adrenalectomised humans. *The Journal of Physiology*, *528*(Pt 2), 371–378.

Klaus, S., Muzzin, P., Revelli, J. P., Cawthome, M. A., Giacobino, J. P., & Ricquier, D. (1995). Control of β3-adrenergic receptor gene expression in brown adipocytes in culture. *Molecular and Cellular Endocrinology*, *109*(2), 189–195.

Kohlie, R., Perwitz, N., Resch, J., Schmid, S. M., Lehnert, H., Klein, J., & Iwen, K. A. (2017). Dopamine directly increases mitochondrial mass and thermogenesis in brown adipocytes. *Journal of Molecular Endocrinology*, *58*(2), 57–66.

Labbé, S. M., Caron, A., Lanfray, D., Monge-Rofarello, B., Bartness, T. J., & Richard, D. (2015). Hypothalamic control of brown adipose tissue thermogenesis. *Frontiers in Systems Neuroscience*, *9*, 150.

Lee, P., Bova, R., Schofield, L., Bryant, W., Dieckmann, W., Slattery, A., Govendir, M. A., Emmett, L., & Greenfield, J. R. (2016). Brown Adipose Tissue Exhibits a Glucose-Responsive Thermogenic Biorhythm in Humans. *Cell Metabolism*, *23*(4), 602–609.

Lelou, E., Corlu, A., Nesseler, N., Rauch, C., Mallédant, Y., Seguin, P., & Aninat, C. (2022). The Role of Catecholamines in Pathophysiological Liver Processes. *Cells*, *11*(6), 1021.

Lidell, M. E. (2019). Brown Adipose Tissue in Human Infants. In A. Pfeifer, M. Klingenspor, & S. Herzig (Hrsg.), *Brown Adipose Tissue* (S. 107–123). Springer International Publishing.

Löschmann, P. A., Smith, L. A., Lange, K. W., Jähnig, P., Jenner, P., & Marsden, C. D. (1992). Motor activity following the administration of selective D-1 and D-2 dopaminergic drugs to MPTP-treated common marmosets. *Psychopharmacology*, *109*(1–2), 49–56.

Lv, Y.-G., & Liu, J. (2007). Effect of transient temperature on thermoreceptor response and thermal sensation. *Building and Environment*, *42*(2), 656–664.

MacGregor, D. A., Smith, T. E., Prielipp, R. C., Butterworth, J. F., James, R. L., & Scuderi, P. E. (2000). Pharmacokinetics of Dopamine in Healthy Male Subjects. *Anesthesiology*, *92*(2), 338.

Mackenzie, R. A., Burke, D., Skuse, N. F., & Lethlean, A. K. (1975). Fibre function and perception during cutaneous nerve block. *Journal of Neurology, Neurosurgery, and Psychiatry*, *38*(9), 865–873.

Manerba, M., Govoni, M., Manet, I., Leale, A., Comparone, A., & Di Stefano, G. (2019). Metabolic activation triggered by cAMP in MCF-7 cells generates lethal vulnerability to combined oxamate/etomoxir. *Biochimica et Biophysica Acta (BBA) - General Subjects*, *1863*(7), 1177–1186.

Maras, B., Barra, D., Duprè, S., & Pitari, G. (1999). Is pantetheinase the actual identity of mouse and human vanin-1 proteins? *FEBS Letters*, *461*(3), 149–152.

Marlatt, K. L., & Ravussin, E. (2017). Brown Adipose Tissue: An Update on Recent Findings. *Current obesity reports*, *6*(4), 389–396.

Maxwell, G. M., Crompton, S., Smyth, C., & Harvey, G. (1985). The action of dopamine upon brown adipose tissue. *Pediatric Research*, *19*(1), 60–63.

McCall, R. B., Lookingland, K. J., Bédard, P. J., & Huff, R. M. (2005a). Sumanirole, a highly dopamine D2-selective receptor agonist: In vitro and in vivo pharmacological characterization and efficacy in animal models of Parkinson's disease. *Journal of Pharmacology and Experimental Therapeutics*, *314*(3), 1248–1256.

McCall, R. B., Lookingland, K. J., Bédard, P. J., & Huff, R. M. (2005b). Sumanirole, a highly dopamine D2-selective receptor agonist: In vitro and in vivo pharmacological characterization and efficacy in animal models of Parkinson's disease. *The Journal of Pharmacology and Experimental Therapeutics*, *314*(3), 1248–1256.

Morrison, S. F., Madden, C. J., & Tupone, D. (2012). Central Control of Brown Adipose Tissue Thermogenesis. *Frontiers in Endocrinology*, *3*.

Motomura, W., Yoshizaki, T., Takahashi, N., Kumei, S., Mizukami, Y., Jang, S.-J., & Kohgo, Y. (2012). Analysis of vanin-1 upregulation and lipid accumulation in hepatocytes in response to a high-fat diet and free fatty acids. *Journal of Clinical Biochemistry and Nutrition*, *51*(3), 163–169.

Nedergaard, J., Bengtsson, T., & Cannon, B. (2007). Unexpected evidence for active brown adipose tissue in adult humans. *American Journal of Physiology - Endocrinology and Metabolism*, *293*(2), 444–452.

Nedergaard, J., & Cannon, B. (2013). UCP1 mRNA does not produce heat. *Biochimica Et Biophysica Acta*, *1831*(5), 943–949.

Nunes, J. L., Sharif, N. A., Michel, A. D., & Whiting, R. L. (1991). Dopamine D2-receptors mediate hypothermia in mice: ICV and IP effects of agonists and antagonists. *Neurochemical Research*, *16*(10), 1167–1174.

Olsen, J. V., De Godoy, L. M. F., Li, G., Macek, B., Mortensen, P., Pesch, R., Makarov, A., Lange, O., Horning, S., & Mann, M. (2005). Parts per Million Mass Accuracy on an Orbitrap Mass Spectrometer via Lock Mass Injection into a C-trap. *Molecular & Cellular Proteomics*, *4*(12), 2010–2021.

Ootsuka, Y., Heidbreder, C. A., Hagan, J. J., & Blessing, W. W. (2007). Dopamine D2 receptor stimulation inhibits cold-initiated thermogenesis in brown adipose tissue in conscious rats. *Neuroscience*, *147*(1), 127–135.

Park, H., He, A., & Lodhi, I. J. (2019). Lipid Regulators of Thermogenic Fat Activation. *Trends in endocrinology and metabolism: TEM*, *30*(10), 710–723.

Patra, C., Foster, K., Corley, J. E., Dimri, M., & Brady, M. F. (2023). Biochemistry, cAMP. In *StatPearls*. StatPearls Publishing.

Petito, G., Cioffi, F., Magnacca, N., de Lange, P., Senese, R., & Lanni, A. (2023). Adipose Tissue Remodeling in Obesity: An Overview of the Actions of Thyroid Hormones and Their Derivatives. *Pharmaceuticals*, *16*(4), Article 4.

Pulinilkunnil, T., He, H., Kong, D., Asakura, K., Peroni, O. D., Lee, A., & Kahn, B. B. (2011). Adrenergic regulation of AMP-activated protein kinase in brown adipose tissue in vivo. *Journal of Biological Chemistry*, *286*(11), 8798–8809.

Purves, D., Augustine, G. J., Fitzpatrick, D., Katz, L. C., LaMantia, A.-S., McNamara, J. O., & Williams, S. M. (2001). Catecholamine Receptors. In *Neuroscience. 2nd edition*. Sinauer Associates.

Qu, L., Zhou, Q., Xu, Y., Guo, Y., Chen, X., Yao, D., Han, G. W., Liu, Z.-J., Stevens, R. C., Zhong, G., Wu, D., & Zhao, S. (2019). Structural Basis of the Diversity of Adrenergic Receptors. *Cell Reports*, *29*(10), 2929-2935.e4.

Raffaelli, F.-M., Resch, J., Oelkrug, R., Iwen, K. A., & Mittag, J. (2020). Dopamine receptor D1- and D2-agonists do not spark brown adipose tissue thermogenesis in mice. *Scientific Reports*, *10*(1).

Reed, N., & Fain, J. N. (1968). Stimulation of Respiration in Brown Fat Cells by Epinephrine, Dibutyryl-3',5'-adenosine Monophosphate, and m-Chloro(carbonyl Cyanide)phenylhydrazone. *Journal of Biological Chemistry*, *243*(11), 2843–2848.

Reinholz, J., Skopp, O., Breitenstein, C., Bohr, I., Winterhoff, H., & Knecht, S. (2008). Compensatory weight gain due to dopaminergic hypofunction: New evidence and own incidental observations. *Nutrition & Metabolism*, *5*, 35.

Ricquier, D. (2000). The uncoupling protein homologues: UCP1, UCP2, UCP3, StUCP and AtUCP. In *Biochem. J* (Bd. 345, S. 161–179).

Roth, J., Qiang, X., Marbán, S. L., Redelt, H., & Lowell, B. C. (2004). The Obesity Pandemic: Where Have We Been and Where Are We Going? *Obesity Research*, *12*(S11), 88S-101S.

Rothwell, N. J., & Stock, M. J. (1983). Luxuskonsumption, Diet-Induced Thermogenesis and Brown Fat: The Case in Favour. *Clinical Science*, *64*(1), 19–23.

Rothwell, N. J., Stock, M. J., & Wyllie, M. G. (1982). Dopaminergic mechanisms in diet-induced thermogenesis and brown adipose tissue metabolism. *European Journal of Pharmacology*, *77*(1), 45–48.

Sánchez-Soto, M., Bonifazi, A., Cai, N. S., Ellenberger, M. P., Newman, A. H., Ferré, S., & Yano, H. (2016). Evidence for noncanonical neurotransmitter activation: Norepinephrine as a dopamine D2-like receptor agonist. *Molecular Pharmacology*, *89*(4), 457–466.

Seale, P. (2015). Transcriptional Regulatory Circuits Controlling Brown Fat Development and Activation. *Diabetes*, *64*(7), 2369–2375.

Seeman, P. (2010). Historical Overview: Introduction to the Dopamine Receptors. In K. A. Neve (Hrsg.), *The Dopamine Receptors* (S. 1–21). Humana Press.

Shepherd, R. E., Noble, E. G., Klug, G. A., & Gollnick, P. D. (1981). Lipolysis and cAMP accumulation in adipocytes in response to physical training. *Journal of Applied Physiology: Respiratory, Environmental and Exercise Physiology*, *50*(1), 143–148.

Sialana, F. J., Gulyassy, P., Májek, P., Sjöstedt, E., Kis, V., Müller, A. C., Rudashevskaya, E. L., Mulder, J., Bennett, K. L., & Lubec, G. (2016). Mass spectrometric analysis of synaptosomal membrane preparations for the determination of brain receptors, transporters and channels. *Proteomics*, *16*(22), 2911–2920.

Simon, G. E., Arterburn, D., Rohde, P., Ludman, E. J., Linde, J. A., Operskalski, B. H., & Jeffery, R. W. (2011). Obesity, depression, and health services costs among middle-aged women. *Journal of general internal medicine*, *26*(11), 1284–1290.

Simonds, S. E., & Cowley, M. A. (2019). Speed-dieting: Dopamine agonists promote weight loss. *Nature Metabolism*, *1*(9), 851–852.

Sonne, J., Goyal, A., & Lopez-Ojeda, W. (2022). Dopamine. In *StatPearls*. StatPearls Publishing.

Sonne, J., Goyal, A., & Lopez-Ojeda, W. (2023). Dopamine. In *StatPearls*. StatPearls Publishing.

Stojanovic, T., Orlova, M., Sialana, F. J., Höger, H., Stuchlik, S., Milenkovic, I., Aradska, J., & Lubec, G. (2017). Validation of dopamine receptor DRD1 and DRD2 antibodies using receptor deficient mice. *Amino Acids*, *49*(6), 1101–1109.

Sturgill, M. G., Kelly, M., & Notterman, D. A. (2011). Pharmacology of the Cardiovascular System. In *Pediatric Critical Care* (S. 277–305). Elsevier Inc.

Suchacki, K. J., & Stimson, R. H. (2021). Nutritional Regulation of Human Brown Adipose Tissue. *Nutrients*, *13*(6), Article 6.

Tapia, P., Fernández-Galilea, M., Robledo, F., Mardones, P., Galgani, J. E., & Cortés, V. A. (2018). Biology and pathological implications of brown adipose tissue: Promises and caveats for the control of obesity and its associated complications. *Biological Reviews*, *93*(2), 1145–1164.

Tran, A. H., Tamura, R., Uwano, T., Kobayashi, T., Katsuki, M., & Ono, T. (2005). Dopamine D1 receptors involved in locomotor activity and accumbens neural responses to prediction of reward associated with place. *Proceedings of the National Academy of Sciences*, *102*(6), 2117–2122.

Tran, L. T., Park, S., Kim, S. K., Lee, J. S., Kim, K. W., & Kwon, O. (2022). Hypothalamic control of energy expenditure and thermogenesis. *Experimental & Molecular Medicine*,

54(4), Article 4.

Underland, L. J., Mark, E. R., Katikaneni, R., & Heptulla, R. (2018). The impact of dopamine on insulin secretion in healthy controls. *Indian Journal of Critical Care Medicine*, *22*(4), 209–213.

Valentine, J. M., Ahmadian, M., Keinan, O., Abu-Odeh, M., Zhao, P., Zhou, X., Keller, M. P., Gao, H., Yu, R. T., Liddle, C., Downes, M., Zhang, J., Lusis, A. J., Attie, A. D., Evans, R. M., Rydén, M., & Saltiel, A. R. (2021). B3-Adrenergic receptor downregulation leads to adipocyte catecholamine resistance in obesity. *The Journal of Clinical Investigation*, *132*(2), e153357.

van Diepen, J. A., Jansen, P. A., Ballak, D. B., Hijmans, A., Rutjes, F. P. J. T., Tack, C. J., Netea, M. G., Schalkwijk, J., & Stienstra, R. (2016). Genetic and pharmacological inhibition of vanin-1 activity in animal models of type 2 diabetes. *Scientific Reports*, *6*, 21906.

Vasse, M., Chagraoui, A., Henry, J. P., & Protais, P. (1990). The rise of body temperature induced by the stimulation of dopamine D1 receptors is increased in acutely reserpinized mice. *European Journal of Pharmacology*, *181*(1–2), 23–33.

Vincent, S. (2004). Norepinephrine Transporter. In L. Martini (Hrsg.), *Encyclopedia of Endocrine Diseases* (S. 382–386). Elsevier.

Virtanen, K. A., Lidell, M. E., Orava, J., Heglind, M., Westergren, R., Niemi, T., Taittonen, M., Laine, J., Savisto, N.-J., Enerbäck, S., & Nuutila, P. (2009). Functional Brown Adipose Tissue in Healthy Adults. *New England Journal of Medicine*, *360*(15), 1518–1525.

Walsh, C. T., Stupack, D., & Brown, J. H. (2008). G Protein–Coupled Receptors Go Extracellular. *Molecular interventions*, *8*(4), 165–173.

Warner, A., & Mittag, J. (2014). Brown fat and vascular heat dissipation: The new cautionary tail. *Adipocyte*, *3*(3), 221–223.

Warner, A., & Mittag, J. (2016). Breaking BAT: Can browning create a better white? *Journal of Endocrinology*, *228*(1), R19–R29.

Weiner, J., Kranz, M., Klöting, N., Kunath, A., Steinhoff, K., Rijntjes, E., Köhrle, J., Zeisig, V., Hankir, M., Gebhardt, C., Deuther-Conrad, W., Heiker, J. T., Kralisch, S., Stumvoll, M., Blüher, M., Sabri, O., Hesse, S., Brust, P., Tönjes, A., & Krause, K. (2016). Thyroid hormone status defines brown adipose tissue activity and browning of white adipose tissues in mice. *Scientific Reports*, *6*(1), Article 1.

Wettschureck, N., & Offermanns, S. (2005). Mammalian G Proteins and Their Cell Type Specific Functions. *Physiological Reviews*, *85*(4), 1159–1204.

Whybrow, P. C., & Prange, A. J. (1981). A Hypothesis of Thyroid-Catecholamine-Receptor Interaction: Its Relevance to Affective Illness. *Archives of General Psychiatry*, *38*(1), 106–

113.

Wiglusz, Z., & Jedrzejak, R. (2011). Dopamine acts peripherally on rat tail arteries. *Journal of Pharmacy and Pharmacology*, *32*(1), 719–721.

Williams, L. T., Lefkowitz, R. J., Watanabe, A. M., Hathaway, D. R., & Besch, H. R. (1977). Thyroid hormone regulation of beta-adrenergic receptor number. *Journal of Biological Chemistry*, *252*(8), 2787–2789.

Wiśniewski, J. R., Zougman, A., Nagaraj, N., & Mann, M. (2009). Universal sample preparation method for proteome analysis. *Nature Methods*, *6*(5), 359–362.

World Health Organization. (2018). Noncommunicable Diseases Country Profiles 2018. In *World Health Organization* (Bd. 369, Nummer 14). World Health Organization.

Wu, J., Boström, P., Sparks, L. M., Ye, L., Choi, J. H., Giang, A.-H., Khandekar, M., Virtanen, K. A., Nuutila, P., Schaart, G., Huang, K., Tu, H., van Marken Lichtenbelt, W. D., Hoeks, J., Enerbäck, S., Schrauwen, P., & Spiegelman, B. M. (2012). Beige adipocytes are a distinct type of thermogenic fat cell in mouse and human. *Cell*, *150*(2), 366–376.

Yu, J., Zhu, J., Deng, J., Shen, J., Du, F., Wu, X., Chen, Y., Li, M., Wen, Q., Xiao, Z., & Zhao, Y. (2022). Dopamine receptor D1 signaling stimulates lipolysis and browning of white adipocytes. *Biochemical and Biophysical Research Communications*, *588*, 83–89.

Yu, S., Matsusue, K., Kashireddy, P., Cao, W.-Q., Yeldandi, V., Yeldandi, A. V., Rao, M. S., Gonzalez, F. J., & Reddy, J. K. (2003). Adipocyte-specific Gene Expression and Adipogenic Steatosis in the Mouse Liver Due to Peroxisome Proliferator-activated Receptor γ1 (PPARγ1) Overexpression*. *Journal of Biological Chemistry*, *278*(1), 498–505.

Zekri, Y., Flamant, F., & Gauthier, K. (2021). Central vs. Peripheral Action of Thyroid Hormone in Adaptive Thermogenesis: A Burning Topic. *Cells*, *10*(6), Article 6.

Zhang, S., Reljić, B., Liang, C., Kerouanton, B., Francisco, J. C., Peh, J. H., Mary, C., Jagannathan, N. S., Olexiouk, V., Tang, C., Fidelito, G., Nama, S., Cheng, R.-K., Wee, C. L., Wang, L. C., Duek Roggli, P., Sampath, P., Lane, L., Petretto, E., … Ho, L. (2020). Mitochondrial peptide BRAWNIN is essential for vertebrate respiratory complex III assembly. *Nature Communications*, *11*(1), Article 1.

Zhang, W., & Bi, S. (2015). Hypothalamic Regulation of Brown Adipose Tissue Thermogenesis and Energy Homeostasis. *Frontiers in Endocrinology*, *6*, 136.

Zhou, H., Zhang, H., Ye, R., Yan, C., Lin, J., Huang, Y., Jiang, X., Yuan, S., Chen, L., Jiang, R., Zheng, K., Cheng, Z., Zhang, Z., Dong, M., & Jin, W. (2022). Pantothenate protects against obesity via brown adipose tissue activation. *American Journal of Physiology. Endocrinology and Metabolism*, *323*(1), E69–E79.